PHASE AND VOLUMETRIC BEHAVIOR OF CO_2 AND BAKKEN OIL SYSTEM UNDER RESERVOIR CONDITIONS

By

Yuhao Yang

Submitted to the graduate degree program in Chemical and Petroleum Engineering Department and the Graduate Faculty of the University of Kansas in partial fulfillment of the requirements for the degree of Master of Science

---

Chair: Xiaoli Li

Member: Reza Barati

Member: Shahin Negahban

Date Defended: December 11, 2020

The thesis committee for Yuhao Yang certifies that this is the approved version of the following thesis:

PHASE AND VOLUMETRIC BEHAVIOR OF CO_2 AND BAKKEN OIL SYSTEM UNDER RESERVOIR CONDITIONS

Chair: Dr. Xiaoli Li

Date Approved: December 14, 2020

ABSTRACT

The Bakken Petroleum System (BPS) is one of the largest unconventional petroleum and natural gas resource and the most prolific tight oil plays in the North America. It is estimated that 10 to 400 billion barrels of oil has been generated and charged into the Bakken region. It is reported that the production rate drops drastically and stabilizes at a low value, which results in an unsatisfying recovery factor in the primary recovery stage. Either secondary recovery process or enhanced oil recovery (EOR) process is required since a small improvement in recovery factor can result in a huge improvement in oil production. CO_2 based EOR process is the most favorable method for Bakken reservoirs due to favorable hydrocarbon properties. In consequence, it is important to quantify and investigate parameters such as CO_2 solubility and oil swelling factor of this hydrocarbon system. In addition, experiments are designed to visualize phase behaviors at real reservoir conditions for comprehensive investigation and analysis of the CO_2 EOR mechanism.

CO_2 dissolution and oil swelling effect are key mechanisms in the CO_2 EOR process. CO_2 solubility, oil swelling factor, and extraction pressure are systematically examined at elevated temperatures and pressures. In the phase behavior experiments, excessive CO_2 and desirable Bakken crude oil is injected into a piston-equipped pressure/volume/temperature (PVT) cell. Different experiments on CO_2 and Bakken oil system are performed at 27, 80, and 120 °C in order to visualize different phase behaviors. For each phase behavior experiment, the system is pressurized step by step by moving the piston forward. Each stabilized pressure is recorded as equilibrium pressure, and the oil phase volume is measured at each equilibrium pressure for swelling factor calculation. The pressurization process is repeated until CO_2 and oil phases become miscible. In the simulation section, flash calculations are performed by using CMG WinProp.

Bakken oil components are lumped into seven pseudo-components. Properties such as binary interaction coefficient, critical properties, and volume shift value of each pseudo-component are modified in order to match the oil swelling factor determined in the phase behavior experiment in order to develop an accurate equation of state (EOS) model. Then, the tuned EOS model is used in a cell-to-cell simulation for minimum miscibility pressure (MMP) calculation. The MMP determined in this section is compared with two pressures determined in the former section (the pressure results in a zero swelling factor and the pressure result in a zero interfacial tension). Overall, it is found that the extraction pressure decreases with system temperature. When the system temperature is below the CO_2 critical temperature (31.1 °C), there are three phase behaviors, liquid-vapor (LV), liquid-liquid-vapor (L_1L_2V), and liquid-liquid (L_1L_2) observed in this system. However, there are only two types of phase behaviors observed when the system temperature exceeds the CO_2 critical temperature. According to the CMG WinProp calculation at 80 and 120°C, the interfacial tension (IFT) between CO_2 phase and Bakken oil phase is 0 at 1897 and 2732 psi, respectively, at which the super-critical CO_2 starts to become liquid-like and a LV phase behavior in observed. Results from the cell-to-cell simulations show that the multiple contact MMP at 80 and 120°C are 2011 and 2812 psi, respectively, at which the interfacial tension across two phases reduces to zero. In conclusion, the multiple contact MMP is achieved when the super-critical CO_2 behaves liquid-like.

ACKNOWLEGEMENT

I would like to express my deepest gratitude and respect to my academic advisor, Dr. Xiaoli Li, for her invaluable encouragement and guidance during the past two-year graduate studies at the University of Kansas. In addition to her technical expertise, I really appreciate her mentorship in other aspects such as work ethics and communication.

I am sincerely thankful to Dr. Reza Barati, Dr. Shapour Vossoughi, Dr. Shahin Negahban, Dr. Russ Ostermann, Dr Jyun-Syung Tsau and Dr. Masoud Kalantari from our Chemical and Petroleum Engineering Department for their endless guidance during my undergraduate and graduate studies at the University of Kansas. In addition, I would like to expand my thanks to the Chemical and Petroleum Engineering Department for the financial support by offering the Graduate Teaching Assistant appointment.

I'm truly thankful for my past and present research group members, Ms. Xuejia Du, Mr. Di Chai, Mr. Gang Yang, Ms. Ruyi Zheng, Ms. Julia Espinoza and Mr. Zhixing Wang, for their encouragements and technical discussions.

I would like to thank my friends, Ms. Ruo Yang, Ms. Qinwen Fu and Mr. Hongtian Ren for their caring and comfort during my tough time.

Last but not the least, I would like to express my appreciation to my families, Mr. Jun Yang, Mrs. Hong Yu, Doufu, Mr. Min Yu, Mrs. Ping Yu, Mrs. Bo Yu, Mr. Chuan Yang and Mrs. Hongying Yang, for their endless love.

DEDICATION

This thesis is dedicated to my dearest parents, Mr. Jun Yang and Mrs. Hong Yu, and my beloved grandfather, Xingliang Yang. I love you forever.

TABLE OF CONTENTS

LIST OF FIGURES

LIST OF TABLES

CHAPTER 1 INTRODUCTION

The Bakken Petroleum System (BPS) is one of the largest unconventional petroleum and natural gas resource and the most prolific tight oil plays underlying parts of North Dakota, Montana and the Canadian provinces of Saskatchewan and Manitoba (Zhang, 2016). U.S. oil industry has been stimulated by the unconventional resource technology breakthrough of hydraulic fracturing and horizontal drilling and become the largest oil productively country in the world (Yu et al., 2015; Wang and Yu, 2019). According to the report from the U.S. Energy Information Administration (EIA), the oil production in the Bakken region has accelerated from 300 thousand to 1500 thousand barrels/day in the last decade, which implies that the Bakken region is one of the major oil production regions in the North American. However, the natural properties of reservoirs in Bakken region lead to a low recovery factor ranging from 5 to 10% (Hoffman, 2012). It is reported that there are 10 to 400 billion barrels of oil in the Bakken region (Price and Lefever, 1992; Pitman et al., 2001; Jin and Sonnenberg, 2013). In consequence, even a small improvement in the recovery factor will lead to a huge increase in oil production with such a large resource base. As a result, other recovery methods such as secondary recovery process and enhanced oil recovery (EOR) process are implemented in order to maintain the production rate. However, waterflooding methods, which is commonly used in conventional reservoirs as a secondary recovery method, is proved to be unfeasible in Bakken reservoirs (Du and Nojabaei, 2019). Gas injection method is the most suitable method for Bakken reservoirs among different enhanced oil recovery methods since the typical Bakken reservoir is 9000 ft below the surface and produces the oil with the viscosity of 1 cP (Poellitzer et al., 2009; Zhang, 2016).

Two main purposes of this study are addressed in this thesis. First, a series of phase behavior experiments are performed to extend the phase behavior database for CO_2 and the Bakken crude oil. In the phase behavior experiment, equilibrium parameters such as CO_2 solubility, oil swelling factor, extraction pressure, and the pressure that leads to a zero swelling factor are determined. With the data acquired from the phase behavior experiment, an equation of state (EOS) model can be obtained for further simulation and investigation studies. Second, the mechanism of CO_2 EOR method, especially at real reservoir conditions, can be comprehensively investigated and analyzed by the visualization of interactions between CO_2 and oil during the entire experiment process.

This thesis includes six chapters. Chapter 1 is an introduction of background information and objectives about this thesis. Chapter 2 is the literature review that provides the background knowledge of the BPS and mechanisms of the CO_2-based EOR method such as oil swelling, CO_2 dissolution, and oil components extraction. Moreover, different minimum miscibility pressure (MMP) determination methods are also introduced in this chapter. Chapter 3 illustrates experimental setups and procedures for the phase behavior experiment and it also demonstrates how the equilibrium parameters such as CO_2 solubility and oil swelling factor are calculated. Chapter 4 illustrates general steps in the simulation study and presents theories used in this research. It demonstrates how CMG WinProp performs the flash calculation to get phase behaviors and parameters at given equilibrium pressure and temperature. Chapter 5 concludes results from experiments and simulations of this thesis. The last chapter summarizes major findings of this thesis and recommendations for the future work.

CHAPTER 2 LITERATURE REVIEW

2.1 Overview of the Bakken Petroleum System

The Bakken formation lays in the Williston Basin. Williston Basin is a sedimentary basin (Carlson and Anderson, 1965). As shown in Figure 1, Nesson, Cedar Creek, and Billings anticlines are major structures in the Williston Basin (Jin et al. 2015). Figure 2 shows the generalized stratigraphic column of the Bakken formation. It illustrates that Bakken formation consists of four major members. These four members are Pronghorn calcareous siltstone member, lower Bakken siliceous organic-rich shale member, middle Bakken dolomite siltstone and sandstone member, and upper Bakken shale member in an ascending order (Sonnenberg and Pramudito, 2009; LeFever et al., 2011). Both lower and upper Bakken shale members are the world class source, sourcing reservoirs in the Bakken formation, upper part of the Three Forks formation, and lower part of the Lodgepole formation. These three formations (Three Forks formation, Bakken formation, and Lodgepole formation) make up the BPS. In conclusion, oil is generated from the mature upper and lower Bakken shale members and then migrates to reservoirs in the BPS (Jin and Sonnenberg, 2013).

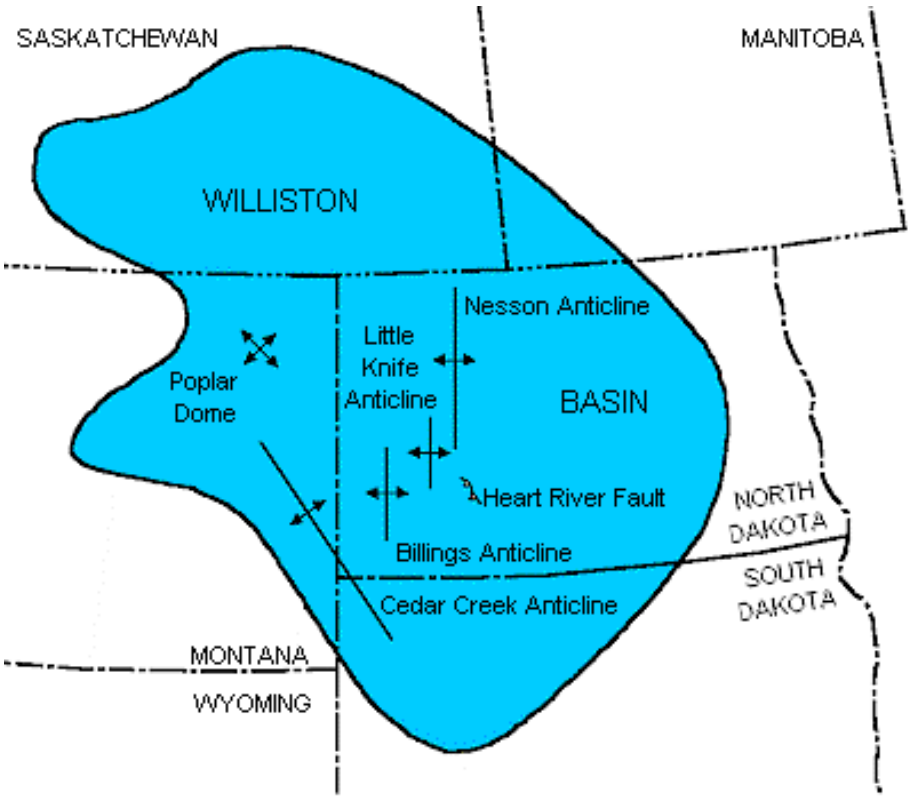

Figure 1 Geo-location of the Williston Basin (Heck et al., 2007)

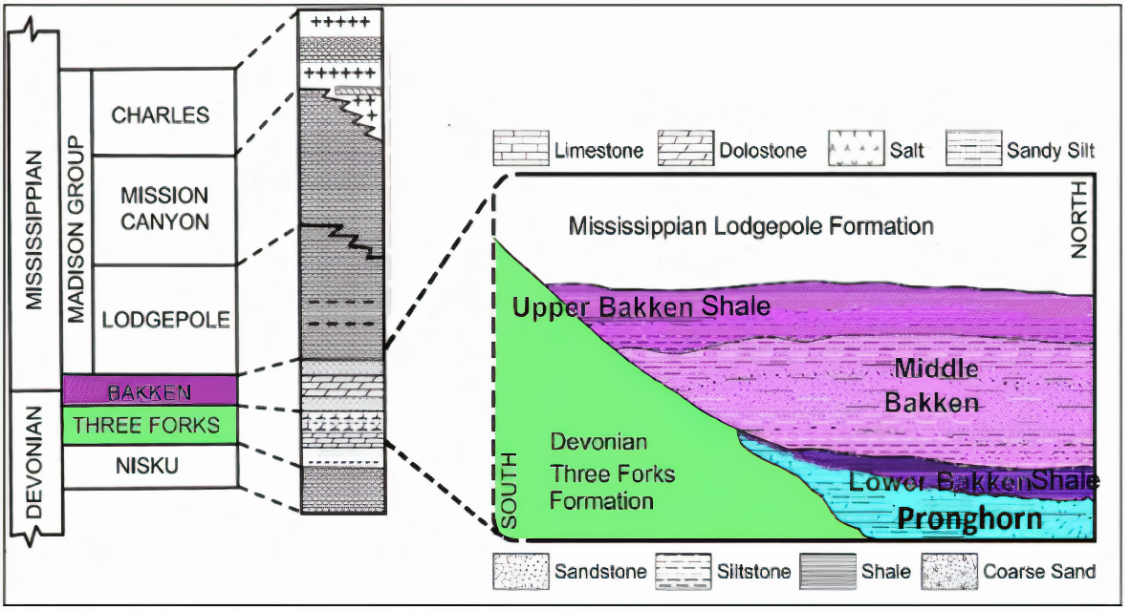

Figure 2 Generalized stratigraphic column of the Bakken formation (Xu and Sonnenberg, 2016)

The BPS is economically essential. Shale members in the Bakken formation are rich in organic matters, which has been proved to be one of the major petroleum source rock (Dow, 1974; Williams, 1974; Schmoker and Hester, 1983; Webster, 1984; Meissner 1984). There are estimated 10 to 400 billion barrels of oil that have been generated and charged into Bakken reservoirs (Price and Lefever, 1992; Pitman et al., 2001; Jin and Sonnenberg, 2013). Figure 3 shows the oil production in the Bakken region, except for some fluctuations, has accelerated from 300 thousand barrels/day to around 1500 thousand barrels/day in the last decade. Figure 4 shows the oil production comparison between different regions. It demonstrates that oil production rate in Permian region is around 4500 thousand barrels/day in August 2019, and the production rate in August 2020 is predicted to be around 4000 thousand barrels/day. Bakken and Eagle Ford regions has almost the same oil production rate. It is around 1500 thousand barrels/day in August 2019 and predicted to be around 1000 thousand barrels/day in August 2020. The production rate in other regions is much lower than these three regions mentioned above, which implies the Bakken region

is one of major oil productive regions in the U.S., and the BPS is considered the world class reservoir (Jin et al., 2015).

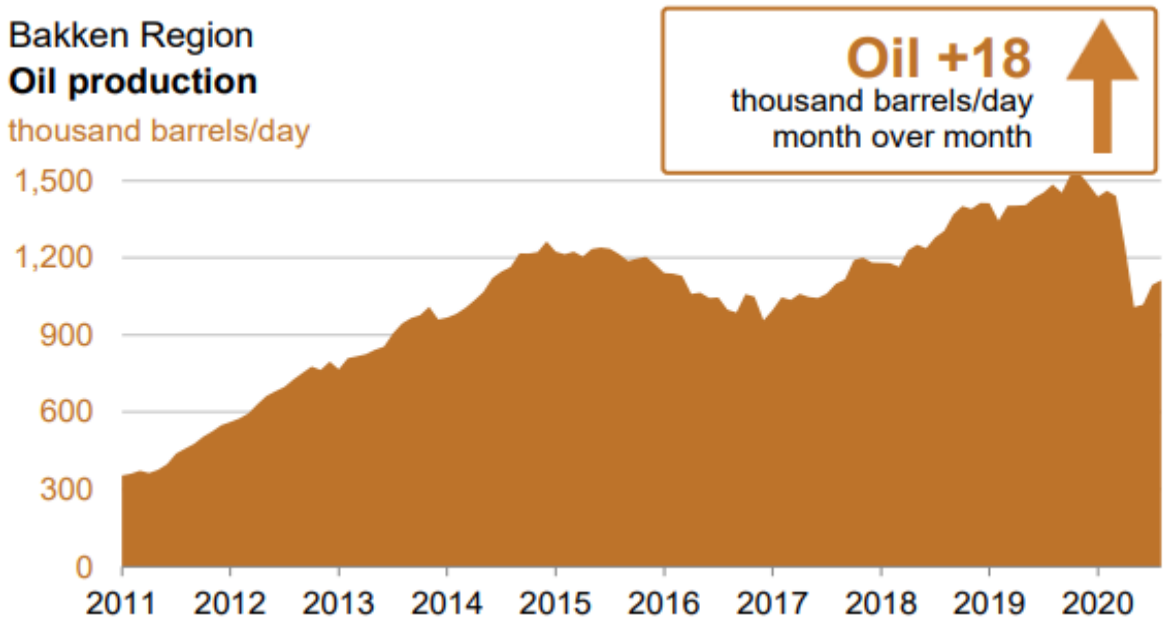

Figure 3 Oil production in the Bakken region in the last decade (EIA, 2020)

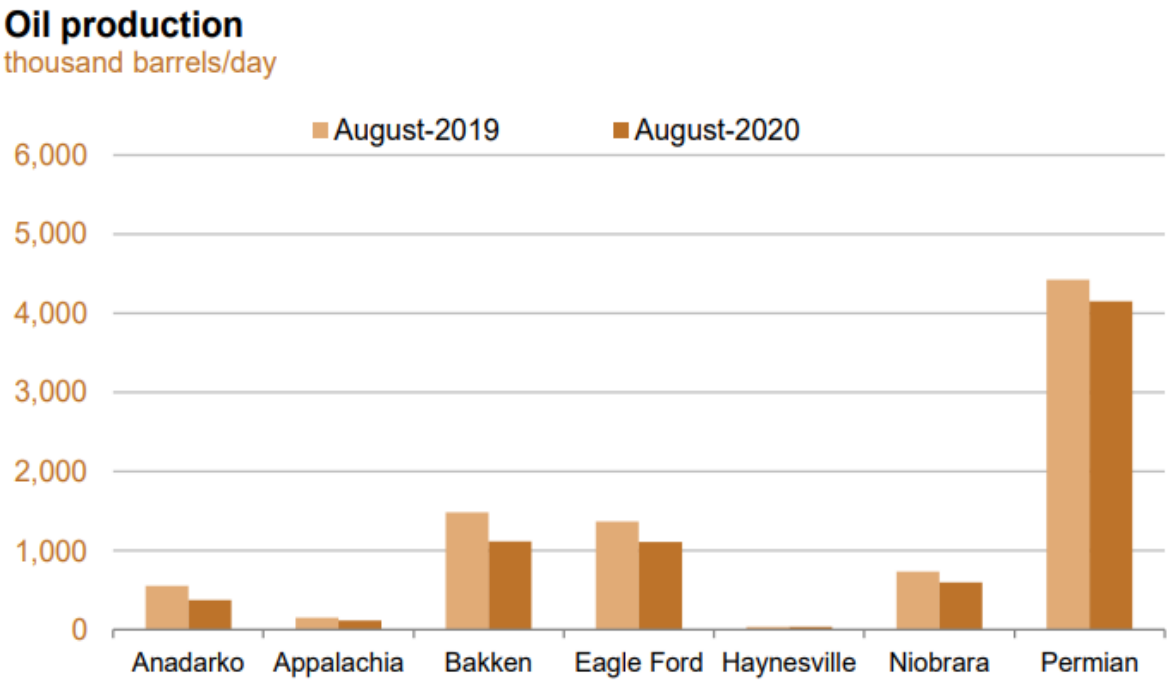

Figure 4 Oil production comparison between different regions in the U.S. (EIA, 2020)

2.2 Enhanced Oil Recovery and Different EOR Options

It is reported that hydrocarbons have been known to exist in the Bakken formation for decades, but the exploitation is not economic because of the extremely low permeability (micro to nano-Darcy). Although recent advanced multi-stage hydraulic fracturing and horizontal drilling have improved the oil overall production, the primary oil recovery factor is still extremely unsatisfied (5 to 10%) because of the natural rock properties such as extremely small pore size, low porosity, and low permeability (Hoffman, 2012; Du and Nojabaei, 2019). Once the production rate tends to decline and stabilize at a low rate, other processes are implemented in order to maintain the production rate to increase the recovery factor. Other processes refer to secondary recovery process (waterflooding) or enhanced oil recovery process. The rock characteristics such as wettability need to be clarified before designing a waterflooding or EOR project. In general, the wettability is the

preference of a surface to be in contact with one fluid rather than another. The wettability for the rock in Bakken reservoirs is oil-wet, indicating that the surface prefers contact with oil. In consequence, a greater entry pressure is required in order to overcome the capillary barrier to water. Therefore, the waterflooding method, which is a common option in conventional reservoirs, is not favorable in the Bakken formation due to low injectivity and the oil-wet natural properties (Zhang, 2016).

Poellitzer et al. (2009) summaries the most suitable EOR method corresponding to different reservoir properties such as reservoir depth and reservoir in-situ oil viscosity. In general, there are mainly six major EOR techniques, which are CO_2/hydrocarbon gas injection, N_2/Air injection, polymer injection, surfactant/alkali surfactant polymer injection, steam injection, and in-situ combustion. Each technique has its suitable using scenario. Figure 5 shows CO_2/hydrocarbon gas injection and N_2/Air injection are favorable EOR techniques when the reservoir is 500 to 3000 ft below the surface and the in-site oil viscosity ranges from 1 to 10 cP. When the depth of the reservoirs is between 200 to 2000 ft and the oil is more viscous (1 to 100 cP), surfactant/alkali surfactant polymer injection is more favorable. When the reservoir depth is between 200 to 1500 ft and the oil viscosity is between 5 to 100 cP, polymer injection is more suitable. Steam injection is considered as the best technique when the reservoir is 50 to 750 ft below the surface and the oil viscosity ranges from 500 to 100000 cP. When the reservoir depth is 300 to 1500 ft and the viscosity is between 1000 to higher than 100000 cP, in-situ combustion is the most suitable EOR method. Researches and experiments show that a typical Bakken reservoir is at least 9000 ft deep, and produces light oil with the viscosity less than 1 cP at reservoir conditions (Zhang, 2016).

Therefore, gas injection is the most favorable method in Bakken reservoirs considering these two properties.

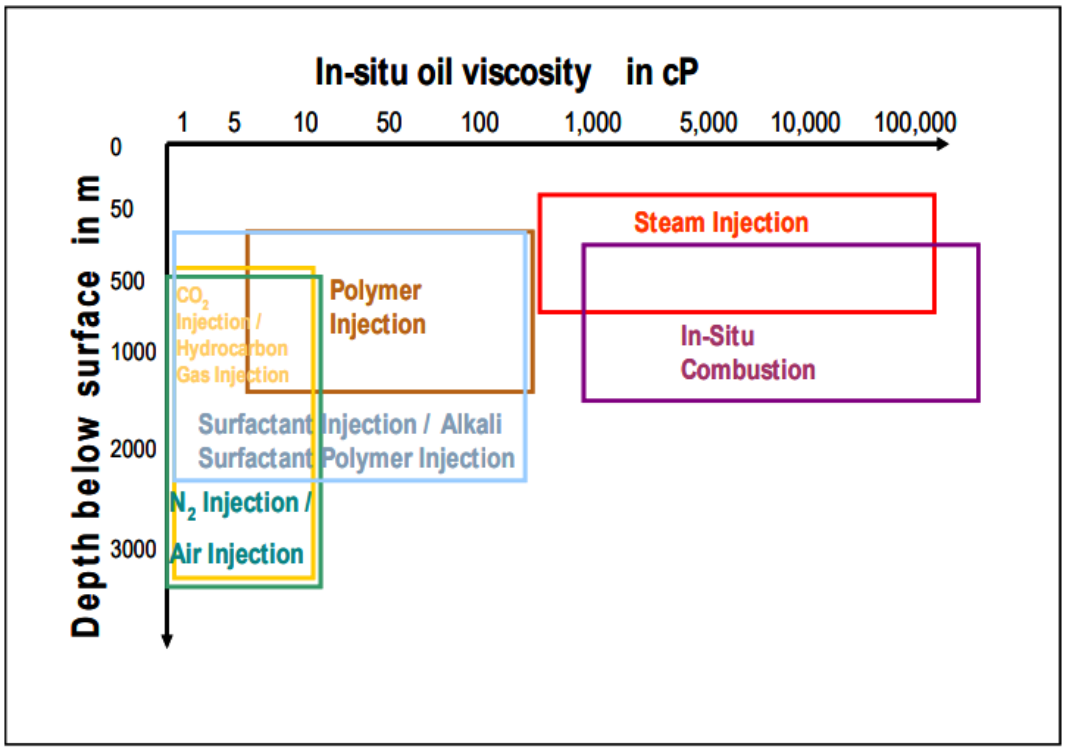

Figure 5 The most suitable EOR method at various reservoir conditions (Poellitzer et al., 2009)

Moreover, CO_2 is the most optimized option among these injected gas candidates for Bakken reservoirs based of the following reasons (Zhang, 2016):

1. The dissolution process of CO_2 is easier compared with other injected gases. Crude oil will be swelled due to CO_2 dissolution, which results in the oil viscosity reduction.
2. The MMP of CO_2 is lower compared with other injected gases. In general, CO_2 requires a minimum reservoirs pressure of 1100 psi at temperature ranging from 90 to 250 °F (90 to 120 °C). Research shows the pressure is greater than 4000 psi, and temperature ranges from 150 to 240 °F (65 to 115 °C) for Bakken reservoirs.

3. The optimum crude oil gravity for CO_2 injection ranges from 27 to 48 °API. Experiments show the typical gravity of light oil produced from Bakken reservoirs is 36 to 48 °API.
4. The injected CO_2 will re-pressurize the reservoir, which can lead to re-establish the drive mechanisms.
5. The injection of CO_2 can be recycled at the surface, and the usage of injected CO_2 can help to mitigate the carbon emission to the atmosphere, which can effectively reduce the greenhouse emissions (Song and Yang, 2013; Adekunle and Hoffman, 2014).

2.3 CO_2 Injection EOR Method

2.3.1 CO_2 properties

CO_2 is a colorless, odorless, and incombustible gas at atmospheric temperature and pressure (Yin, 2015). The phase diagram of the pure CO_2 on the pressure-temperature (P-T) chart is shown in Figure 6. It shows that the critical pressure is 73.9 bar (1073 psi), and the critical temperature is 304 K (31.1 °C). Therefore, CO_2 mainly behaves as a supercritical fluid under Bakken reservoir conditions since the average pressure and temperature of the Bakken reservoir is greater than 4000 psi and 65 °C.

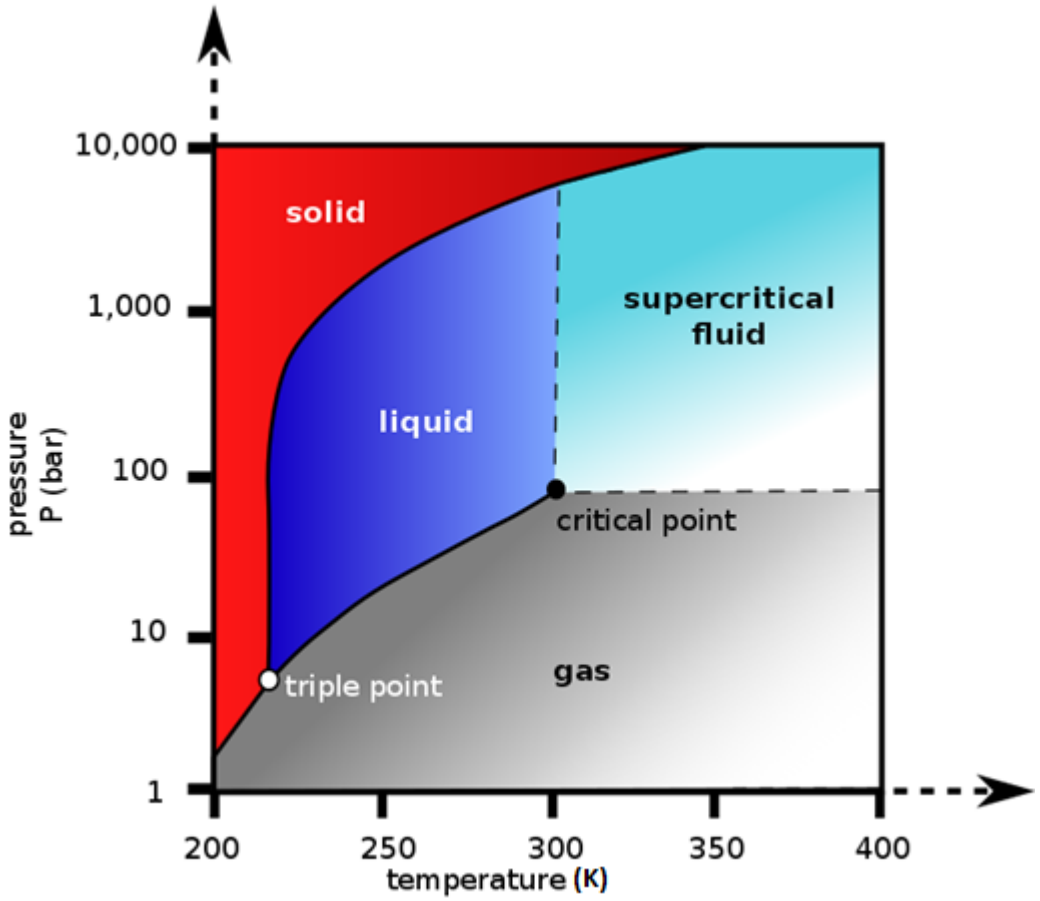

Figure 6 P-T chart of pure CO_2 (en.wikipedia.org)

2.3.2 CO_2 immiscible displacement

CO_2 immiscible flooding can result in oil viscosity reduction, oil phase swelling, oil light components extraction, and the fluid drive (Holm and Josendal, 1982). This immiscible displacement happens when the reservoir pressure is below the MMP or the reservoir oil composition is not favorable (CO_2 and oil will not form a single phase). However, a higher production rate can be achieved compared with the production rate in the primary production due to:

1. The swelling of oil due to CO_2 dissolution.

2. The oil viscosity reduction due to the oil swelling effect.

The oil swelling effect and the oil viscosity reduction can help to release the residual oil. Another CO_2 immiscible displacement mechanism is the solution gas drive. When the reservoir pressure goes below the pseudo-bubble point pressure during the production life, saturated CO_2 comes out of the oil phase, forming a continuous CO_2 gas phase. This gas phase provides energy for the oil production. It is reported that immiscible displacement is favorable in field with low-gravity, high-viscosity crude oil (Holm, 1987).

2.3.3 CO_2 miscible displacement

Two or more phases are considered miscible if there is no interface between the phases. First contact miscible displacement and multiple contact miscible displacement are two main processes in miscible displacement. First contact miscibility happens when the injected fluid is directly miscible with the reservoir oil at the condition of pressure and temperature existing in the reservoir (Green and Willhite, 1998). Multiple contact miscibility process happens when the injected gas does not achieve miscibility with reservoir oil at the first contact. However, the miscibility can still be achieved through some extra processes such as in-situ mass transfer between oil and CO_2 after repeated contacts. This phenomenon is called multiple contact miscibility. The mechanism for oil displacement will be discussed in the next section.

2.3.4 CO_2 near miscible displacement

Many displacement processes are not considered as miscible displacement because the maximum reservoir pressure can be attained is lower that the MMP. Near miscible displacement refers to a

process occurring at pressure slightly below the MMP, but the actual injection pressure range is not clearly defined (Bui, 2010). The CO_2 MMP is estimated to be 1350 psig at 110 °F and 1650 psig at 125 °F, the slim tube experiment performed by Bui (2010) shows at least 80% of the original oil in place is recovered at the pressure of 1150 psig and at a temperature ranging from 110 to 125 °F. In addition, the swelling and extraction test performed by Bui (2010) implies that the extraction of oil components is the primary recovery mechanism in the near miscible displacement. Moreover, it was found that the oil viscosity was reduced by a factor of five due to the dissolution CO_2. In conclusion, the efficiency of the near miscible displacement process is between immiscible process and miscible process. Mechanisms of the near miscible displacement includes oil swelling, oil viscosity reduction and the reduction of interfacial tension between CO_2 and oil.

2.3.5 Mechanisms for oil displacement by CO_2

The mechanisms of oil displacement highly rely on the reservoir temperatures and pressures. Klins (1984) generates and describes main mechanisms for the oil displacement at different temperatures and pressures (Figure 7).

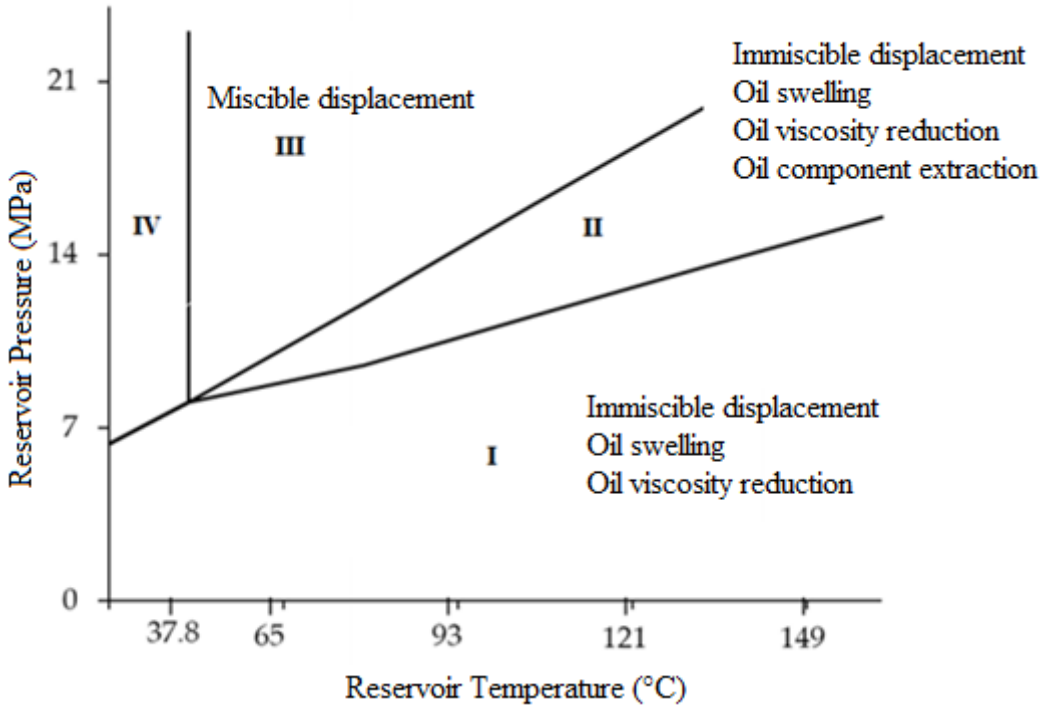

Figure 7 Different mechanisms of oil displacement at different reservoir temperatures and pressures (Klins, 1984)

In the low-pressure range (Region I), the oil displacement is driven by the oil swelling and oil viscosity reduction. In addition, the undissolved gas is trying to merge into oil phase. This phenomenon is defined as solution gas drive that can also provide energy for oil displacement.

When the system pressure increases and the oil and gas system is in Region II, crude oil component extraction is another key mechanism. In this region, light oil components are extracted by the injected gas enhancing the viscosity reduction. Region III is an essential region that demonstrates the mechanism for the miscible displacement. In this region, CO_2 extracts a significant amount of oil components so miscibility will be achieved in a very short time range (Bui, 2010).

2.3.6 Mechanisms for CO_2 and oil miscibility

Miscibility between two phases can be achieved by either first contact miscibility or multiple contact miscibility. If CO_2 and oil are not miscible at the first contact in the suitable pressure range, additional contact processes between oil and CO_2 are required to enrich the CO_2 phase until oil-enriched CO_2 cannot be distinguished from the CO_2-enricheh oil. These processes can be classified into vaporing process and condensing process that can be describe by a ternary diagram (Green and Willhite, 1998).

The ternary diagram is used to describe the vaporing and condensing process in order to achieve multiple contact miscibility. In a general diagram, apexes demonstrate the 100% concentration of light components (methane, nitrogen, and CO_2), intermediate oil components (C_2-C_6), and heavy oil components (C_{7+}). Each diagram represents a certain pressure and temperature. As shown in Figure 8, Point A represents the composition of the injected gas. Point C represents the composition of the crude oil. Point O is the critical point. The enclosed area is the two-phase region, and the outside area is the single-phase region. VO is the saturated vapor curve. LO is the saturated liquid curve.

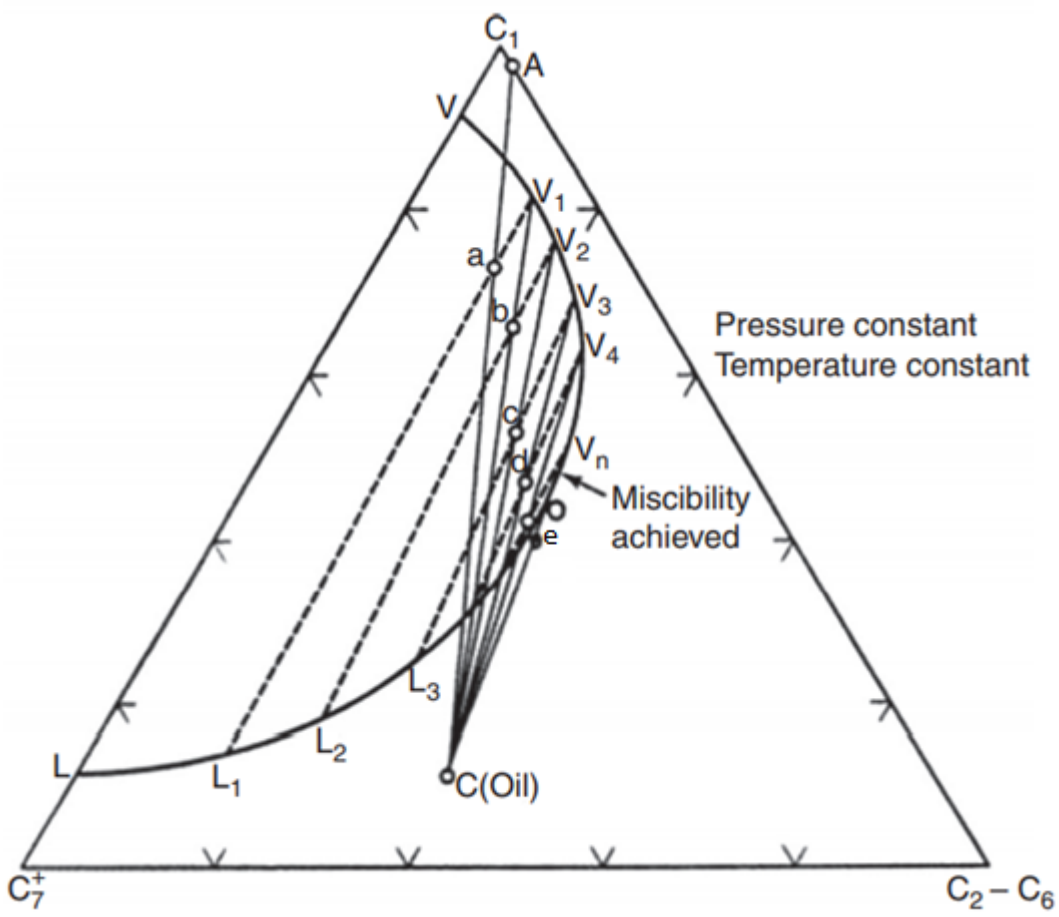

Figure 8 Demonstration of vaporization process of multiple contact miscibility (Green and Willhite, 1998)

Figure 8 demonstrates the vaporing process in order to achieve multiple contact miscibility. The injected gas is relatively lean gas, and it mostly contains methane and light hydrocarbons. In this process, the composition of injected gas and crude oil continuously modified, which means the injected gas is enriched through multiple contacts with the crude oil. During this process, intermediate components are extracted from the crude oil into the injected gas. The vaporing process is described as follows:

1. When the injected gas A contacts with the crude oil C, the composition of this gas-oil mixture is along the line AC (Point a).

2. Point a is in the two-phase region, which means the mixture has two different phases (vapor phase V_1 and liquid phase L_1).
3. Vapor phase of the mixture V_1 continuously contacts with the crude oil C. The composition of this mixture is along the line V_1C (Point b).
4. Point b is in the two-phase region, which means the mixture has two different phases (vapor phase V_2 and liquid phase L_2).
5. Vapor phase of the mixture V_2 continuously contacts with the crude oil C. The composition of this mixture is along the line V_2C (Point c).
6. The similar contact process continues happening until Point e is reached, which indicates two phases achieve miscible since the line between C and e is in the single- phase region, which means multiple contact miscibility is achieved.

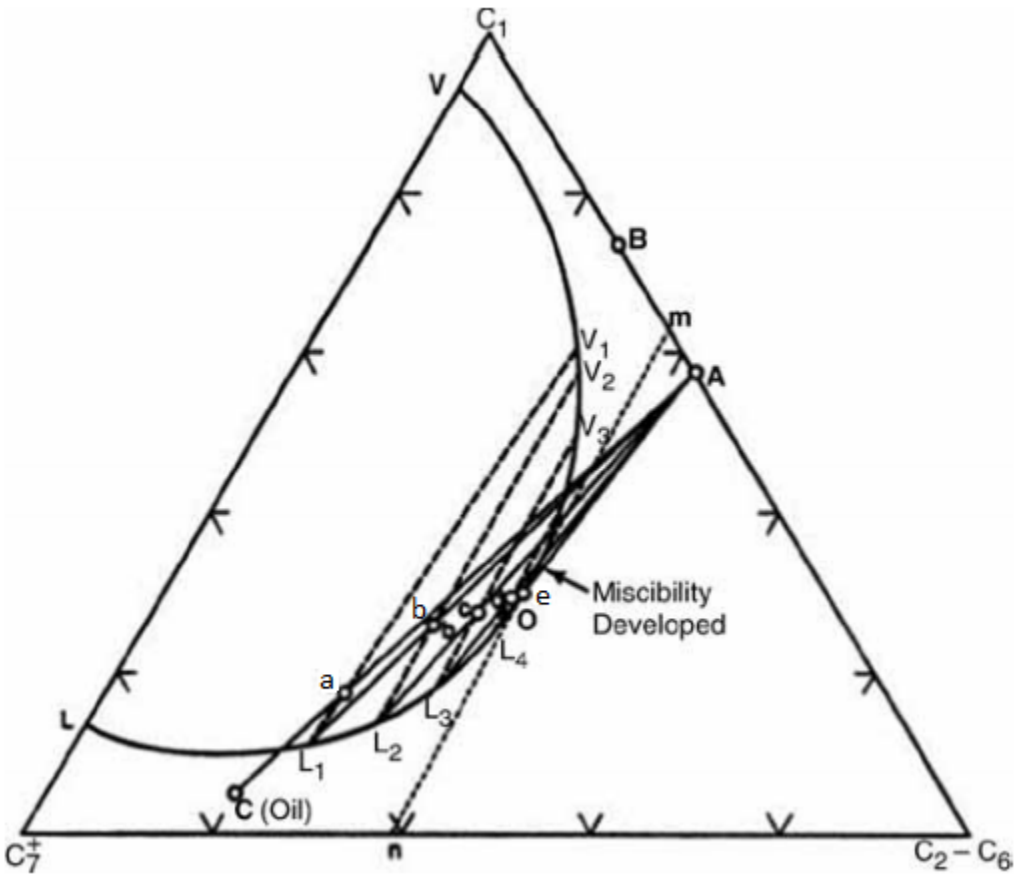

Figure 9 Demonstration of condensation process of multiple contact miscibility (Green and Willhite, 1998)

Figure 9 demonstrates the condensation process in order to achieve multiple contact miscibility. When the injected gas contains relatively large amount of intermediate oil components (Point A), the condensation process is described as follows:

1. The crude oil near the injection well is enriched by the injected gas A. The composition of this mixture is along the line AC (point a).
2. Point a is a two-phase mixture since it is in the two-phase region (vapor phase V_1 and liquid phase L_1).

3. Due to the enrichment of injected gas, liquid phase L_1 is more mobile that the vapor phase V_1, and L_1 continuously contacts with the injected gas again. The composition of mixture of along the L_1A line (Pint b).
4. The similar contact process continues until the mixture reaches Point e because line between point C and e is in the single-phase region, which indicates multiple contact miscibility is achieved by condensing process.

2.4 Phase Behaviors of CO_2 and Oil

The phase behavior study between the injected gas and the crude oil is essential since the experimental data from phase behavior experiment is required for further reservoir simulation, evaluation, and production prediction. The following section lists key parameters analyzed in the phase behavior experiment a CO_2 and crude oil system.

2.4.1 Oil swelling effect and CO_2 solubility

Oil swelling factor is the ratio of the volume of expanded or shrunken oil at reservoir temperature and pressure to the volume of the original deal oil at standard pressure and reservoir temperature (Welker, 1963). As aforementioned, oil swelling is an essential mechanism in CO_2 oil displacement. The non-mobile oil becomes mobile after swelling that can be displaced by the injected CO_2 (Huang and Tracht, 1974). In addition, the expanded oil can also displace the reservoir brine, which can improve the relative permeability and reduces the residual oil saturation in this reservoir (Du, 2016). In the swelling and extraction test, it is reported that there are two distinct regions. The oil swelling factor is found to continuously increase with pressure due to the CO_2 dissolution. However, it immediately starts decreasing after it reaches the maximum pressure

due the appearance of oil component extraction (Tsau et al., 2010). Aforementioned, in the low-pressure range, oil swelling factors increase with pressure due to the CO_2 dissolution. In consequence, the solubility of CO_2 can be calculated or measured in this low-pressure range. CO_2 solubility is the maximum amount of gas that dissolves into oil at reservoir temperature and saturated pressure. It shows that the solubility of CO_2 is proportional to the pressure and oil API gravity, while it is inversely proportional to the temperature. A correction has been developed by Welker (1963) in order to predict the CO_2 solubility using oil composition.

2.4.2 Oil components extraction by CO_2

Several oil components can be selectively extracted by CO_2 after oil swelling since these components are more readily soluble in CO_2 (Holm and Josendal, 1982). The interaction between CO_2 and the crude oil has three stages, CO_2 condensation, extraction-condensation, and extraction (Wang 1986). In the lower pressure range, the oil swells to some extend since CO_2 is condensing into oil (Holm and Josendal, 1982; Tsau et al., 2010). The oil component extraction is observed as the pressure continuously increases further (Tsau et al., 2010). In general, the oil phase swells when the dissolution of CO_2 is dominated in the system (Yang and Gu, 2005). In a higher-pressure range, the oil phase shrinks since some oil components can be extracted by the CO_2. Moreover, CO_2 will have a liquid-like density when the system reaches the critical condition (Lansangan et al., 1987), which will enhance the extraction process (Chaback, 1989).

2.5 Minimum Miscibility Pressure Determination

As aforementioned, miscible displacement will yield a higher recovery factor. In consequence, the MMP prediction and determination are essential for designing a CO_2 EOR. In general, there are

three main methods for MMP determination: experimental method, numerical method, and analytical method.

2.5.1 Experimental method

Slim tube method, interfacial intension vanished technique, and rising bubble apparatus are three main experimental methods used to determine the MMP.

Slim tube method

There was not a standard method available in oil industry to determine the MMP until Yelling and Metcalfe propose the slim tube experiment. Figure 10 demonstrates the equipment setup for this technique. A long stainless-steel tube is used and packed with sand that is saturated with reservoir oil at typical a temperature and pressure. The coil is placed horizontally with a very low dip angle in order to reduce gravity impact on the displacement. CO_2 is injected into the coil at the desirable injection pressure. With this setup, the oil recovery factor is calculated after 1.2 pore volume of CO_2 is injected. Figure 11 shows the recovery factor increases quickly with pressure at beginning (immiscible displacements). However, the recovery factor trend will eventually reach the plateau. The turning point on the curve indicates that the displacement changes from immiscible to miscible, at which the pressure is defined as MMP.

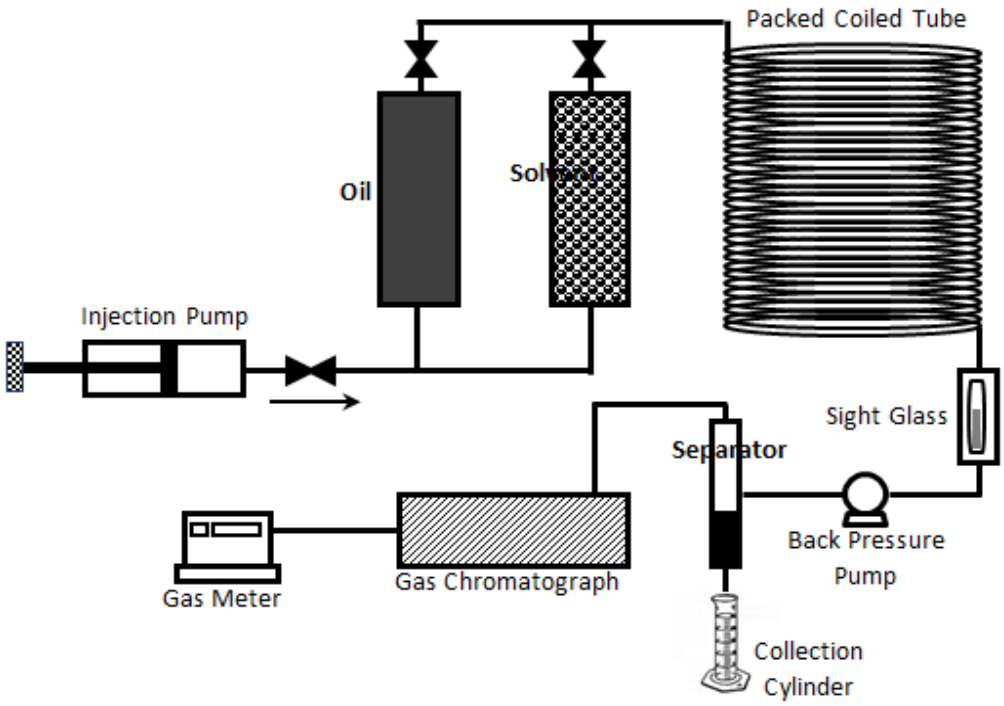

Figure 10 Experimental setup of slim tube experiment for MMP determination (perminc.com)

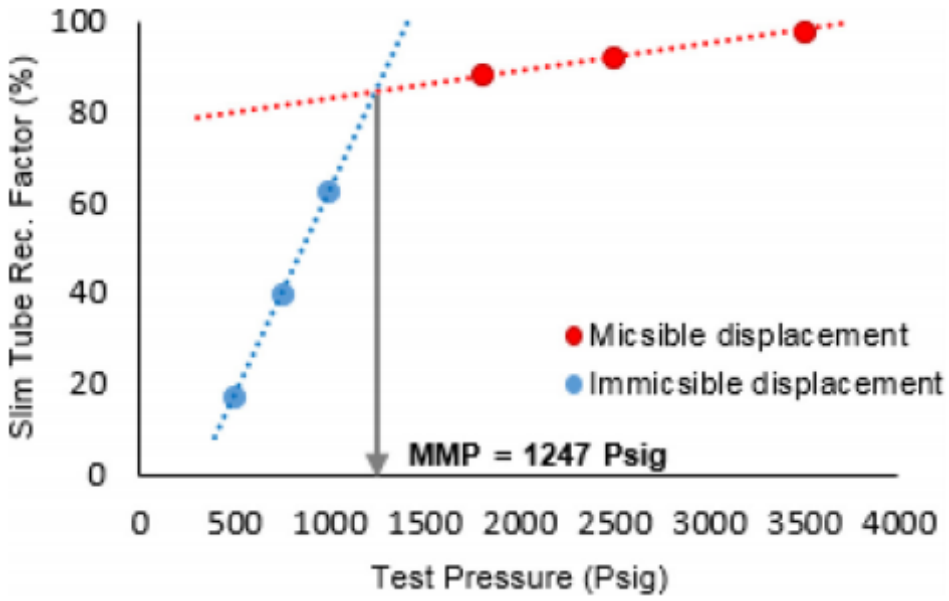

Figure 11 Data interpretation of slim tube experiment for MMP determination (Adel et al. 2016)

With the same idea, many researchers have tried to standardize the parameters for the slim tube method such as coil length, coil diameter, and injection rate. Different experiments have been conducted in different formats (Holm and Josendal, 1974; Flock and Nouar, 1984; Elsharkawy et al., 1992). Moreover, although slim method is time-consuming and expensive, it still is the standard MMP determination method in oil and gas industry

Vanish interfacial tension technique

Vanished interfacial tension (VIT) technique is another experimental method for MMP determination. Figure 12 shows the general setup to conduct this experiment (Zhang and Gu, 2016). In this experiment, the interfacial tension (IFT) across the fluid phase against different injection pressures are measured. The miscibility occurs when the interfacial tension reduces to zero, and the pressure is defined MMP (Figure 13).

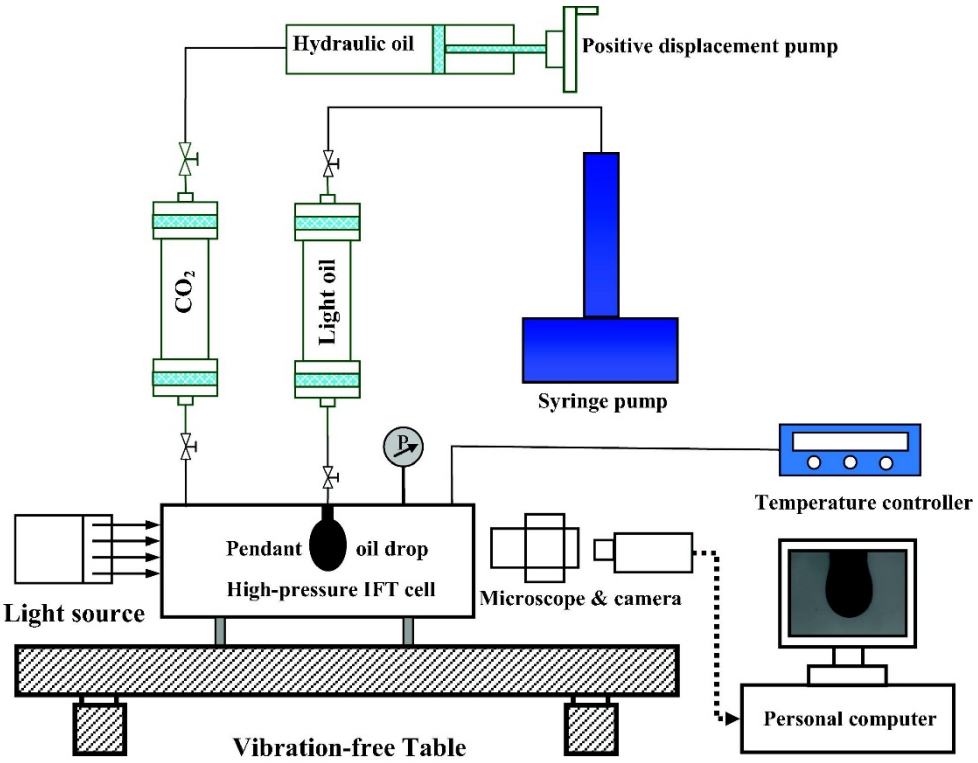

Figure 12 Experimental setup of vanished interfacial tension for MMP determination (Zhang and Gu, 2016)

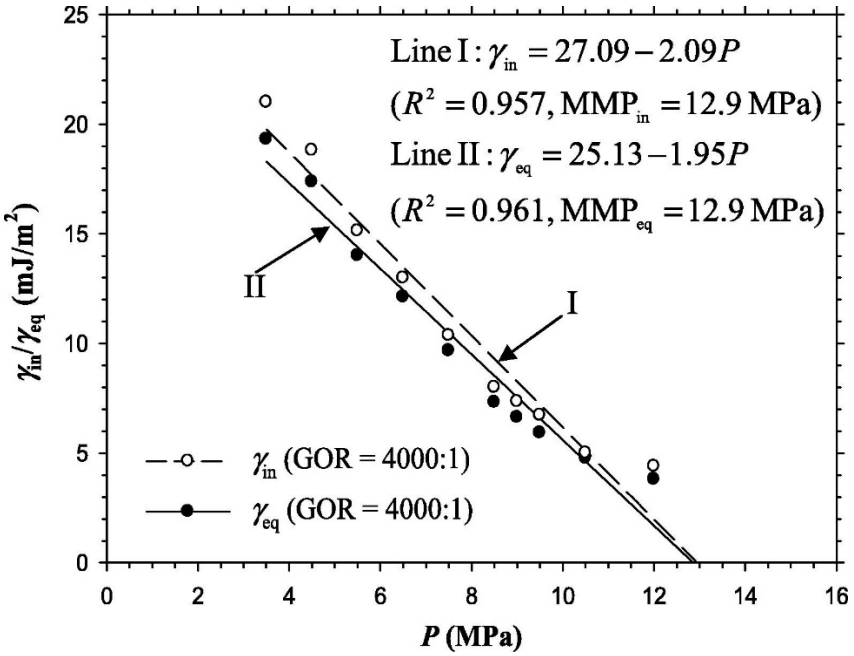

Figure 13 Data interpretation of slim tube experiment for MMP determination (Zhang and Gu, 2016)

Rising bubble technique

Compared to slim tube method and vanished interfacial technique, rising bubble technique is not based on the measurement of recovery factor or interfacial tension. Instead, the determination of MMP of then rising bubble method is based in the direct visual observation (Yin, 2015). Figure 14 shows the general setup for this rising bubble method. The glass tube is initially filled with distilled water. Then, the oil is injected to the glass tube from the top. As a result, the bottom portion of the glass tube is filled with distilled water and the top portion is filled with crude oil. A small bubble of gas is injected into the tube from the needle. Because of the density difference, the gas bubble will rise through the entire water and oil column. The whole rising process and bubble shape will be recorded. The MMP can be visually determined by the shape of the rising bubble.

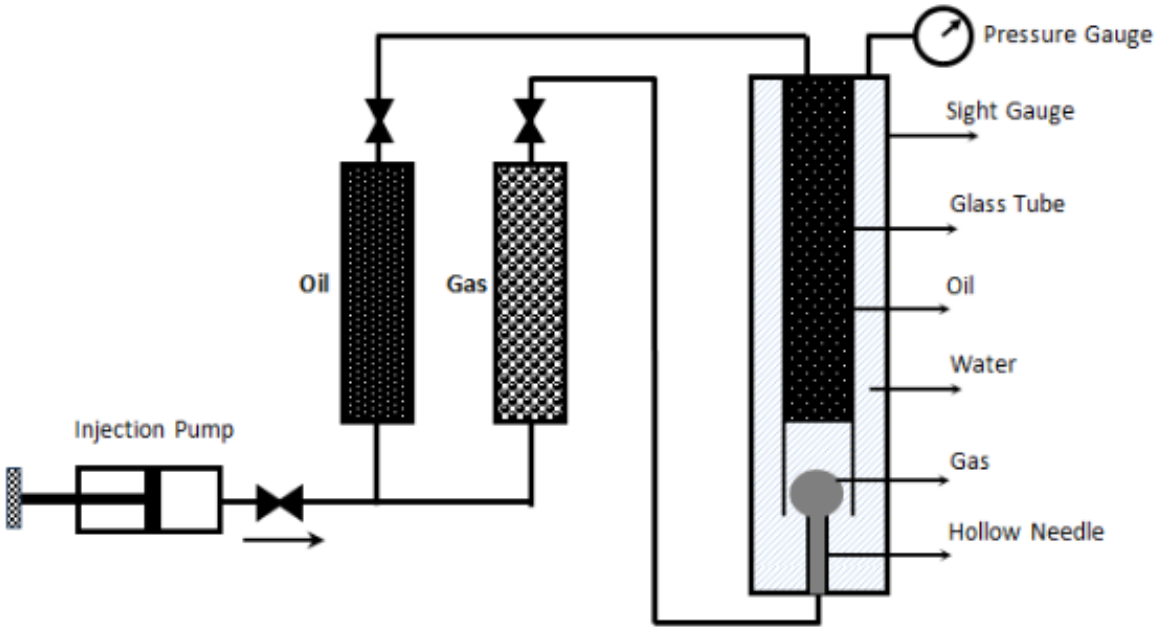

Figure 14 Experimental setup of rising bubble technique for MMP determination (perminc.com)

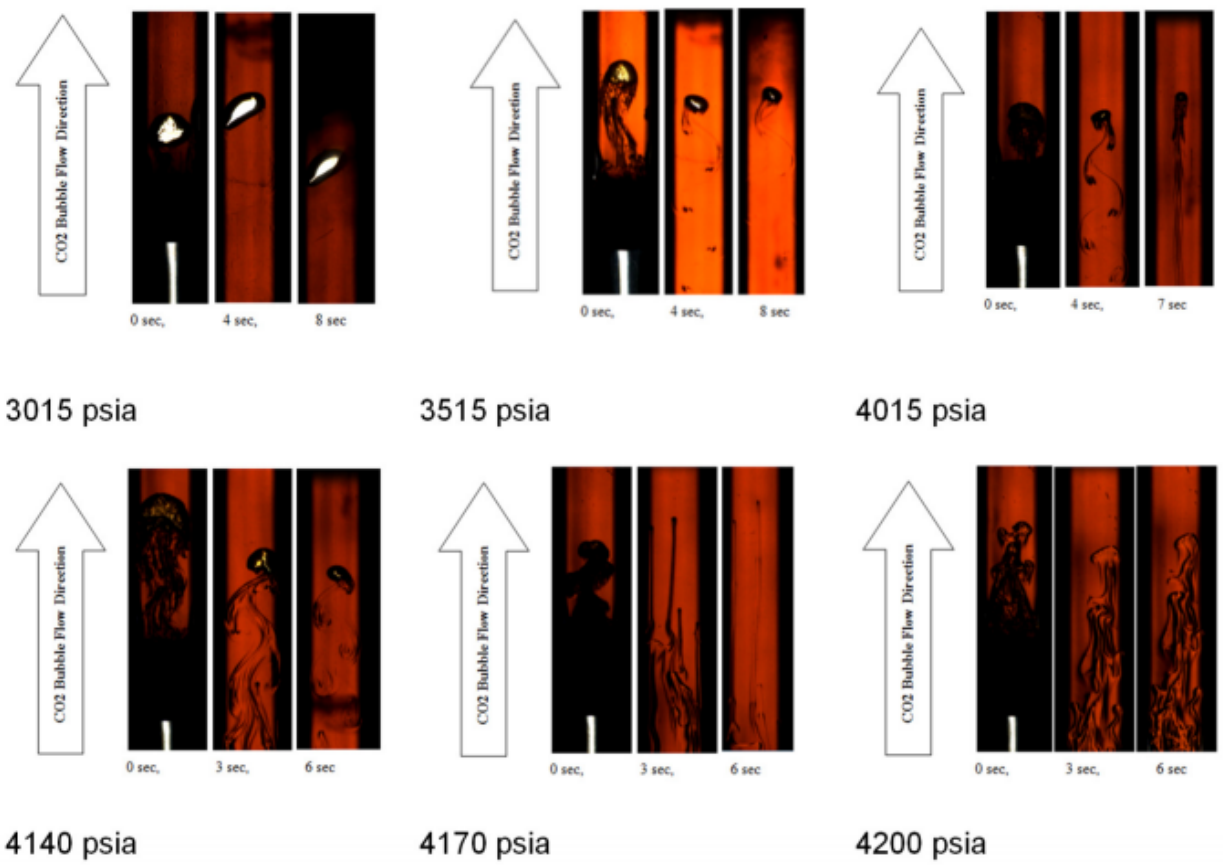

Figure 15 Behaviors of bubbles in rising bubble method at different pressures (Khabibullin et al., 2017)

Figure 15 shows different shapes of bubbles in the rising bubble experiment at different pressures. When the pressure is below the MMP (3515 pisa), the bubble retains the spherical shape during the entire rising process. However, the size of the bubble reduces during the rising process. When the pressure is approaching the MMP (4015 and 4140 psia), the upper part of the bubble remains the same shape. However, the interface in the lower part of the bubble becomes vague. It is hard to distinguish the interface of the lower part of the bubble. When the pressure is at or above the MMP (>= 4200 psia), the bubble will disperse rapidly and disappear in the oil column.

Compared to slim tube method, rising bubble is much more time efficient since it only takes 5 to 30 second for the entire rising process (Yin, 2015). However, the rising bubble technique doesn't completely model the multiple contact mechanisms between gas and oil, and this method needs more quantitative information to support the result.

2.5.2 Numerical method

Numerical computational method is also developed for MMP determination in order to avoid heavy experimental workloads in experimental methods. However, numerical methods require an accurate EOS model to for a reliable prediction.

One dimensional slim tube simulation is an optimization to the slim tube experiment since the experiment is time-consuming and expensive. The 1D slim tube simulation mimics the oil displacement in porous media by using a well-characterized EOS fluid model. In addition, CMG WinProp provides three different numerical methods, which are cell-to-cell simulation, semi-analytical method, and multiple mixing-cell method. Cell-to-cell method is used for MMP determination in this thesis, and the theory will be introduced in Chapter 4.

2.5.3 Analytical method

Holm and Josendal (1974) propose the first MMP correlation based on the reservoir temperature and C_{5+} oil components. Alston et al. (1985) propose a correlation with temperature, oil composition, and averaged weight critical temperature for impure CO_2 (Yin, 2015). Most of these correlations are used for the estimation for MMP used on the regressions of experimental data.

These correlations (Alston correlation and Cronquist correlation) are listed in the following section.

Alston correlation (1985)

The correlation developed by Alston (1985) is based on the experimental result of the slim tube method for pure CO_2, contaminated CO_2, and enriched CO_2 injection gas. Moreover, results for MMP measurements for oil from Alameda, Steelman, and Weyburn reservoirs are used to verify this correlation.

$$MMP_{CO_2} = 0.000878 \times T^{1.06} \times M_{C_{5+}}^{1.78} \times \left(\frac{x_{vol}}{x_{int}}\right)^{0.136} \quad 2.1$$

$$MMP_{imp-CO_2} = MMP_{CO_2} \times F_{imp} \quad 2.2$$

$$F_{imp} = \left(\frac{87.8}{T_{cm}}\right)^{1.935 \times \frac{87.8}{T_{cm}}} \quad 2.3$$

where

MMP_{CO_2} is the MMP for pure CO_2, psi.

MMP_{imp-CO_2} is the MMP for impure CO_2, psi.

T_{cm} is the pseudocritical temperature of weight average mixture, K.

x_{vol} is the mole fraction of volatile oil components.

x_{int} is the mole fraction of intermediate oil components.

T is the reservoir temperature.

Cronquist correlation (1978)

$$MMP_{CO_2} = 16 \times T^{0.744+0.0011M_{C5+}+0.0015x_{vol}} \quad 2.4$$

where

T is the reservoir temperature.

M_{C5+} is the molecular weight of heavy oil components.

x_{vol} is the mole fraction of volatile oil components.

Sebastian correlation (1985)

The correlation is developed to determine the MMP for impure CO_2 based on the mole fraction mixing rule. The correlation is shown as follows,

$$MMP_{imp-CO_2} = MMP_{CO_2} \times [1.0 - 2.13 \times 10^{-2}(T_c - 304.2) + 2.51 \times 10^{-4}(T_c - 304.2)^2 - 2.35 \times 10^{-4}(T_c - 304.2)^3] \quad 2.5$$

$$T_c = \sum_{i=1}^{n} x_i \times T_{ci} \quad 2.6$$

where

T_c is the mole fraction average pseudocritical temperature, K.

T_{ci} is the critical temperature of the *i*th gas component, K.

CHAPTER 3 PHASE BEHAVIOR EXPERIMENTS

The experiments are designed to visualize the interactions between CO_2 and the crude oil phase compared to traditional phase behavior experiments. The visualization helps understand CO_2 EOR mechanisms at real reservoir conditions. The goals of phase behavior experiments are listed as follows:

1. Calculate the oil swelling factor at different equilibrium pressures.
2. Calculate CO_2 solubilities in the swelling factor increasing region at different equilibrium pressures.
3. Visualize different types of phase behaviors at different equilibrium pressures and temperatures.
4. Determine phase boundaries that separate different phase behaviors.
5. Determine the extraction pressure and the pressure that leads to a zero-swelling factor.

The experimental materials, experimental setups, calculation formulas, and experimental procedures will be introduced in following sections.

3.1 Experimental Materials

The oil used in this study is a crude oil sample collected from the Bakken oilfield. Table 1 shows the compositional analysis of the oil sample. It lists the crude oil component distribution in both molar fraction and weight fraction. Figure 16 plots the distribution of each carbon numbers in mole fractions and weight fractions, and Figure 17 shows the oil components C_1-C_9, C_{10}-C_{19}, C_{20}-C_{29}, and C_{30+} in molar percentages are 33.74, 35.17, 16.15%, and 14.89%, respectively. These two figures show that the major components of this Bakken oil sample are light and intermediate oil components (~70%). CO_2 used in this work has the purity of 99.999% (Matheson, USA).

Table 1 Weight fraction and molar fraction for each component of the Bakken crude oil

Symbol	wt%	mol%	Symbol	wt%	mol%
N_2	0.039	0.008	C_{14}	2.534	3.566
CO_2	0.086	0.028	C_{15}	2.159	3.295
C_1	3.205	0.381	C_{16}	1.872	3.078
C_2	7.036	1.567	C_{17}	1.516	2.661
C_3	9.321	3.044	C_{18}	1.395	2.593
iC_4	1.629	0.701	C_{19}	1.259	2.451
nC_4	7.09	3.052	C_{20}	1.115	2.272
iC_5	2.201	1.176	C_{21}	1.001	2.158
nC_5	4.843	2.588	C_{22}	0.77	1.74
C_6	5.904	3.769	C_{23}	0.738	1.739
C_7	8.028	5.656	C_{24}	0.665	1.629
C_8	8.135	6.598	C_{25}	0.596	1.524
C_9	5.724	5.21	C_{26}	0.512	1.362
C_{10}	5.164	5.126	C_{27}	0.515	1.428
C_{11}	3.98	4.333	C_{28}	0.43	1.235
C_{12}	3.331	3.972	C_{29}	0.358	1.065
C_{13}	3.161	4.097	C_{30+}	3.689	14.899

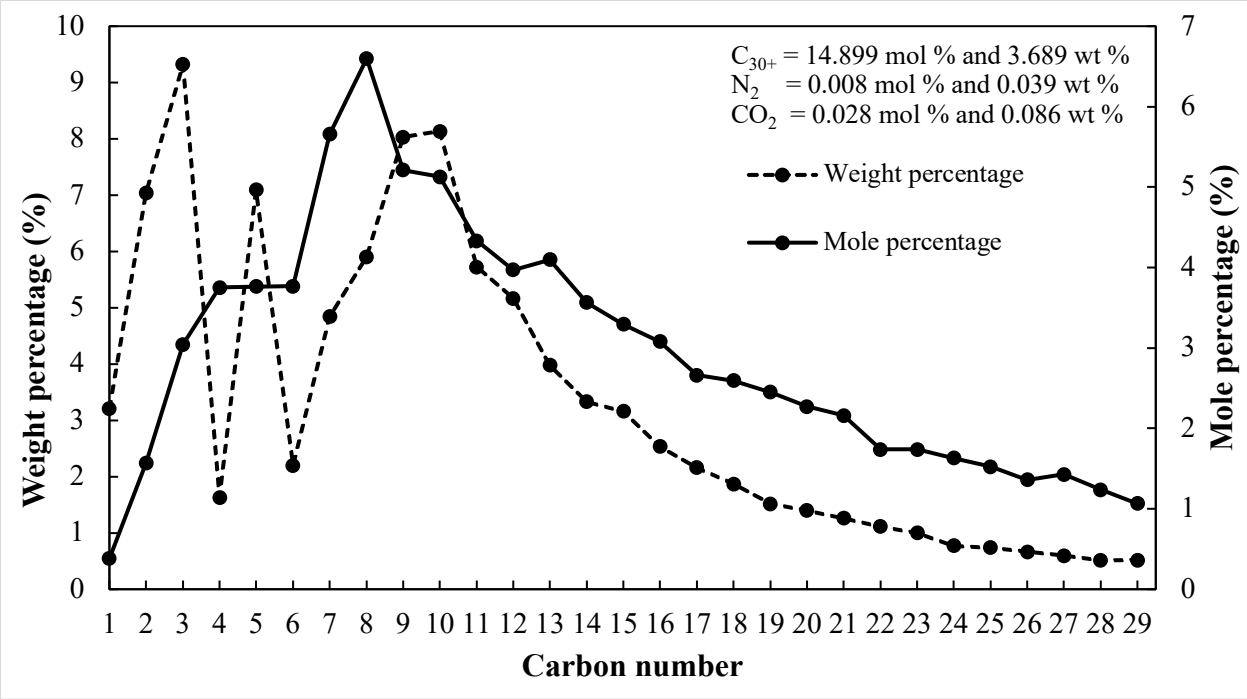

Figure 16 Oil components distribution of the Bakken crude oil

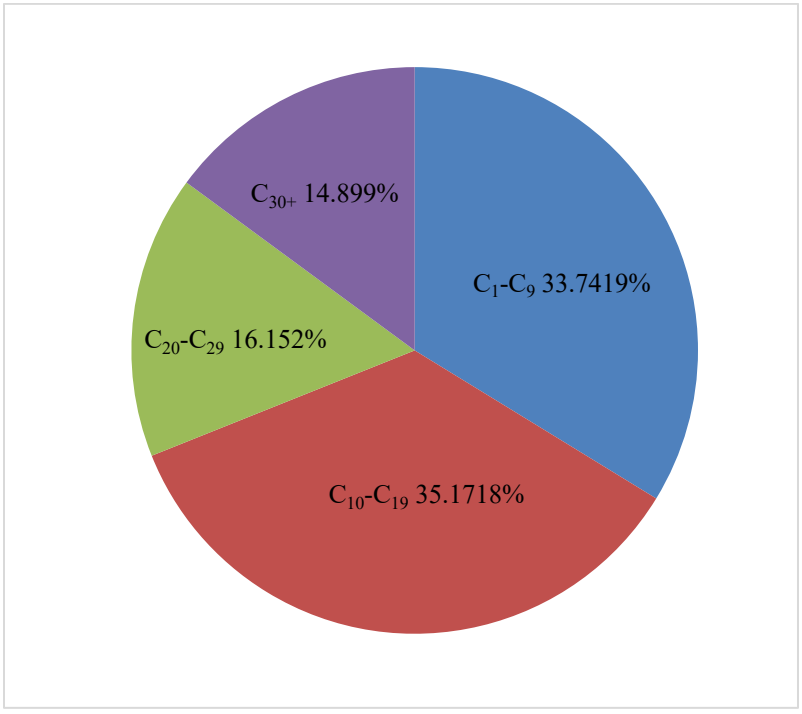

Figure 17 Molar fraction distribution for each oil component group

3.2 Experimental Setup

All phase behavior experiments for the CO_2 and Bakken crude oil system are performed in a piston-equipped pressure-volume-temperature (PVT) equipment. There are three major components in this equipment, which are the high-pressure and high-temperature PVT cell (PVT 300/700 FV, Core Lab), temperature-controlled system (Pilot One Controller, Huber, Germany), and the built-in software (Faclon and Euclide) for equipment monitoring and data acquisition.

3.2.1 PVT cell

In this study, the Core Lab PVT 300/700 FV (PVT Cell 300 ml 700 bar Full Visibility) is used for the phase behavior experiment (Figure 18). This PVT cell has an inner diameter of 5.000 cm and a total length of 15.279 cm. It can sustain the pressure up to 10150.0 psi with the temperature ranging from -10 to 180 °C. In addition, a built-in stirrer is equipped within this PVT cell for sufficiently mixing purpose. The rotation rate of this stirrer can be adjusted to desirable value by the stirrer monitor. Moreover, the cell pressure can be adjusted by moving the built-in piston forwards or backwards. The highlighted feature of this PVT cell is the transparent sapphire visual screen and the in-situ digital camera with the resolution of 6M pixels, which enables to visualize interactions and phase behaviors between the CO_2 and the Bakken crude oil at designed pressures and temperatures.

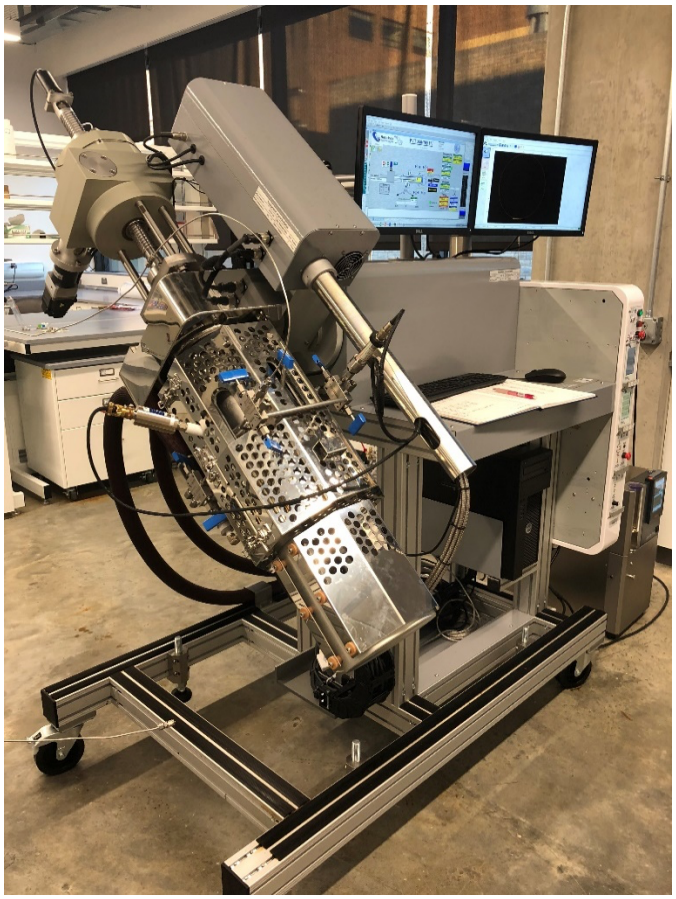

Figure 18 PVT cell (Core Lab PVT 300/700 FV EDU)

3.2.2 Temperature-controlled system

Series of phase behavior experiments are performed at different desirable temperatures (27, 80, and 120 °C). A bath is required in order to keep the PVT cell in a stable temperature environment. In this thesis, the temperature of different experiments is controlled by an automatic oil bath (Huber Grande Fleur dynamic temperature control system). This oil bath has a temperature ranges from -40 to 200 °C with the accuracy of ± 0.01 °C.

Figure 19 Automatic oil bath (Huber Grande Fleur Dynamic Temperature Control System)

3.2.3 Falcon and Eculide software

The Falcon software is connected to the PVT cell and the oil bath. The user interface of this software is shown in Figure 20. Key parameters in this phase behavior experiment such as pressure, volume, and temperature can be automatically measured and recorded by this software. Moreover, the experimental pressure and temperature can be adjusted by adjusting the cell piston and the oil bath through the user interface.

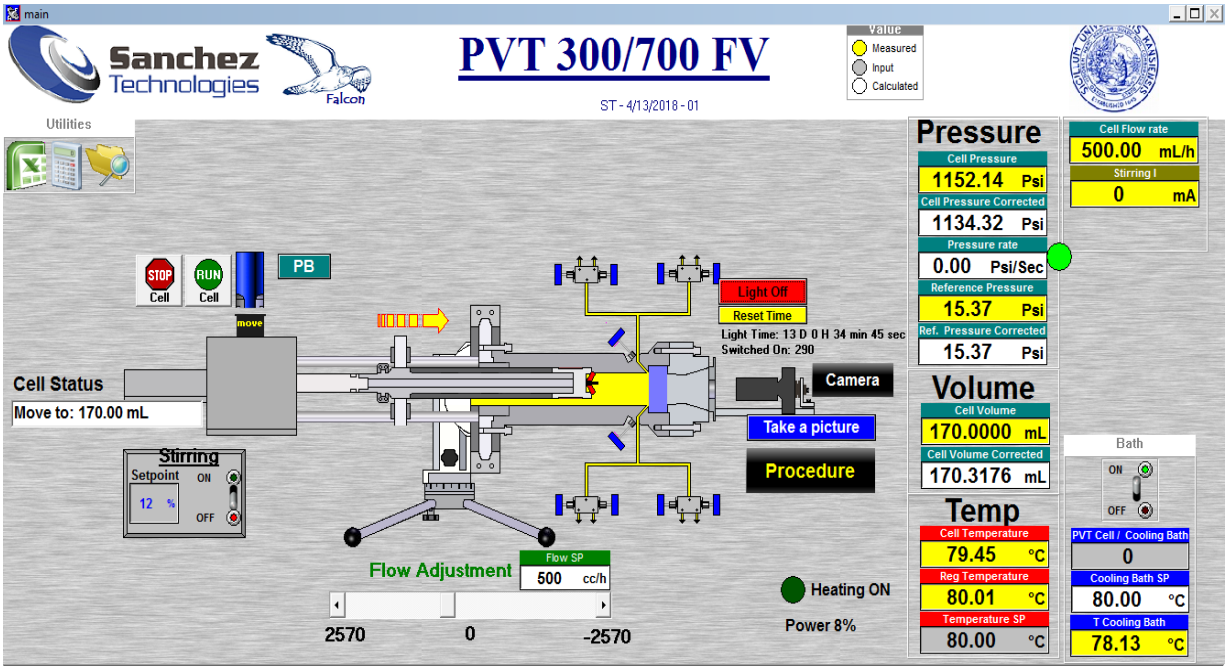

Figure 20 Falcon software user interface

The visualization of the interaction between CO_2 and the Bakken crude oil is the one of the main objectives in this study. This propose is achieved by connecting the in-situ camera with the Euclide software. Figure 21 shows user interface of this software. The phase behavior at the desirable pressure and temperature is directly shown in the interface. In addition, this software enables to automatically measure the volume of the oil phase by matching the yellow line with the interface between two phases.

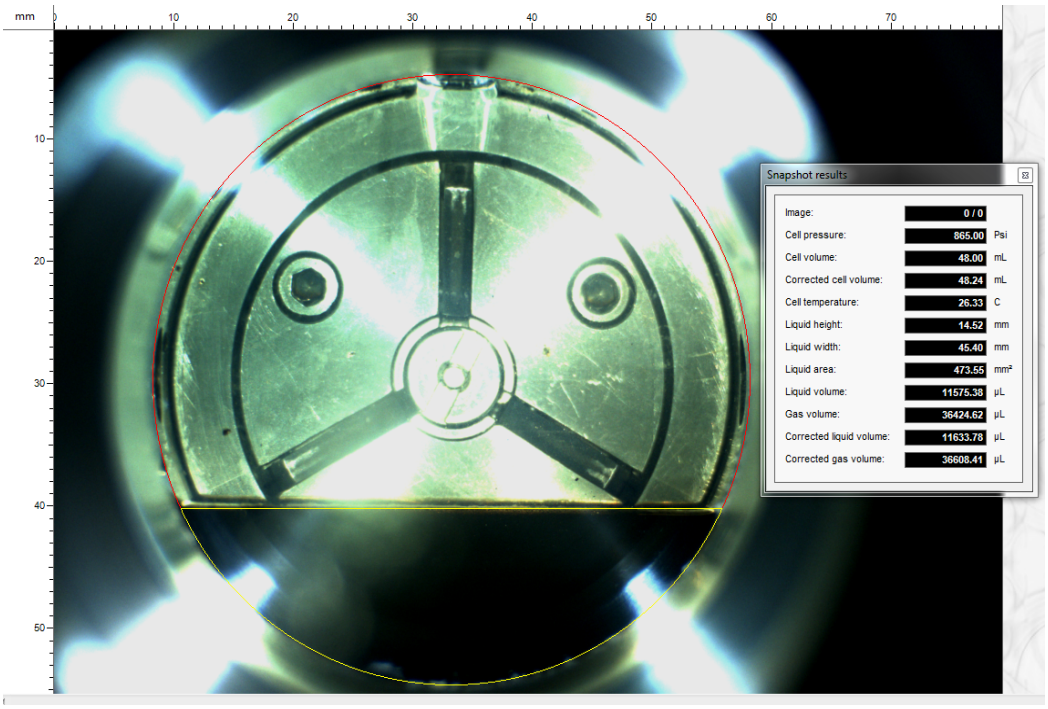

Figure 21 Euclide software user interface

3.2.4 Experimental setups

In the phase behavior experiment, four different experiments with different system temperatures (27, 80, and 120 °C) and different CO_2 and Bakken crude oil ratio are listed in Table 2. Figure 22 shows the schematic diagram for the experiment.

Table 2 Experimental design

Experiment No.	Composition, mol %		Composition, wt%		Temperature, °C
	CO_2	Oil	CO_2	Oil	
1	91.39	8.61	86.79	13.21	27
2	91.39	8.61	86.79	13.21	80
3	91.39	8.61	86.79	13.21	120
4	84.58	15.42	77.25	22.75	120

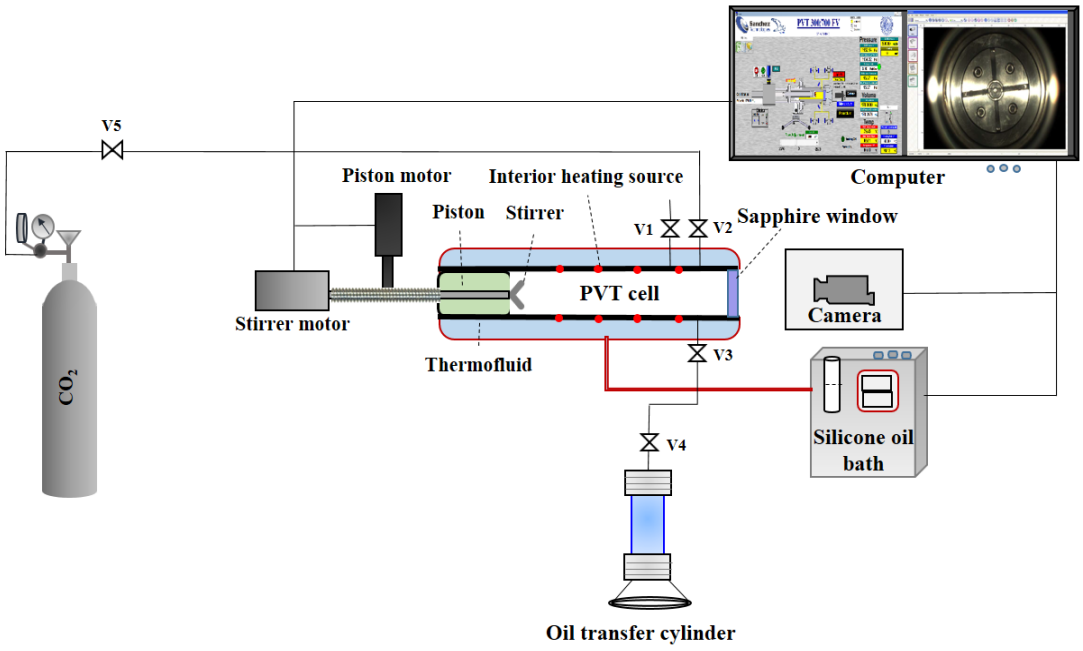

Figure 22 Experimental setups for the phase behavior experiment

3.3 CO_2 Solubility and Swelling Factor Determination

Both CO_2 solubility and oil swelling factor will be determined during the phase behavior experiment. In the relative low-pressure range, the dissolution of CO_2 into the Bakken crude oil

will result in oil swelling. In this region, it is found that the swelling factor increases with pressure until the pressure reaches a maximum value (Tsau et al., 2010). CO_2 solubility can be determined in this swelling increasing region. In this region, the CO_2 dissolution is assumed to be the only interaction between CO_2 and Bakken crude oil. In consequence, the CO_2 solubility can be calculated using the following equation:

$$S = \frac{N_{CO_2}}{N_{oil}+N_{CO_2}} \tag{3.1}$$

where

S is the CO_2 solubility.

N_{oil} is the molar number of the injected Bakken oil.

N_{CO_2} is the molar number of dissolved CO_2 in the oil.

The molar number of dissolved CO2 in the crude oil can be determined using the following equation:

$$N_{CO_2} = N_{injCO_2} - N_{undisCO_2} \tag{3.2}$$

where

N_{injCO_2} is the molar number of injected CO_2.

$N_{undisCO_2}$ is the molar number of undissolved CO_2 in the gas phase at different equilibrium pressures.

N_{injCO_2} and $N_{undisCO_2}$ can be calculated using the following equation:

$$N_{injCO_2} = \frac{PV_{CO_2}}{ZRT} \tag{3.3}$$

$$N_{undisCO_2} = \frac{\rho_{CO_2} V_{undisCO_2}}{M_{CO_2}} \tag{3.4}$$

where

V_{CO_2} is the volume of gas after CO_2 injection.

$V_{undisCO_2}$ is the undissolved CO_2 at equilibrium pressures.

P is the system pressure after CO_2 injection.

Z is the CO_2 compressibility value.

T is the system pressure after CO_2 injection.

R is the universal gas constant.

ρ_{CO_2} is the CO_2 density at equilibrium pressures and system temperature.

M_{CO_2} is the molecular weight of CO_2 (44.01 g/mol).

In this study, excessive CO_2 is injected into the PVT cell, which indicates the CO_2 gas phase cannot entirely dissolve into the oil phase. The swelling factor is calculated using the following equation:

$$SF = \frac{V_p}{V_{atmo}} \tag{3.5}$$

where

SF is the swelling factor.

V_P is the volume of expanded/shrunken oil at each equilibrium pressure.

V_{atmo} is the volume of originally injected oil at atmospherically conditions.

3.4 Experimental Procedures

The procedures for a typical phase behavior experiment is shown briefly introduced as follows:

1. The PVT cell is firstly cleaned by kerosene and toluene. Then, the cell is under gas flash in order to get rid of the excessive cleaning fluid. Open valve v1, v2 and v3 and move the piston forward to until the piston cannot be moved forward anymore in order to discharge excessive air out of the PVT cell. Then, close v1, v2 and v3.
2. Oil transfer cylinder is filled with Bakken crude oil. Open valve v3, v4 and close valve v1, v2. Move piston backwards in order to charge Bakken oil into the PVT cell. After desirable amount of oil is injected into the PVT cell, the piston is stopped. The volume of injected oil is measured by the moving the yellow line in Euclide software.
3. After oil injection, close v3, v4. Open v2 and v5. Adjust the CO_2 regulator to increase the regulator pressure step by step until the PVT cell pressure reaches the desirable pressure. In this step, the molar amount of injected CO_2 (N_{injCO_2}) can be calculated.
4. After CO_2 injection, move piston backwards until the PVT cell reaches the maximum volume. Turn on the oil bath and set the bath temperature to the pre-designed temperature. Wait until the temperature stabilizes.
5. Move the piston forward step by step in order to increase the system pressure. In addition, turn on the stirrer for a sufficient mixing.
6. Wait until the system pressure stabilizes. The stabilized pressure is defined as equilibrium pressure. The oil phase volume is determined by Euclide for swelling factor calculation (Equation 3.5). In addition, the phase behavior of this CO_2 and oil system can also be recorded at this equilibrium pressure.
7. If there is distinct interface between different phases, repeat step 5 and 6 until the distinct interface disappear.

The following flowchart summaries the steps of the PVT experiment.

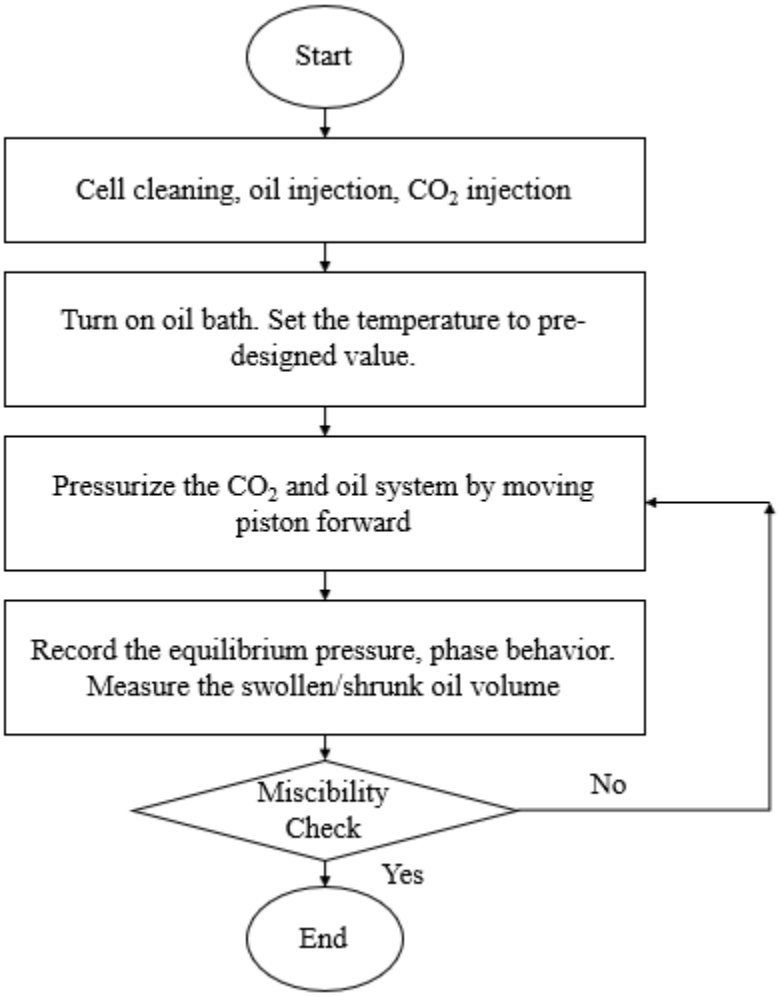

Figure 23 General procedures in the phase behavior experiment

CHAPTER 4 THEORY AND SIMULATION

In this thesis, simulation studies are performed using CMG WinProp in order to get an accurate EOS model. Cell-to-cell simulation for multi-contact MMP determination is then performed by CMG WinProp after the accurate EOS model is obtained. In this chapter, theories about EOS model, oil characterization, flash calculation in CMG WinProp, cell-to-cell simulation and other parameters calculated by CMG WinProp (swelling factor, interfacial tension) are introduced.

4.1. Equation of State

The equilibrium pressure is defined as the pressure at which the oil phase is at equilibrium with the injected gas. Intuitively, the equilibrium pressure is the pressure at which the gas-oil system is stabilized. Moreover, the equilibrium pressure of a gas-oil system can be determined by EOS function, which describes the relation between pressure, temperature, and molar volume of a single components or a mixed system. Peng-Robinson EOS function (PR-EOS) is widely used to demonstrate phase behaviors and interactions between oil and gas. RP-EOS is expressed as follows:

$$P = \frac{RT}{v - b} - \frac{a}{v + 2vb - b^2} \tag{4.1}$$

For a single-component system, the parameter a and b can determined by following equations:

$$a = a_c \alpha(T_r, \omega) \tag{4.2}$$

$$a_c = \frac{0.457235 R^2 T_c^2}{P_c} \tag{4.3}$$

$$b = \frac{0.0777969RT_c}{P_c} \tag{4.4}$$

where

$\alpha(T_r, \omega)$ is the alpha function that is based on the reduced temperature T_r and acentric factor ω.

R is the universal gas constant.

v is the molar volume.

T is the temperature.

For a multiple-component system, the parameter a and b can determined by the using van der Waals mixing rule:

$$a = \sum_{i=1}^{nc}\sum_{j=1}^{nc} x_i x_j (1 - \delta_{ij})\sqrt{a_i a_j} \tag{4.5}$$

$$b = \sum_{i=1}^{nc} x_i b_i \tag{4.6}$$

where

nc is the number of components in this multiple-component system.

x_i is the mole fraction of the *i*th component in this system.

x_j is the mole fraction of the *j*th component in this system.

a_i and b_i are the constant for the *i*th component in this system that can be calculated from Equation 4.2 and Equation 4.4.

a_j and b_j are the constant for *j*th component in this system that can be calculated from Equation 4.2 and Equation 4.4.

δ_{ij} is the binary interaction parameter (BIP) between *i*th and *j*th component.

The application of EOS is relatively straightforward for a single-component system. However, a variety of components in a typical oil sample make the application of EOS impractical. In consequence, the oil characterization process is required when using EOS model in the simulation study.

4.2 Oil Characterization

In this thesis, CMG WinProp is used to obtain the accurate EOS model. For each oil component, WinProp requires parameters such as critical pressure *(*P_c), critical temperature (T_c), acentric factor (ω), molecular weight (M), and binary interaction parameter (δ_{ij}) for each oil components. In addition, volume shift (τ), equation of state parameter Ω_a and Ω_b can also be modified to get a precise EOS model. The determination for these parameters will be discussed in this section.

4.2.1 Oil components properties

Properties for each oil component such as critical temperature, critical pressure, molecular weight, specific gravity, and acentric factor are required for simulations. In this thesis, these properties for each oil component are directly obtained from the CMG WinProp library. According to the CMG manual, properties for the first 20 oil components in the library are obtained from Reid et al. (1977). critical properties of others oil components are calculated by Kesler and Lee correlation (1976) using the average normal boiling point and specific gravity.

Specific gravity of each oil component can be calculated by the following equation:

$$\gamma = 6.0108 M^{0.17947} {K_w}^{-1.18241} \tag{4.7}$$

for oil component of C_{42+},

$$\gamma = \frac{zM}{\sum_{i=1}^{N}(z_i M_i/\gamma_i)} \tag{4.8}$$

where

K_w is the Watson factor.

z_i is the molar fraction of the *i*th oil component.

M_i is the molecular weight of the *i*th oil component.

γ_i is the specific gravity of the *i*th oil component.

Boiling temperature (T_b) is calculated by the Soreide correction (1989)

$$T_b = 1928.3 - (1.695 \times 10^5)M^{-0.03522}\gamma^{3.266} \times exp\,[-(4.922 \times 10^{-3})M - 4.7685\gamma + (3.462 \times 10^{-3})M\gamma \tag{4.9}$$

Critical temperature, critical pressure, and acentric factor are determined by these following equations:

$$T_c = 341.7 + 811\gamma + (0.4244 + 0.1174\gamma)T_b + (0.4669 - 3.2623\gamma) \times 10^5 T_b^{-1} \tag{4.10}$$

$$P_c = exp\{8.3634 - 0.0566\gamma^{-1} - [(0.24244 + 2.898\gamma^{-1}) + 0.118857\gamma^{-2}) \times 10^{-3}]\,T_b + [(1.4685 + 3.648\gamma^{-1} + 0.47227\gamma^{-2}) \times 10^{-7}]T_b^2 - [(0.42019 + 1.6977\gamma^{-2}) \times 10^{-10}]T_b^3\} \tag{4.11}$$

if $T_b/T_c < 0.8$,

$$\omega = \frac{-ln\left(\frac{P_c}{14.7}\right) - 5.92714 + 6.09648T_b^{-1} + 1.28862lnT_b + -0.169347lnT_b^6}{15.2518 + 15.6875T_b^{-1} - 13.4721lnT_b + 0.43577lnT_b^6} \quad (4.12)$$

if $T_b/T_c > 0.8$

$$\omega = -7.904 + 0.1352K_w - 0.007456K_w^2 + 8.359T_b + (1.408 - 0.01063K_w)T_b^{-1} \quad (4.13)$$

4.2.2 Binary interaction coefficient

The interaction coefficient between different oil components is calculated by the following equation:

$$\delta_{ij} = 1 - \left(\frac{2v_{ci}^{1/6}v_{cj}^{1/6}}{v_{ci}^{1/3} + v_{cj}^{1/3}}\right)^{\beta} \quad (4.14)$$

where

v_{ci} is the critical volume of the *i*th component.

v_{cj} is the critical volume of the *j*th component.

β is the hydrocarbon interaction coefficient exponent constant.

It is found that the $\beta = 1.2$ that is recommend by Oellrich et al (1981) provides a good match.

3.2.3 Lumping

There are various types of oil components in a certain oil sample, which will result in different parameters. A larger number of parameters will make the simulation and tuning process

impracticable. Hence, it is every essential to lump different types of oil components into groups and represent this oil sample using multiple pseudo-components. A appropriate lumping method can decrease the simulation time and make the property of this lumped system similar to the original oil (Al-Meshari, 2005). The Hong's mixing rule is widely used to calculate properties for each pseudo-component,

$$\eta_j = \frac{\sum_{i=l}^{u} z_i M_i \eta_i}{\sum_{i=j}^{u} z_i M_i} \tag{4.15}$$

where

η_j express any property (T_b, T_c, P_c, v_c, Z_{RA}, M, γ and ω) of the *j*th pseudo-component.

z_i is the mole fraction of the *i*th oil component

$M_i$is the molecular weight of the *i*th oil component.

4.3 Flash Calculation

Flash calculations are used to split a mixed system into different phases at a certain pressure, temperature, and composition. A typical flash calculation will provide the following results (Pedersen and Christensen, 2007):

1. Number of phases.
2. Molar amounts of each phase.
3. Molar composition of each phase.

In this thesis, two types of flash calculation (vapor-liquid, vapor-liquid-liquid) are applied for CO_2 and Bakken light oil system at given temperatures and pressure.

4.3.1 Two-phase flash calculation

In CMG WinProp, two-phase flash calculation requires the solution from the equilibrium equation and material balance equation. The equilibrium equation is shown as follows:

$$G_i \equiv \ln K_{iv} - \ln \phi_i (x^L) - \ln \phi_i (x^V) = 0 \tag{4.16}$$

The material balance equation is shown as follows:

$$G_N \equiv \sum_k \frac{Z_k(K_k - 1)}{1 + F_v(K_k - 1)} = 0 \tag{4.17}$$

where

Z is the composition of the feed.

F_v is the molar fraction of the vapor phase.

Z and F_v satisfy the following correction:

$$x_i^L = \frac{Z_i}{\{1 + F_v(K_i - 1)\}} \tag{4.18}$$

When the F_v is within the value range from 0 to 1, it means there are two equilibrium phases in this system. A negative value means the system is stable at this pressure and temperature. For the two-phase calculation, the equilibrium equation is solved using the quasi-Newton successive substitution (QNSS) method. In this method, for each variable $\ln K_i$ for each component, the initial guess is determined by the Wilson's correction:

$$\ln K_i = 5.37(1 + \omega_i)\left(1 - \frac{T_{ci}}{T}\right) + \ln(\frac{P_{ci}}{P}) \tag{4.19}$$

A single-phase detection method is used to solve the material balance equation:

$$f_o = \sum_k z_k K_k \tag{4.20}$$

$$f_l = \sum_k \frac{z_k}{K_k} \tag{4.21}$$

$f_o < 1$ indicates there is a single liquid system, and $f_l < 1$ indicates there is a single vapor system. Figure 24 summarizes the steps for a typical two-phase flash calculation. At the beginning, the material balance equation for the vapor phase is solved to calculate F_v, which is used to determine if the system is two-phase or single-phase. If there is a two-phase system, WinProp use the QNSS method to solve the equilibrium equation by updating variable *K* until converges. If there is a single-phase system, Equations 4.20 and 4.21 are used to determine if it is a single-vapor phase or a single-liquid phase.

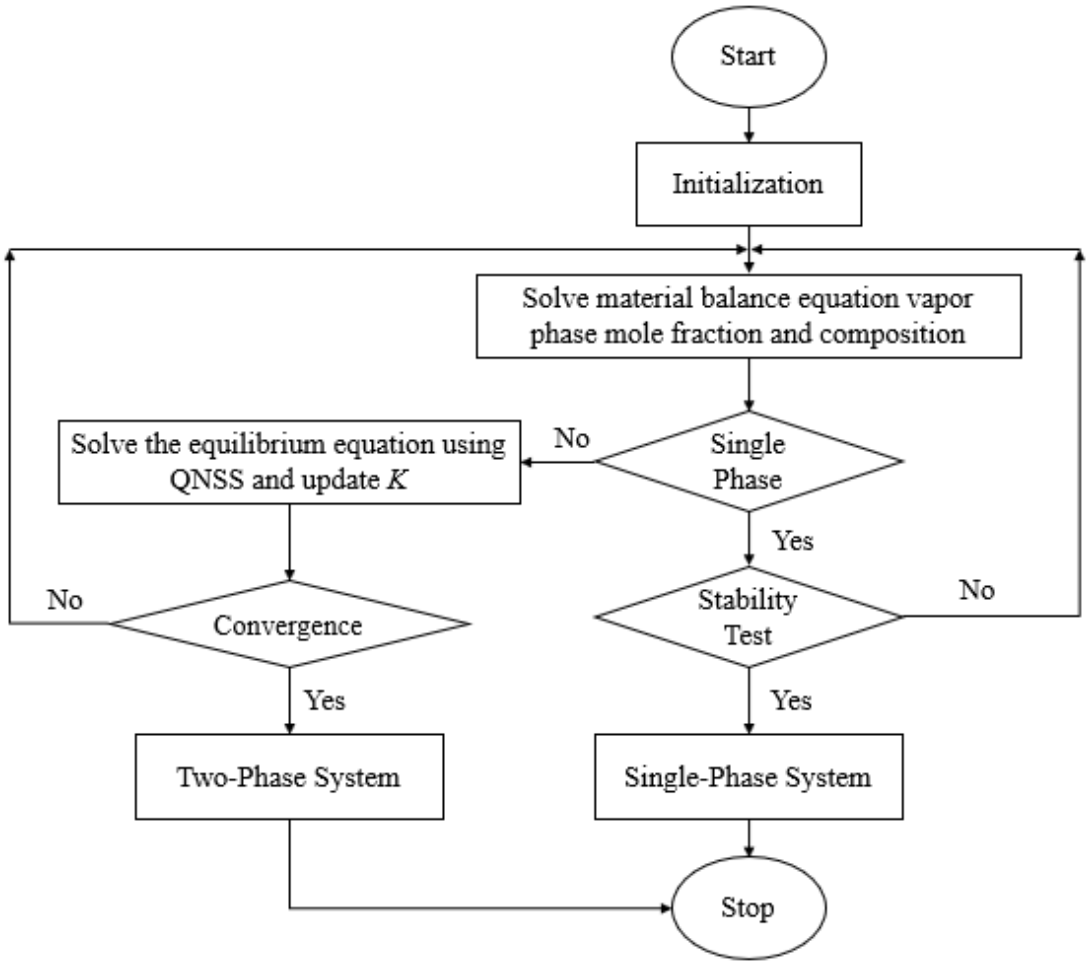

Figure 24 Flowchart of two-phase flash calculation in CMG WinProp (CMG, 2017)

4.3.2 Three-phase flash calculation

For a three-phase (liquid-liquid-vapor) system, the concept of flash calculation is similar to two-phase flash calculation. The governing equilibrium equations are shown as follows:

$$\ln K_{iv} + \ln \phi_i^V - \ln \phi_i^L = 0 \tag{4.22}$$

$$\ln K_{iq} + \ln \phi_i^Q - \ln \phi_i^L = 0 \tag{4.23}$$

where

$$K_{iv} = \frac{x_i^V}{x_i^L} \tag{4.24}$$

$$K_{iq} = \frac{x_i^Q}{x_i^L} \tag{4.25}$$

Material balance equations for the three-phase system are shown as follows:

$$\sum_{i=1}^{nc}(x_i^V - x_i^L) = \sum_{i=1}^{nc}\frac{(K_{iv}-1)Z_i}{F_l + F_v K_{iv} + F_q K_{iq}} \tag{4.26}$$

$$\sum_{i=1}^{nc}(x_i^Q - x_i^L) = \sum_{i=1}^{nc}\frac{(K_{iq}-1)Z_i}{F_l + F_v K_{iv} + F_q K_{iq}} \tag{4.27}$$

$$F_l + F_v + F_q = 1 \tag{4.28}$$

where

F_l is the molar fraction of the first liquid phase.

F_q is the molar fraction of the second liquid phase.

F_v is the molar fraction of the vapor phase.

Similar to the two-phase flash calculation the primary variables are $\ln K_{iv}$, $\ln K_{iq}$, F_l, F_v, and F_q. The mole fractions are determined by these primary variables.

$$x_i^m = \frac{K_{im}Z_i}{K_{im}F_v + K_{il}F_l + K_{iq}F_{iq}} \tag{4.29}$$

In three-phase flash calculation, a two-phase flash calculation is firstly performed. The initial properties guess for the third liquid is obtained from a stability test. Then, the QNSS method is performed to solve the equilibrium equation and update *K* value until the calculation is convergent (Figure 25).

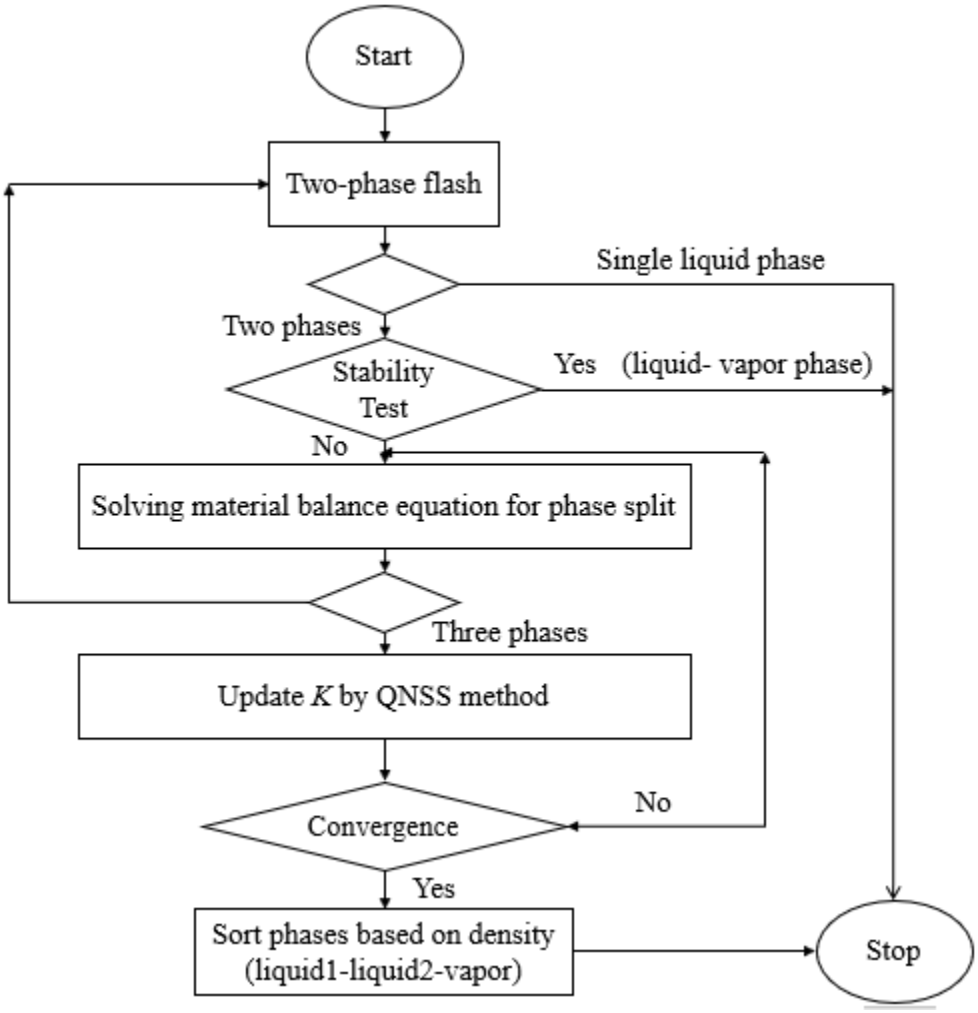

Figure 25 Flowchart of three-phase flash calculation in CMG WinProp (CMG, 2017)

4.4 Oil Swelling Factor

Oil swelling factor describes the swelling effect and it is defined as the ratio of the oil phase at a given pressure to its initial volume at atmospheric condition.

In this thesis, there are two major scenarios that require different equation for the oil swelling factor calculation:

1. The CO_2 dissolution is the only process happening in the CO_2 and crude oil system.
2. The CO_2 dissolution process and the light oil component extraction process are both happening in this CO_2 and crude oil system at the same time.

In the low-pressure region, the CO_2 dissolution is the dominant interaction mechanism between CO_2 and crude oil. In consequence, it is safe to assume that the extraction process of oil components is negligible. In this region, the oil swelling factor can be determined by the following equation:

$$SF = \frac{V_2}{V_1(1-S)} \tag{4.30}$$

where

V_1 is the molar volume of the crude oil at saturation temperature and atmospheric pressure.

V_2 is the molar volume of the CO_2-satruated crude oil at saturation temperature and pressure.

S is the CO_2 solubility in molar fraction.

When the system pressure increases furthermore, there will be a three-phase region. The interactions between CO_2 and oil are the CO_2 dissolution process and the oil component extraction process. In this region, the swelling factor can be calculated by the following equation:

$$SF = \frac{AN_{tot}V_2}{N_{oil}V_1} \tag{4.31}$$

where

A is the mole percentage of the oil phase in this CO_2 and crude oil system at saturation pressure and temperature.

N_{tot} is the total molar number of this CO_2 and crude oil system.

N_{oil} is the total molar number of crude oil system in this system.

4.5 Interfacial Tension

Interfacial tension between different phases is also calculated in flash calculation by WinProp. The general equation for the interfacial tension can be estimated by the following equation.

$$\sigma^{\frac{1}{4}} = p_{ar}(\rho_1 - \rho_2) \tag{4.32}$$

where

σ is the interfacial tension between phase1 and phase2, dyne/cm.

ρ is the molar density of phase1 or phase2, mol/cm^3.

p_{ar} is the parachor parameter.

In a multi-component system, the interfacial tension is determined by the following equation:

$$\sigma^{\frac{1}{4}} = \sum_{i=1}^{n_c} p_{ari}(x_i\rho_1 - y_i\rho_2) \tag{4.33}$$

where

x_i is the mole fraction of *i*th component in phase1.

y_i is the mole fraction of *j*th component in phase2.

4.6 Cell-to-cell Simulation

In CMG WinProp, a pseudo-ternary diagram is generated from CMG WinProp calculations to interpret simulation results. In consequence, oil pseudo-components are grouped into three groups (pseudo-component1: C_1-C_2, N_2, and CO_2, pseudo-component2: C_3-C_6, and pseud-component3:

C_{7+}). Figure 26 shows the ternary diagram of the CO_2 and oil system in this study. The red point represents the gas consists 100% pseudo-component1 (100% CO_2). Another point represents Bakken crude oil (1.97% pseudo-component1, 14.32% pseudo-component2, and 83.71% pseudo-component3).

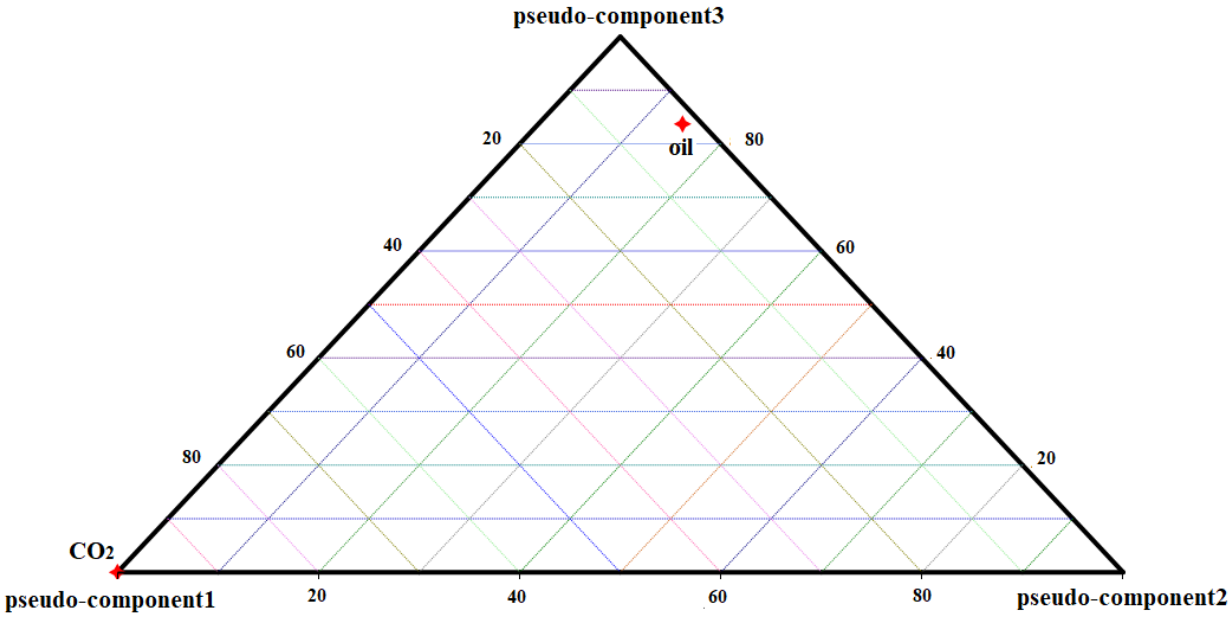

Figure 26 Ternary diagram of the CO_2 and Bakken crude oil in this study

As aforementioned, each ternary diagram can determine whether the gas and oil phase can achieve miscibility at a given pressure and temperature. In the typical diagram, CO_2 is added to the oil such that the CO_2 to oil molar ratio for each mixture increases by a default value (0.01) equilibrium liquid and gas compositions for each mixture are determined by the CMG WinProp flash calculation. As a result, a two-phase envelope in this ternary diagram can be defined, and the first point (point A) in the two-phase region can be detected. Both vaporizing and condensing processes are simulated in cell-to-cell simulation to determine whether multiple-contact miscibility can be achieved. In the vaporizing process, all liquid of A is removed. 0.9 moles of the remaining gas is

mixed with 0.1 moles of the original oil. If the composition of the new mixture is the same as the composition of the former mixture. The vaporizing simulation is terminated. Otherwise, a flash calculation is performed and the simulation process is repeated in order to find out if the multiple contact miscibility can be achieved through vaporizing process. The condensing process is similar to the vaporizing process instead the vapor of the mixture is removed. In addition, ternary diagrams in the selected pressure range are generated to determine the multi-contact MMP through either vaporizing process or condensing process.

4.7 Multiple Mixing Cell Simulation

Multiple mixing cell simulation used in CMG WinProp is developed by Ahamadi and Johns (2011). In the multiple mixing cell method, miscibility is achieved whenever one of the key tie lines becomes zero and the length of the tie line is calculated by the following equation:

$$TL = \sqrt{\sum_{i=1}^{n_c} (x_i - y_i)^2} \tag{4.34}$$

where

TL is the tie line length.

x_i is the liquid equilibrium composition.

y_i is the gas equilibrium composition.

Figure 27 demonstrates the contact process at a given temperature and pressure in the multiple mixing cell method. The process initially begins with two cells, the injected gas is located in the upstream cell while the reservoir fluid is located in the downstream cell. The injected gas and

reservoir fluid are mixed in any desired mole fraction. Then, the flash calculation is performed at this mixture, resulting in two equilibrium compositions (liquid and gas). The equilibrium gas composition is assumed to move ahead of the equilibrium liquid composition. It is the first contact, which results in four cells. The second series contain contacts between the equilibrium gas with the reservoir oil, and the equilibrium liquid with the injected gas. There will be six cells after the second contact. This process will continue until all the key lines develop and converge to within a specific tolerance (10^{-8}). In consequence, there will be $2N + 2$ cells after the Nth contact.

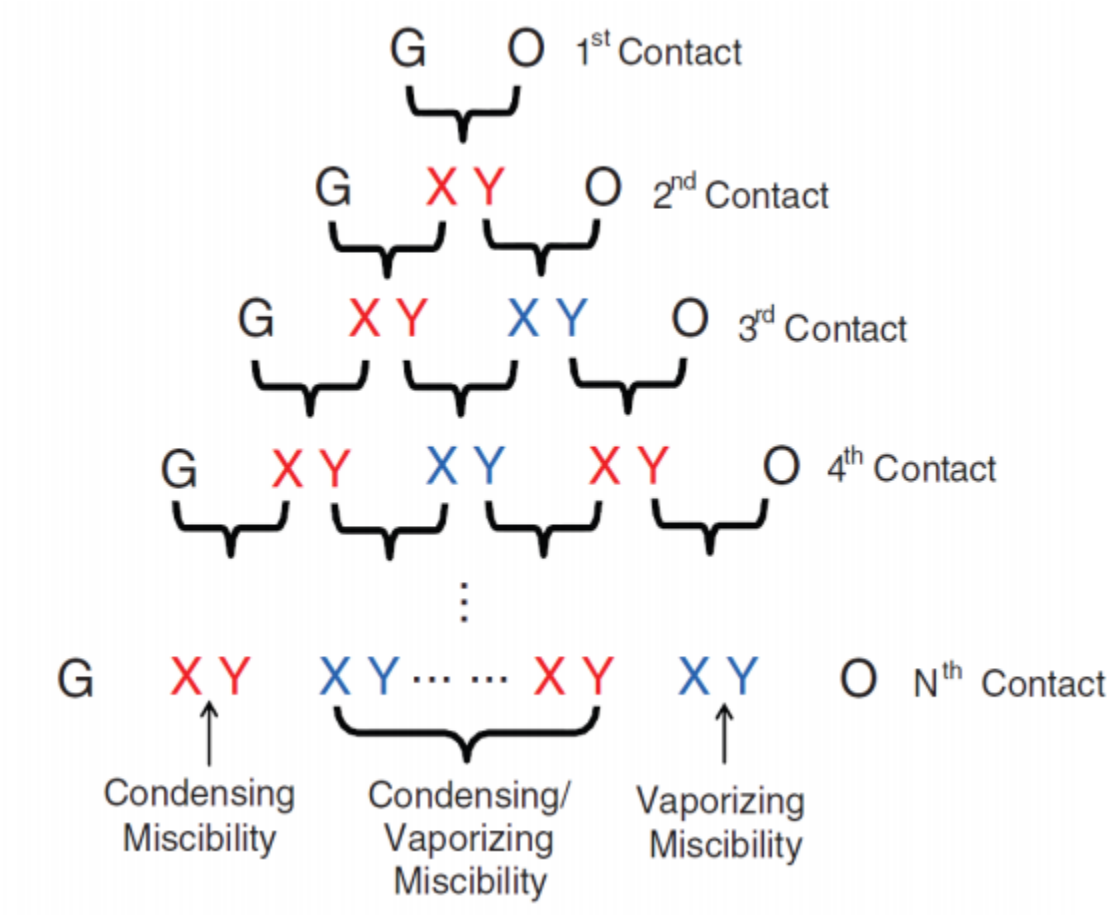

Figure 27 Repeated contacts in the multiple-mixing-cell method. G: injected gas; O: reservoir fluid; X: equilibrium liquid composition; Y: equilibrium gas composition (Ahmadi and Johns, 2011)

The multiple mixing cell algorithm is based on finding the key tie line length at each pressure and procedures of the method are shown in the following:

1. The system temperature and starting pressure are defined.
2. As aforementioned, the contact process starts with two cells filled with the injected gas and the reservoir fluid. Flash calculation is preformed after two cells are mixed, resulting in two equilibrium compositions (liquid and gas).
3. Additional contacts between neighborhood cells continue until all key tie lines develop and converge to the tolerance (10^{-8}).
4. Calculate the tie line length of each key tie line, the smallest tie line length is stored and recorded as TL at this pressure.
5. Increase system pressure and repeat step 2 to 4.
6. The multiple parameter regression is performed to determine the correlation coefficient (n), the lope (m), and the constant (b) in Equation 4.35, and the result is plotted.

$$TL^n = mP + b \tag{4.35}$$

7. The MMP is determined when the power-law extrapolation yields a zero TL value. Repeat Step 5 to 6 until the extrapolated MMP is within the desired accuracy of 20 psi at the latest three pressures.

In conclusion, steps in the simulation study in this thesis are listed as follows:

1. Assign each oil components with physical and critical properties.
2. Lump all the oil components into seven pseudo-components. Calculate physical and critical properties for each pseudo-component based on the oil characterization that has been introduced in this chapter.
3. Perform three-phase flash calculations in WinProp. Optimize pseudo-components properties such as critical pressure, critical temperature, and binary interaction coefficient to match the phase boundaries (LV to L_1L_2V, LV to L_1L and L_1L_2V, L_1L_2) observed in the experimental section.
4. Perform three-phase flash calculations in WinProp. Optimize the pseudo-components properties such as volume shift parameter in order to match the swelling factor calculated in the experiment section.
5. Cell-to-cell and multiple mixing cell simulations for multi-contact MMP are performed by CMG after the accurate EOS model is obtained. The MMP determined in simulation is compared with experimental data for further analysis.

CHAPTER 5 RESULTS FROM EXPERIMENTS AND SIMULATIONS

Results from both experiments and simulations will be discussed in this chapter. In the phase behavior experiment, different phase behaviors are recorded and equilibrium properties such as CO_2 solubility, extraction pressure, and oil swelling factor are determined at different temperatures and pressures. In this simulation study, an accurate EOS model is obtained by CMG WinProp. In addition, the cell-to-cell simulation is performed for multi-contact MMP determination. The determined MMP value is compared and analyzed with the pressure recorded in the experiment.

5.1 Phase Behavior Experiments

5.1.1 Phase and volumetric behaviors

CO_2 and oil at 27 °C. At the temperature of 27 °C, three different types of phase behaviors are recorded in the whole pressurization process, which are liquid-vapor (LV), liquid-liquid-vapor (L_1L_2V), and liquid-liquid (L_1L_2). At the beginning of this experiment, the system pressure stabilizes at 598.72 psi when the system temperature is set to be 27 °C. It shows that a liquid vapor phase behavior exists in the PVT cell. Figure 28 shows the LV phase behavior at 718 psi. The LV phase behavior is observed until the system pressure reaches 824.90 psi.

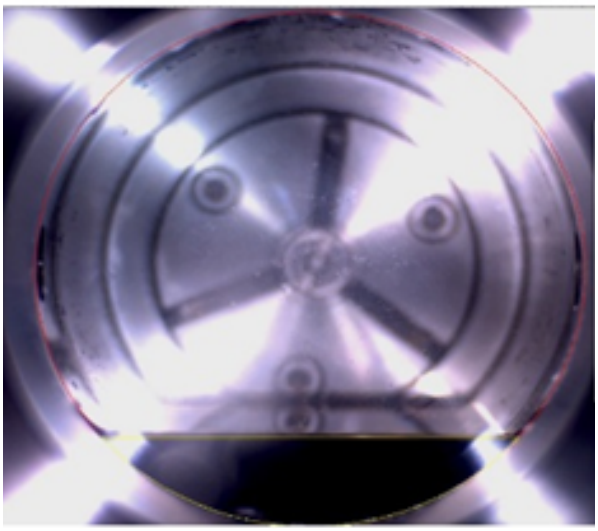

Figure 28 LV phase behavior at 718 psi between CO_2 and oil at 27 °C

At the pressure ranging from 824.90 to 866.04 psi, some of CO_2 in the upper gas phase condenses into liquid phase resulting in a three-phase phase behavior. Figure 29 shows the L_1L_2V phase behavior at 843 psi. The light brown liquid CO_2 phase indicates the oil component extraction.

Figure 29 L_1L_2V phase behavior at 843 psi between CO_2 and oil at 27 °C

As equilibrium pressure continuously increases to 866.04 psi, all the CO_2 in the upper gas phase condense into liquid CO_2 resulting in a L_1L_2 phase behavior. Experiment shows the interface between liquid CO_2 and crude oil becomes vague at the pressure of 3034 psi. In Figure 30, the interface between oil phase and CO_2 liquid phase become "uneven" compared interfaces in Figures 28 and 29.

Figure 30 L_1L_2 phase behavior at 3034 psi between CO_2 and oil at 27 °C

Figure 31 shows the oil extraction column at 3219 psi, and Figure 32 shows the interface disappears and two distinct phases achieve miscibility at 3253 psi.

Figure 31 Oil extraction column between CO_2 and oil at 3219 psi at 27 °C

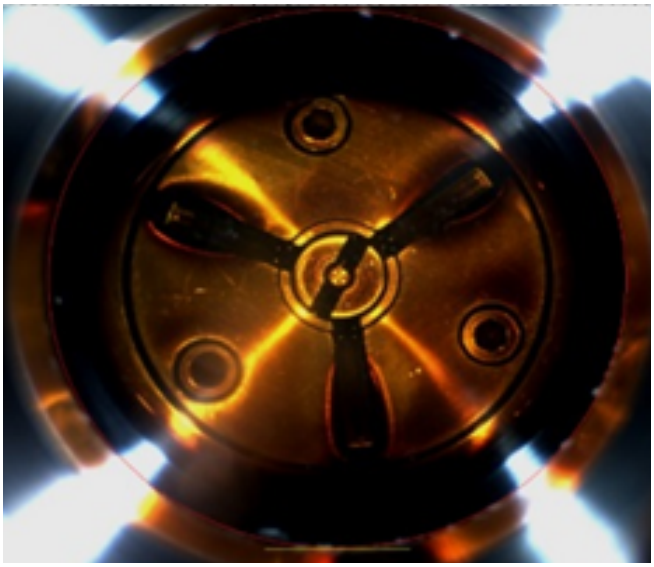

Figure 32 Miscible phase behavior at 3253 psi between CO_2 and oil at 27 °C

CO_2 and oil at 80 °C. Different from experiment results at 27 °C, there are only two types of phase behaviors (LV, L_1L_2) in this CO_2 and oil system during the entire pressurization process. According to the CO_2 P-T diagram, the critical temperature of CO_2 is 31.1 °C, and the critical pressure is 1070.38 psi. In this experiment (80 °C), the CO_2 is super-heated when system pressure

is below critical pressure, while it is super-critical when the system pressure is above the critical pressure. At the start of this experiment, the system pressure is 762.24 psi when the temperature is stabilized 80 °C. Figure 33 shows the system has a LV phase behavior at equilibrium pressure of 1013.87 psi.

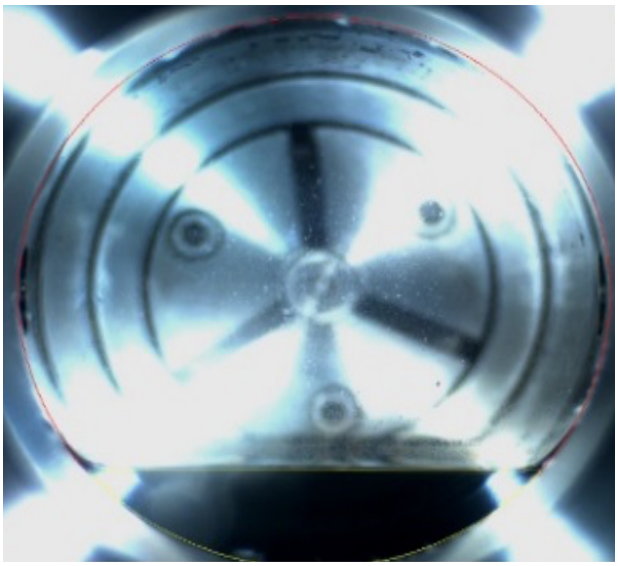

Figure 33 LV phase behavior at 1013.87 psi between CO_2 and oil at 80 °C

The LV phase behavior exists until the system pressure reaches 1897.81 psi. CO_2 is super-critical at this pressure, which has properties of both gaseous CO_2 and liquid CO_2. Starting from a certain pressure (1897.81 psi), the upper CO_2 will become liquid-like. Figure 34 shows the L_1L_2 phase behavior at 2765.64 psi where the CO_2 performs the characteristic of liquid CO_2. Visualized phase behaviors (Figures 34 and 35) show the CO_2 phase color changes from light yellow to light brown as the equilibrium pressure increased from 2765.64 to 3335.52 psi.

Figure 34 L_1L_2 phase behavior at 2765.64 psi between CO_2 and oil at 80 °C

Figure 35 L_1L_2 phase behavior at 3335.52 psi between CO_2 and oil at 80 °C

The color change in the upper CO_2 phase shows the oil component extraction is continuously taking place in this gas and oil system. In addition, the shrunk volume of oil phase also indicates the extraction. Finally, the oil column disappears when the system pressure reaches 4420.13 psi

(Figure 36), which indicates the whole oil phase is extracted by the CO_2 phase and these two phases achieve miscibility.

Figure 36 Miscible phase behavior at 4420.13 psi behaviors between CO_2 and oil at 80 °C

CO_2 and oil at 120 °C. Results from Experiment #3 and #4 is similar to results from Experiment #2. There are two types of phase behaviors. In Experiment #3, the system pressure stabilizes at 897.18 psi when the temperature is set to 120 °C. Similarly, CO_2 becomes super-critical when the system pressure is greater than a certain pressure (2782.93 psi), at which CO_2 becomes a liquid-like fluid. Figure 37 shows the super-critical CO_2 act as gaseous CO_2 resulting in a LV phase behavior at the equilibrium pressure of 2138.45 psi.

Figure 37 LV phase behavior at 2138.45 psi between CO_2 and oil at 120 °C

Results show the system maintains a LV phase behavior until the equilibrium pressure reaches 2354.73 psi, at which a L_1L_2 phase behavior is observed. Similar to the temperature of 80 °C, the color of CO_2 phase changes from light yellow to dark brown (Figures 38 and 40) when the equilibrium pressure increases from 2992.20 to 4270.45 psi. This phenomenon indicates the extraction of oil components from oil phase to upper CO_2 phase. Similarly, since the oil component is continuously extracted by the upper CO_2 phase. It is clearly that the volume of oil phase gradually decreases due to the extraction. Eventually, the entire of oil column disappeared, which means two liquid phases achieved miscibility.

Figure 38 L_1L_2 phase behavior at 2992.20 psi between CO_2 and oil at 120 °C

Figure 39 L_1L_2 phase behavior at 3642.76 psi between CO_2 and oil at 120 °C

Figure 40 Miscible phase behavior at 4270.45 psi between CO_2 and oil at 120 °C

5.1.2 Oil swelling factor

CO_2 and oil at 27 °C. As aforementioned, there are three different phase behaviors between CO_2 and oil at 27 °C, which corresponding to three distinct regions in the chart of swelling factor versus the equilibrium pressure (Figure 41).

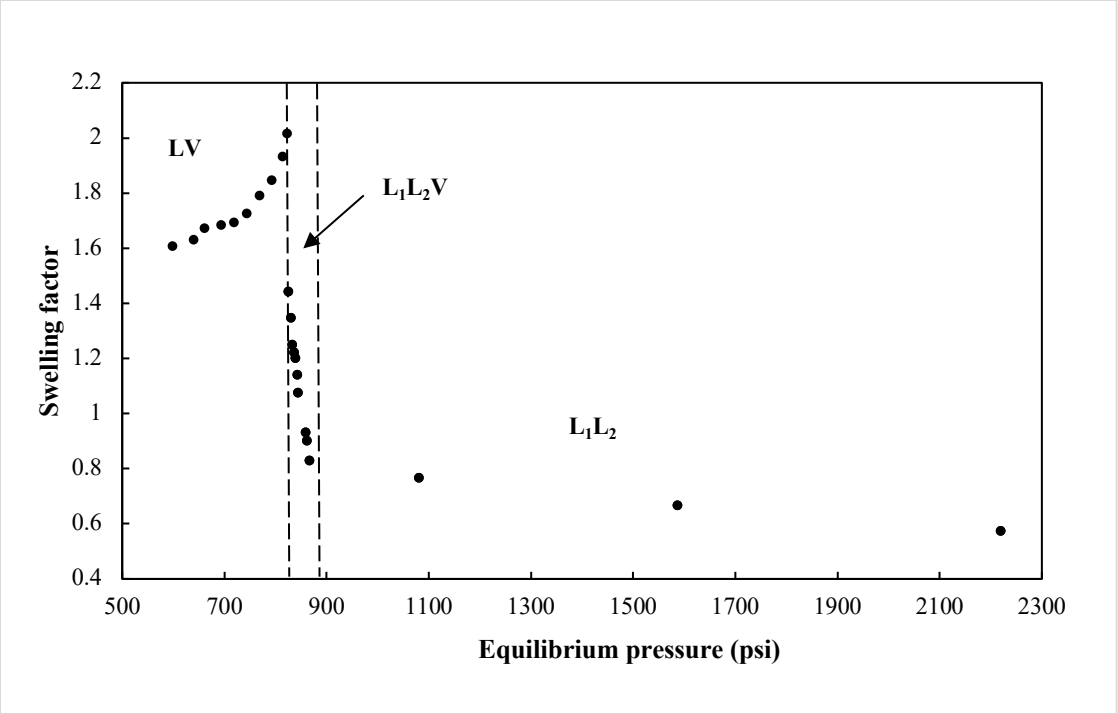

Figure 41 Oil swelling factor at elevated equilibrium pressure at 27 °C

After desirable amount of CO_2 is injected into the PVT cell, the oil swells as the CO_2 continuously dissolves into the oil. As a result, the swelling factor increases to 2.01 in the LV phase behavior region. As pressure increases furthermore (> 823.12 psi), a L_1L_2V phase behavior is observed when the CO_2 starts to be liquified. A lower interfacial tension between the liquid CO_2 phase and the oil phase, which allows the light oil component extraction. Hence, the oil swelling factor decreases in the L_1L_2V region. As shown in Figure 41, in this three-phase region, the swelling factor drops drastically from 2.02 to 0.83. When the equilibrium pressure increases furthermore, all of the CO_2 was liquefied and a L_1L_2 phase behavior is observed. In this region the intermediated to heavy oil components starts to be extracted. Therefore, the swelling factor drops slightly from 0.83 to 0.53 in a pressure ranging from 824.98 to 2688.49 psi.

CO_2 and oil at 80 °C. Figure 42 is the chart of swelling factor versus equilibrium pressure at 80 °C. In the beginning, the state of CO_2 is super-heated because the system temperature is above the CO_2 critical temperature while the pressure is less than the critical pressure. After the system pressure reaches CO_2 critical pressure, CO_2 becomes super-critical. Compared to Experiment #1, there are only two types of phase behaviors. In the LV phase behavior region, the oil welling factor increases from 2.08 to 2.19 with the pressure due to CO_2 dissolution. As equilibrium pressure reaches 801.47 psi, oil components are extracted leading to the decreasing in oil swelling factor. As the pressure increases furthermore (greater than 1897.81 psi), super-critical CO_2 shows liquid CO_2 properties forming a LV phase behavior. In this LV phase behavior region, oil extraction is boosted and swelling factor restarts decreasing with equilibrium pressure until these two phases achieve miscibility.

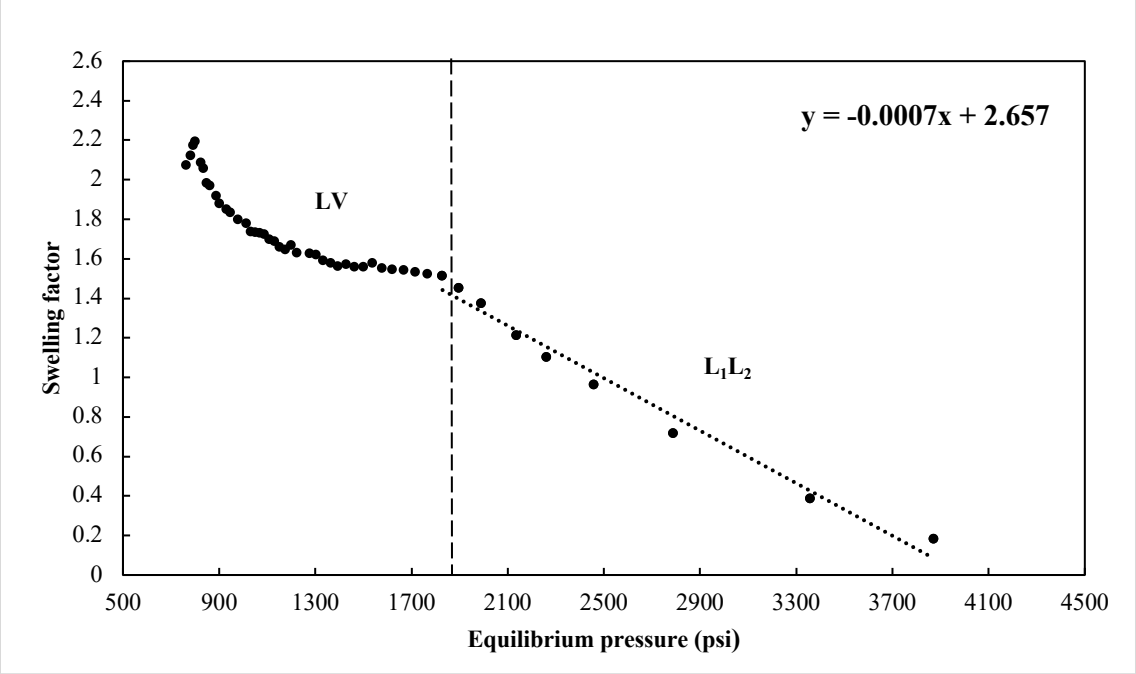

Figure 42 Oil swelling factor at elevated equilibrium pressure at 80 °C

CO_2 and oil at 120 °C. Similar to the swelling factor trend in Experiment #2, the system pressure is measured to be 897.18 psi when the system temperature stabilizes at 120 °C. Compared to Experiment #2, The only difference in Experiment #3 is that the swelling factor starts decreasing at the beginning. The lack of swelling factor increasing region indicates the extraction of oil components has already started in this system. As shown in Figure 43, the result show that the swelling factor decreases from 1.99 to 1.39 in LV region, and finally reaches the plateau. Starting from 2165.17 psi, the upper CO_2 becomes liquid-like forming to a LV phase behavior. Since the extraction ability of liquid CO_2 is stronger than the gaseous CO_2, the swelling factor restarts to drop until the whole oil column is extracted by the upper phase.

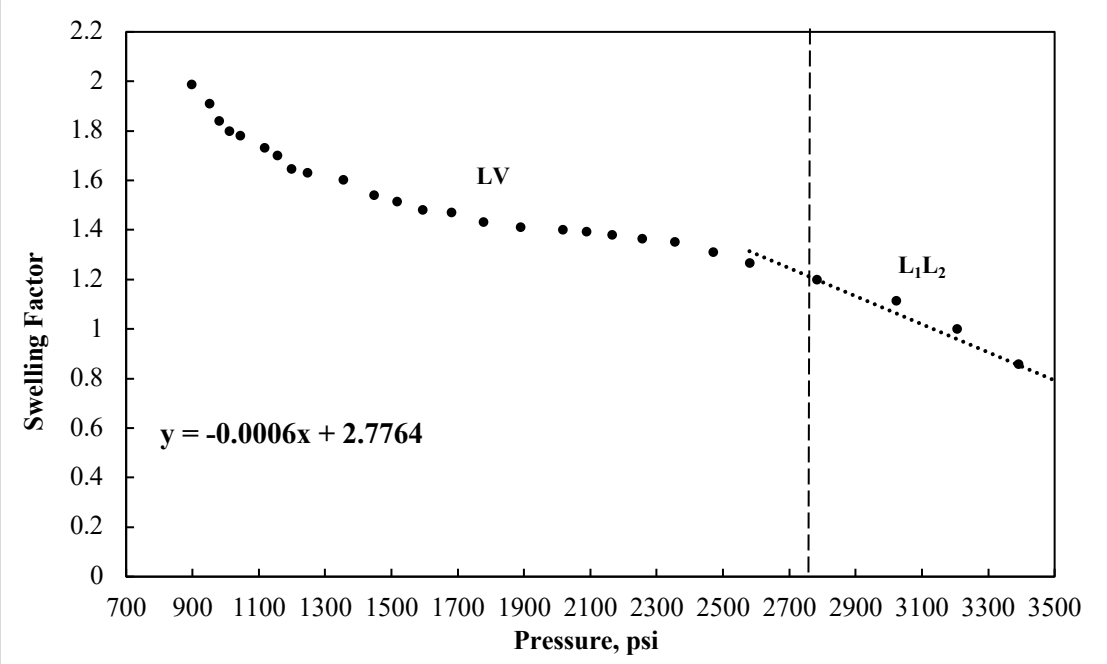

Figure 43 Oil swelling factor at elevated equilibrium pressure at 120 °C (Experiment #3)

Experiment #4 is conducted to find the swelling factor increasing region. Compared to Experiment #3, less CO_2 is injected into the PVT cell, and the system pressure is measured to be 476.73 psi when the system temperature stabilizes at 120 °C. The swelling factor is calculated to be 1.96 at

the beginning of this experiment. As the system pressure increases from 476.73 to 526.31 psi, the swelling factor increases from 1.96 to 2.00 due to CO_2 dissolution. After 526.31 psi, the swelling factor starts to decrease indicating the start of oil component extraction.

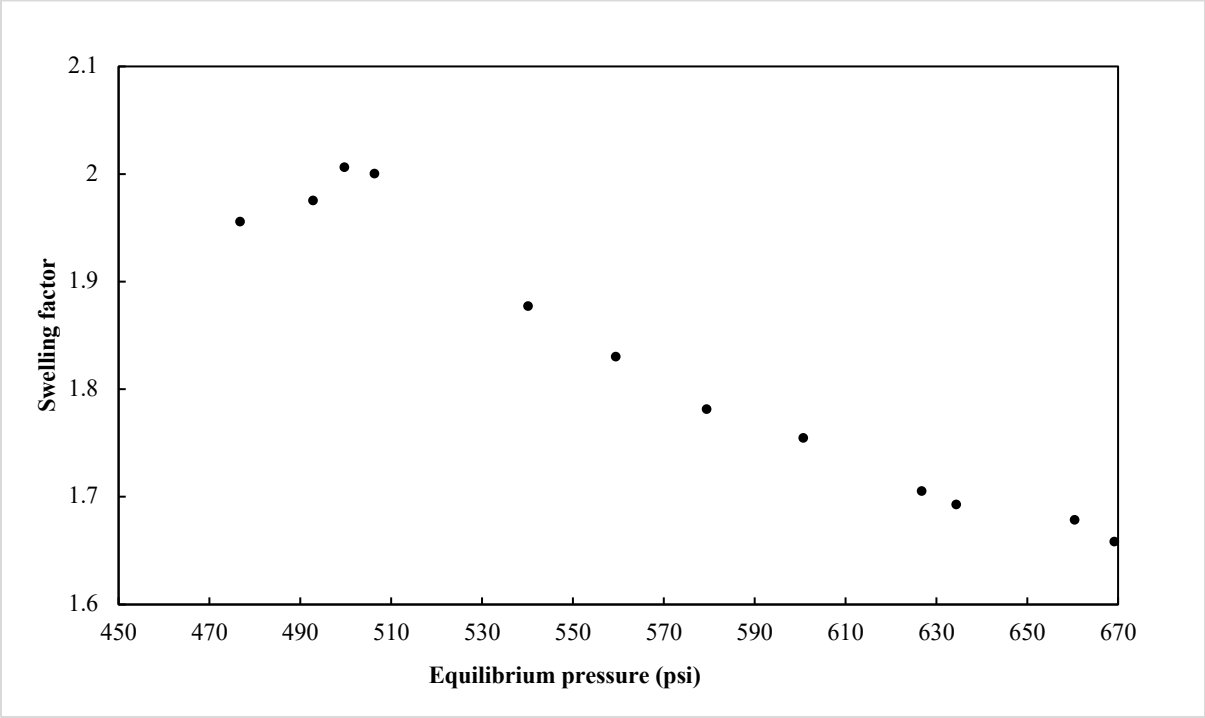

Figure 44 Oil swelling factor at elevated equilibrium pressure at 120 °C (Experiment #4)

5.1.3 Extraction pressure and CO_2 solubility

Compare the swelling factor trend in Experiment #1, Experiment #2, and Experiment #4, the similarity in these three experiments is the swelling factor increasing region. As aforementioned, the oil swelling factor increases with pressure due to the CO_2 dissolution into crude oil. However, when the system pressure reaches a maximum value, the swelling factor reaches a peak and starts to decrease. The swelling factor in this region decreases due to the oil component extraction. In consequence, the turning point at which swelling factor starts to drop is defined as extraction pressure in this thesis. According to this definition, the extraction pressures at 27, 80, and 120 °C

are measured to be 823.50, 801.47, and 499.70 psi. Table 3 concludes the extraction pressure of this CO_2 and oil system in three different experiments. Results shows the extraction pressure decreases with temperature, which indicates the CO_2 extraction ability gets stronger in higher temperature.

Table 3 Extraction pressure at different experiments

Temperature, °C	**Extraction Pressure, psi**
27	823.50
80	801.47
120	499.70

It is assumed that there is only CO_2 dissolution taking place in the CO_2 and oil system before the pressure reaches the extraction pressure. In this case, the CO_2 solubility at each saturation pressure at each temperature can be determined. Figure 45 demonstrates the calculated solubility at elevated pressures for each experiment. It shows that CO_2 solubility at each temperature increases with pressure. In addition, Table 4 concludes the CO_2 maximum solubility at different temperatures. Result shows the maximum solubility decreases with temperature, which enhance the conclusion that the CO_2 extraction capability is enhanced with temperature.

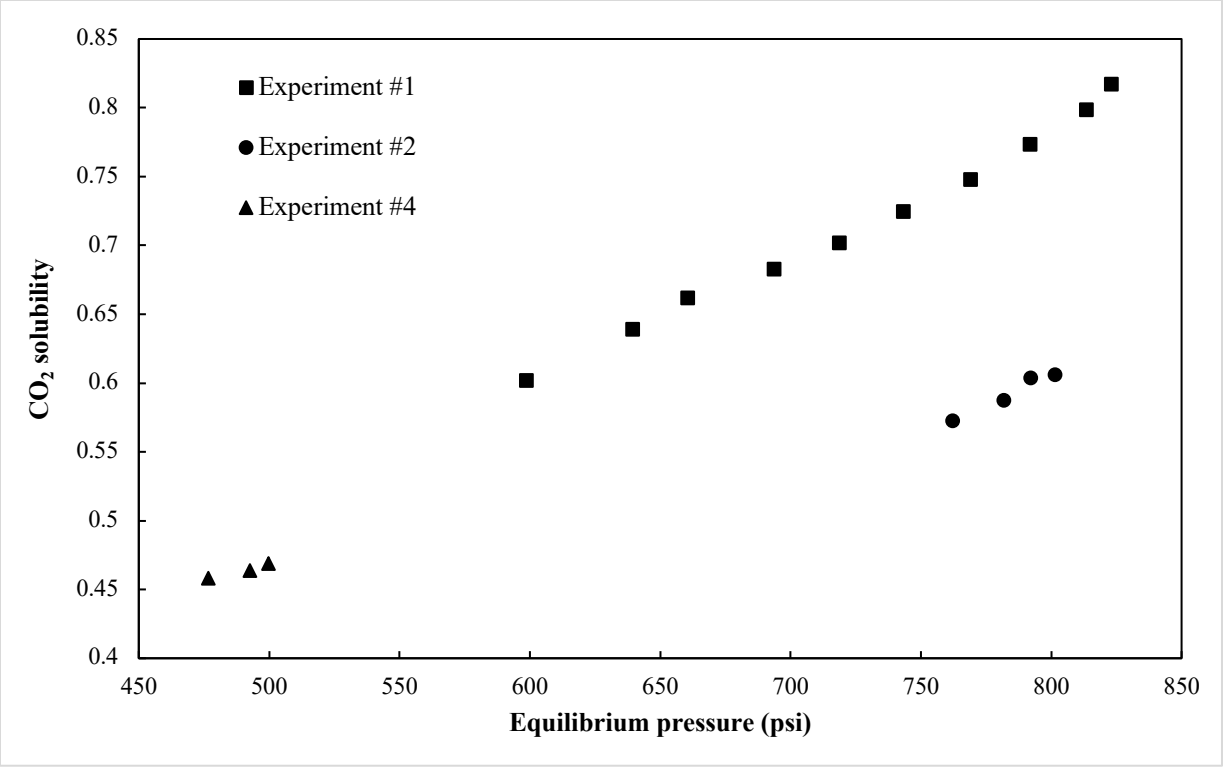

Figure 45 CO_2 solubility at elevated pressures in different experiment

Table 4 Maximum CO_2 solubility at different temperatures

Temperature, °C	Maximum solubility
27	0.82
80	0.61
120	0.47

5.2 CMG Simulation

5.2.1 Bakken crude oil characterization

In the oil characterization, properties are assigned to each oil component using the CMG WinProp library. As aforementioned in Chapter 4, oil components are grouped into seven pseudo-

components in order to reduce the simulation time and simplify the tuning process in order to get an accurate EOS model.

5.2.2 Swelling factor matching

CMG WinProp software is used for the swelling factor matching. In this step, critical properties of heavy oil components are adjusted to match the phase boundary in each experiment. To be specific, the phase boundary is the turning point (marked as red) along with the swelling factor changing path (Figures 45, 47, and 48). After the phase boundary matches with the experimental phase boundary. The swelling factors are calculated by equations in according to different phase behaviors. Moreover, the swelling factor is matched with experimental swelling factor by adjusting the volume shift coefficient of each oil pseudo-component. The following charts shows the history matching result for each experiment.

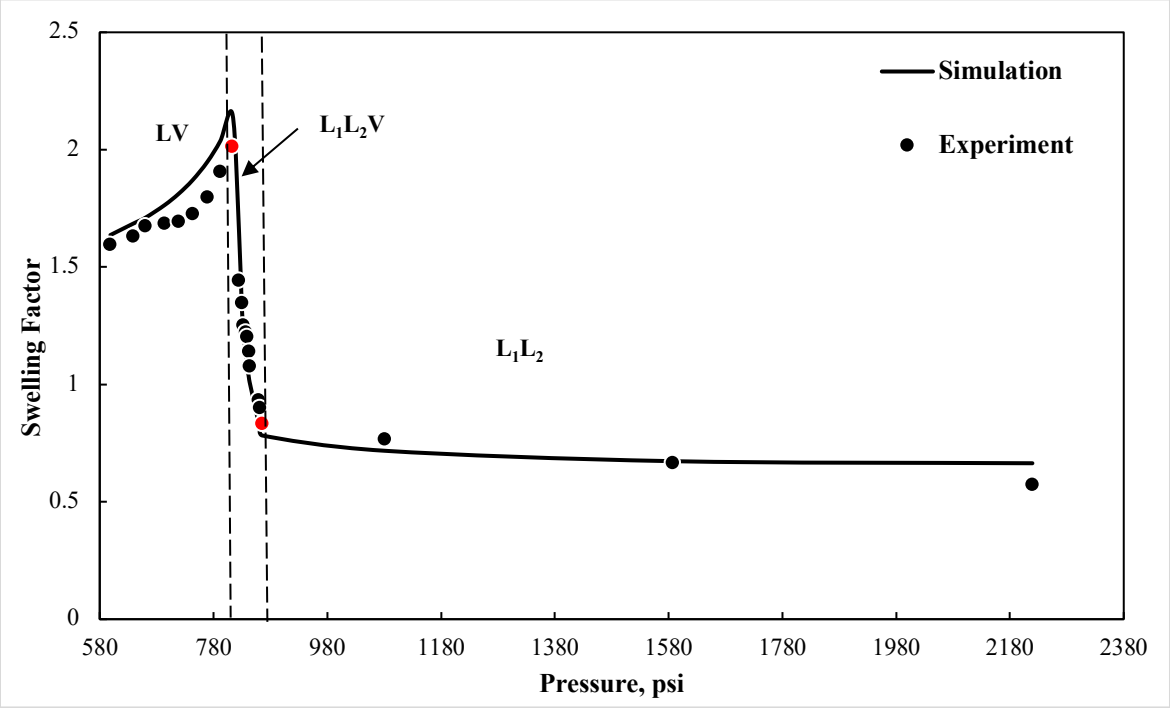

Figure 46 Swelling factor matching result for Experiment #1

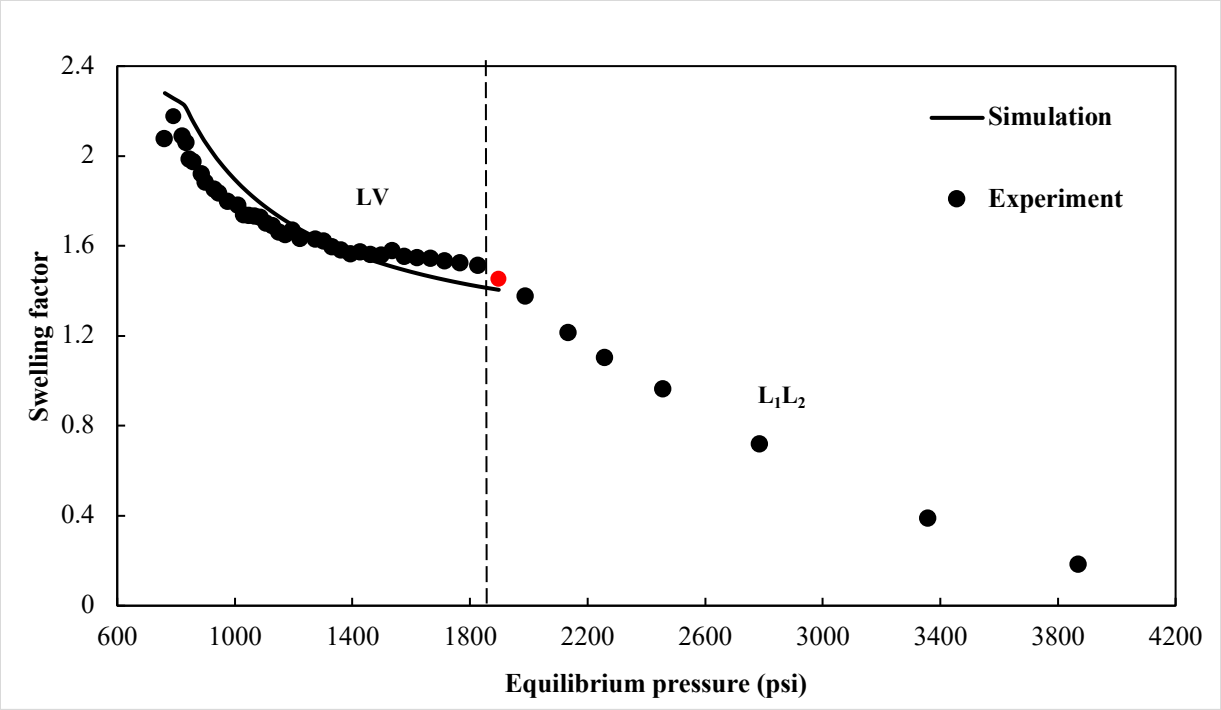

Figure 47 Swelling factor matching result for Experiment #2

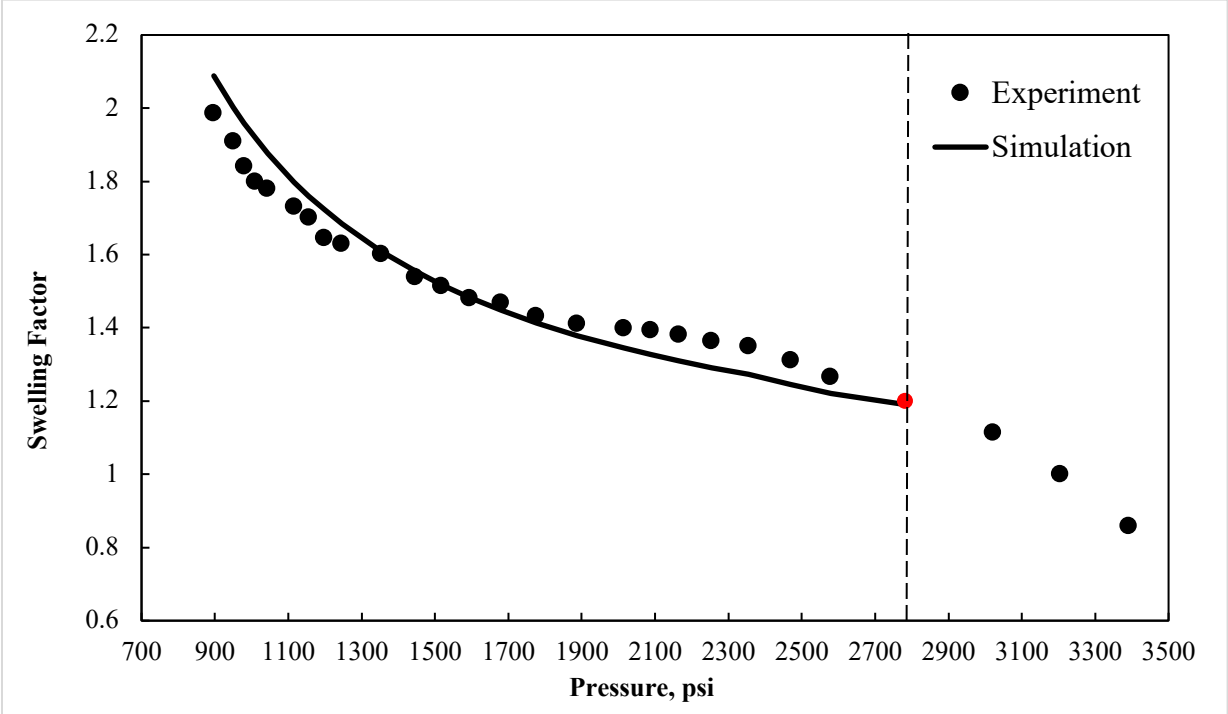

Figure 48 Swelling factor matching result for Experiment #3

Figures 46 to 48 shows the swelling factor matching result for each experiment. In general, the error is 6.62 % for Experiment #1, 4.61% for Experiment #2, and 3.66% for Experiment #3. It is worthy to highlight that in Experiments #2 and #3, history matching for swelling factor is not performed after the red turning point (phase boundary between LV and LL). Multi-phase flash calculation result demonstrates that at the red turning point, the interfacial tension between super-critical CO_2 and oil reduced to zero. WinProp yields the interfacial tension reduce to 0 dyne/cm at 1897.81 psi in Experiment #2 and 0.0007 dyne/cm at 2732.93 psi in Experiment #3. However, the interface between two phases can be still observed. It is also reported that the interface between two phases are still visible when the interfacial tension is zero (Hawthorne et al. 2019).

After the swelling factor matching step, a fine-tuned EOS model is obtained. Table 5 lists the EOS model with tuned properties for each pseudo-component for this CO_2 and Bakken crude oil at 80 and 120 °C.

Table 5 Physical and critical properties of each pseudo-component

Group No.	P_c, atm	T_c, K	Acentric factor	M, g/mol
1	45.167	189.21	0.00866	16.289
2	72.8	304.2	0.225	44.01
3	48.2	305.4	0.098	30.07
4	41.9	369.8	0.152	44.097
5	34.313	466.87	0.23618	72.11
6	22.642	654.56	0.50052	157.04
7	10.092	892.12	1.06925	417.37

5.2.3 CO_2 density

In Experiments #2 and #3, the color change in the upper CO_2 phase indicates the appearance of the oil component extraction in this PVT system. After accurate EOS models at 80 and 120 °C are obtained by matching the oil swelling factor in the previous step, CMG WinProp calculates densities of CO_2 in the upper phase at different equilibrium pressures at 80 and 120 °C. The black curve in Figure 49 shows the density of CO_2 in the upper phase increases from 0.27 to 0.41 g/cm^3 when the system is pressurized from 823 to 1828 psi at 80 °C. In addition, the black curve in Figure 50 shows the density of the upper CO_2 increases from 0.24 to 0.39 g/cm^3 in the pressure range from 897 to 2782 psi at 120 °C. Compared with the red curve in Figures 49 and 50, which is the pure CO_2 density in the same pressure range at 80 and 120 °C, the density of the upper CO_2 is larger than the pure CO_2 at the same pressure and temperature. Extracted oil components enrich the upper CO_2, resulting in a larger density value, which indicates the appearance of the oil component extraction.

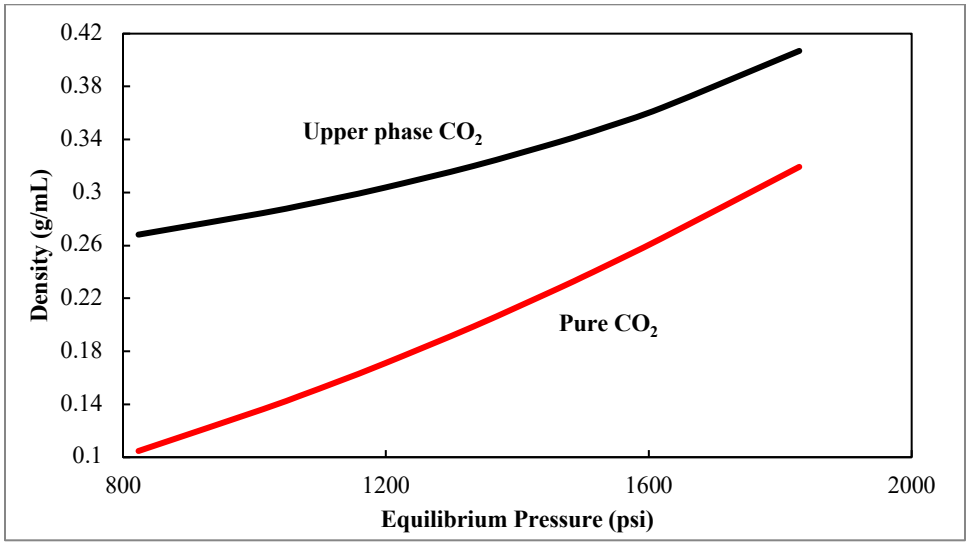

Figure 49 Density of CO_2 in the upper phase and pure CO_2 in the pressure range from 823 to 1828 psi in Experiment #2

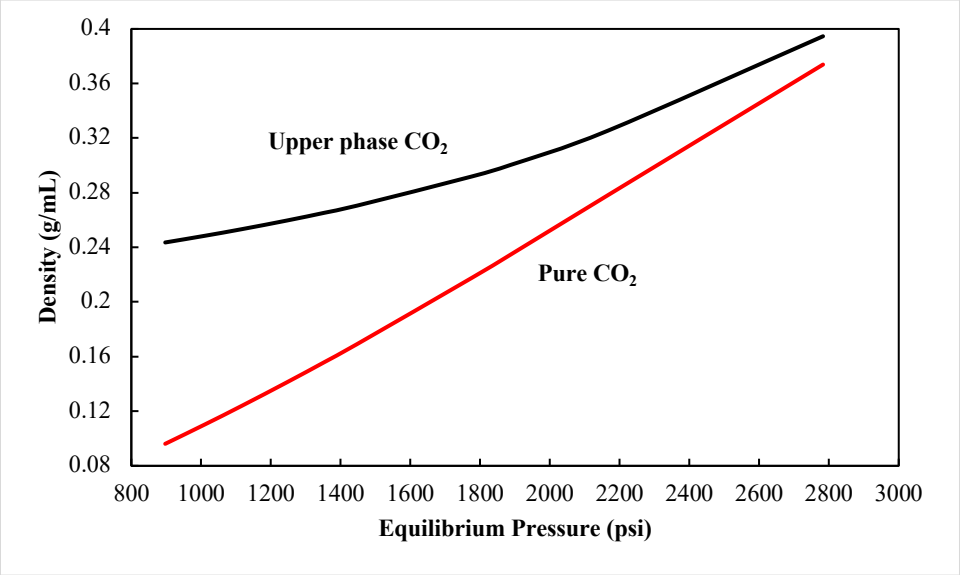

Figure 50 Density of CO_2 in the upper phase and pure CO_2 in the pressure range of 897 to 2782 psi in Experiment #3

5.2.4 MMP analysis

In Experiments #2 and #3, the results show that the oil column continuously decreases in the L_1L_2 region because of oil component extraction. In consequence, the swelling factor continuously decreases in this region, and the extrapolated point at which the swelling factor reduces to zero indicates the entire oil phase is extracted by the upper CO_2 phase. The extrapolated pressures at 80 and 120 °C are determined to be 3795 and 4627 psi. Figures 51 and 52 show the miscible phase behavior at 4420 psi in Experiment #2 and 5532 psi at Experiment #3. The extrapolated pressure can be defined as miscibility pressure that is denoted as $MP_{swelling}$.

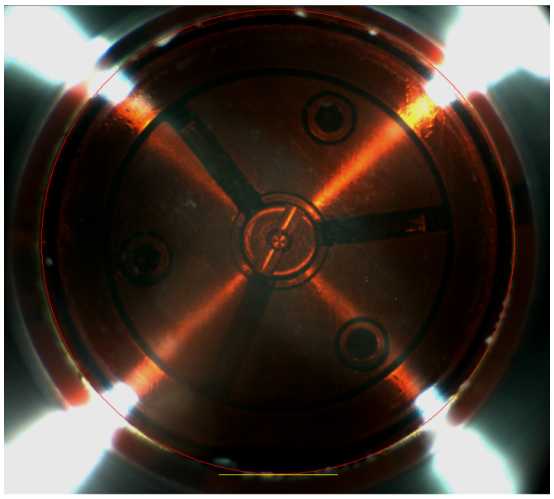

Figure 51 Miscibility phase behavior at pressure that is greater than the extrapolated pressure of Experiment #2

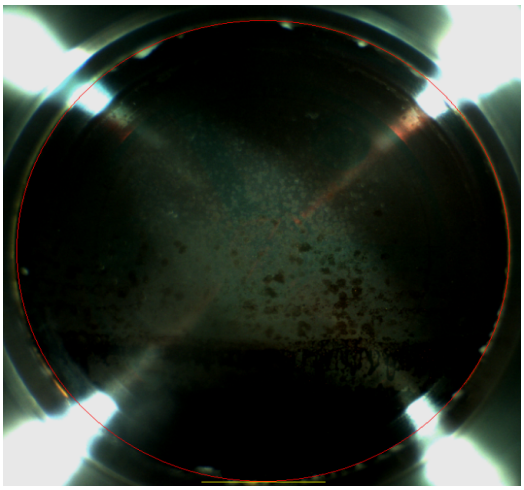

Figure 52 Miscibility phase behavior at pressure that is greater than the extrapolated pressure of Experiment #3

In Chapter 2, the use of vanished interfacial tension technique is widely used for rapid and cos-effective determination of MMP (Ayirala and Rao 2011). In this method, the miscibility pressure is defined at which the IFT between two phases reduces to zero. In the CMG simulation, multiphase flash calculation is performed by the CMG WinProp. The flash calculation yields the

interfacial tension between oil phase and CO_2 phase at different equilibrium pressures, and the interfacial tension determined by WinProp flash calculation at different equilibrium pressures is shown in the following figures (Figures 53 and 54). The pressure that leads to a zero IFT is denoted as MP_{IFT}. Simulation results show that the MP_{IFT} in Experiment #2 and Experiment #3 is 1897 and 2732 psi, respectively.

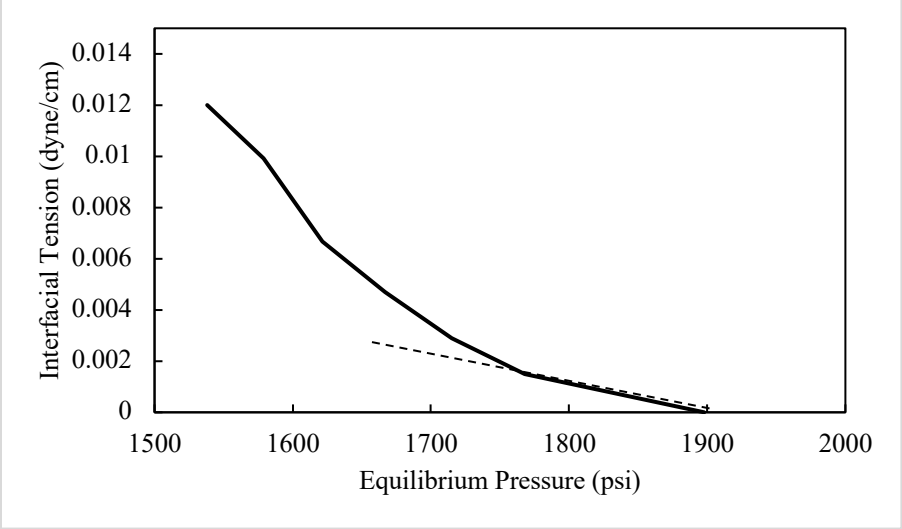

Figure 53 Interfacial tension at each equilibrium pressure calculated by WinProp flash calculation for Experiment #2

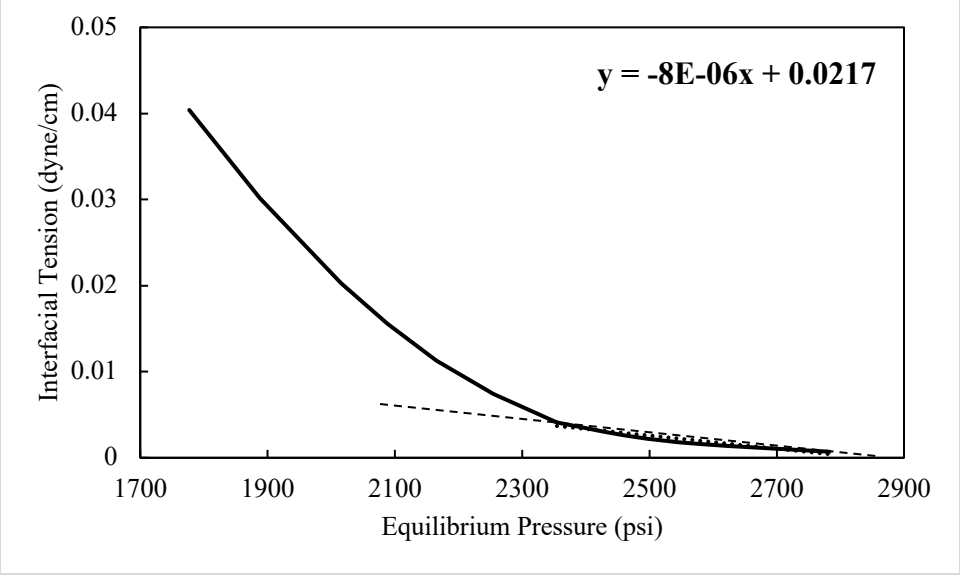

Figure 54 Interfacial tension at each equilibrium pressure calculated by WinProp flash calculation for Experiment #3

In this thesis, there are two key pressures that are highly related to the miscibility. One is the pressure that leads to a zero-swelling factor, while another is the pressure that leads to a zero interfacial intension. In order to analyze which pressure is the MMP, cell-to-cell multi-contact MMP simulation is performed by CMG WinProp using the EOS model obtained from the previous step. Results from cell-to-cell simulation with the pressure step of 100 psi at 120 °C under different pressures (500, 2000, and 2900 psi) are listed. Tables 6 and 7 conclude the CO_2 and Bakken crude oil mixture through both vaporizing and condensing multiple contact process at 500 psi. In Table 6, V_1 stands for the mixture composition after the first contact through the vaporizing process, and V_2 means the mixture composition after the second contact. CMG calculation results show the mixture composition after point V_2 doesn't change. In consequence, the vaporizing process is terminated. Similarly, the condensing process is terminated since the mixture composition after point A_{52} remains the same. Figure 55 shows points V_2 and A_{52} are in the two-phase region, which indicates multi-contact miscibility cannot be achieved through neither vaporizing nor condensing process.

Table 6 Mixture composition in the vaporizing multiple contact process at 500 psi

Mixture	**mol% of each pseudo-component**		
	Pseudo-component1	**Pseudo-component2**	**Pseudo-component3**
V_1	80.107	11.106	8.787
V_2	80.088	11.125	8.787

Table 7 Mixture composition in the condensing multiple contact process at 500 psi

Mixture	mol% of each pseudo-component		
	Pseudo-component1	**Pseudo-component2**	**Pseudo-component3**
A_1	12.69	12.676	74.634
A_2	12.126	11.784	76.09
A_3	11.783	10.981	77.236
A_4	11.565	10.256	78.178
A_5	11.423	9.6	78.978
A_6	11.327	9.002	79.671
A_7	11.262	8.457	80.282
A_8	11.216	7.956	80.828
A_9	11.184	7.495	81.321
A_{10}	11.161	7.07	81.769
A_{11}	11.144	6.676	82.18
A_{12}	11.131	6.309	82.559
A_{13}	11.122	5.968	82.91
A_{14}	11.114	5.649	83.237
A_{15}	11.108	5.351	83.541
A_{16}	11.103	5.071	83.826
A_{17}	11.099	4.808	84.094
A_{18}	11.095	4.56	84.345
A_{19}	11.092	4.327	84.581
A_{20}	11.089	4.107	84.805
A_{21}	11.086	3.899	85.015
A_{22}	11.083	3.703	85.214
A_{23}	11.08	3.517	85.403
A_{24}	11.078	3.341	85.581
A_{25}	11.076	3.174	85.75
A_{26}	11.073	3.016	85.911
A_{27}	11.071	2.866	86.063
A_{28}	11.069	2.724	86.207
A_{29}	11.067	2.589	86.344
A_{30}	11.065	2.461	86.474

Table 7 (Continued) Mixture composition in the condensing multiple contact process at 500 psi

Mixture	mol% of each pseudo-component		
	Pseudo-component1	**Pseudo-component2**	**Pseudo-component3**
A_{31}	11.063	2.339	86.598
A_{32}	11.061	2.224	86.715
A_{33}	11.059	2.114	86.827
A_{34}	11.058	2.01	86.933
A_{35}	11.056	1.91	87.034
A_{36}	11.054	1.816	87.13
A_{37}	11.052	1.727	87.221
A_{38}	11.051	1.642	87.308
A_{39}	11.049	1.561	87.39
A_{40}	11.048	1.484	87.469
A_{41}	11.046	1.411	87.543
A_{42}	11.044	1.341	87.614
A_{43}	11.043	1.275	87.682
A_{44}	11.041	1.212	87.746
A_{45}	11.04	1.153	87.807
A_{46}	11.039	1.096	87.866
A_{47}	11.037	1.042	87.921
A_{48}	11.036	0.99	87.974
A_{49}	11.034	0.941	88.024
A_{50}	11.033	0.895	88.072
A_{51}	11.032	0.851	88.117
A_{52}	11.03	0.809	88.161

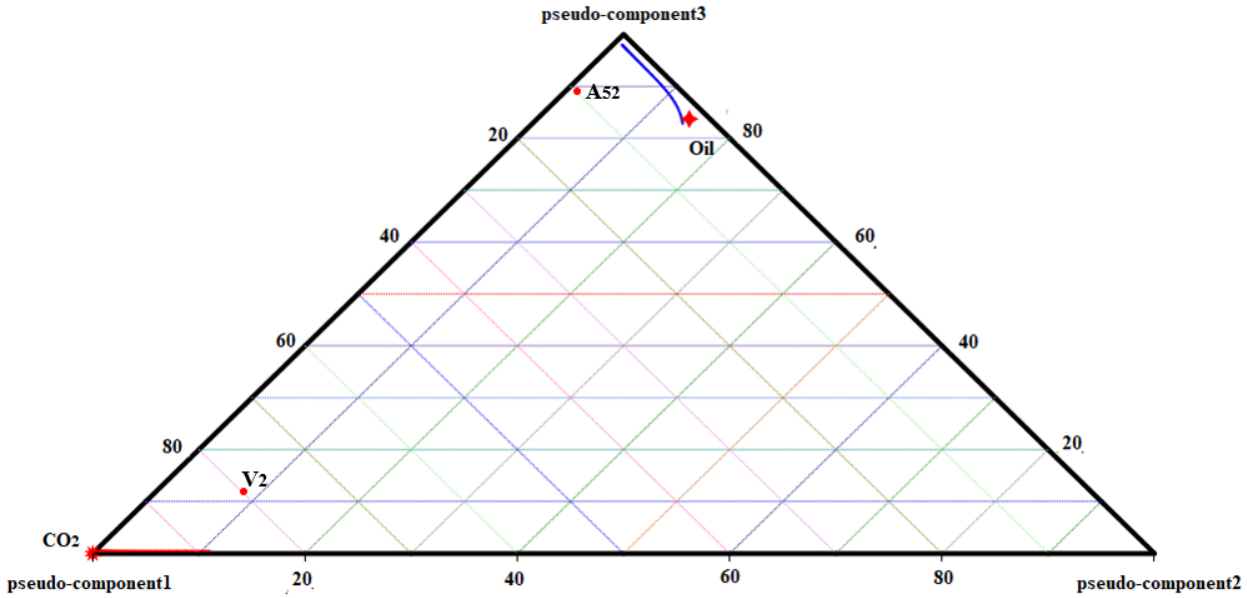

Figure 55 Ternary diagram at 500 psi generated by CMG WinProp

Similarly, Tables 8 and 9 conclude the CO_2 and Bakken crude oil mixture through both vaporizing and condensing multiple contact process at 2000 psi. Both vaporizing and condensing processes are terminated since the composition of the mixture remains the same after points V_{14} and A_{116}. Figure 56 shows these last two points are located in the two-phase region, which indicates multiple contact miscibility cannot be achieved.

Table 8 Mixture composition in the vaporizing multiple contact process at 2000 psi

Mixture	mol% of each pseudo-component		
	Pseudo-component1	**Pseudo-component2**	**Pseudo-component3**
V_1	30.308	15.738	53.954
V_2	30.185	15.768	54.047
V_3	30.074	15.795	54.131
V_4	29.974	15.82	54.207
V_5	29.884	15.842	54.274
V_6	29.803	15.862	54.335
V_7	29.73	15.881	54.389
V_8	29.664	15.898	54.437
V_9	29.605	15.914	54.481
V_{10}	29.552	15.928	54.52
V_{11}	29.504	15.941	54.554
V_{12}	29.461	15.953	54.585
V_{13}	29.423	15.964	54.613
V_{14}	29.388	15.974	54.638

Table 9 Mixture composition in the condensing multiple contact process at 2000 psi

Mixture	mol% of each pseudo-component		
	Pseudo-component1	**Pseudo-component2**	**Pseudo-component3**
A_1	13.274	12.628	74.099
A_2	12.801	10.873	76.326
A_3	12.457	9.371	78.172
A_4	12.189	8.084	79.726
A_5	11.971	6.983	81.046
A_6	11.788	6.04	82.171
A_7	11.634	5.235	83.131
A_8	11.53	4.833	83.637
A_9	11.422	4.469	84.109
A_{10}	11.334	4.138	84.528
A_{11}	11.262	3.836	84.902
A_{12}	11.202	3.56	85.238
A_{13}	11.152	3.307	85.541
A_{14}	11.111	3.075	85.814
A_{15}	11.077	2.861	86.062
A_{16}	11.048	2.665	86.287
A_{17}	11.023	2.484	86.493
A_{18}	11.003	2.317	86.681
A_{19}	10.985	2.162	86.853
A_{20}	10.97	2.019	87.011
A_{21}	10.957	1.886	87.157
A_{22}	10.945	1.763	87.291
A_{23}	10.935	1.649	87.415
A_{24}	10.927	1.543	87.53
A_{25}	10.919	1.445	87.636
A_{26}	10.912	1.353	87.735
A_{27}	10.906	1.268	87.826
A_{28}	10.9	1.188	87.912
A_{29}	10.895	1.114	87.991
A_{30}	10.89	1.045	88.065
A_{31}	10.886	0.98	88.134

Table 9 (Continued) Mixture composition in the condensing multiple contact process at 2000 psi

Mixture	mol% of each pseudo-component		
	Pseudo-component1	**Pseudo-component2**	**Pseudo-component3**
A_{32}	10.882	0.92	88.198
A_{33}	10.878	0.864	88.258
A_{34}	10.874	0.811	88.315
A_{35}	10.871	0.762	88.367
A_{36}	10.868	0.716	88.417
A_{37}	10.864	0.672	88.463
A_{38}	10.861	0.632	88.507
A_{39}	10.859	0.594	88.547
A_{40}	10.856	0.559	88.586
A_{41}	10.853	0.525	88.622
A_{42}	10.85	0.494	88.656
A_{43}	10.848	0.465	88.688
A_{44}	10.845	0.437	88.718
A_{45}	10.843	0.411	88.746
A_{46}	10.84	0.387	88.772
A_{47}	10.838	0.364	88.798
A_{48}	10.836	0.343	88.821
A_{49}	10.834	0.323	88.844
A_{50}	10.831	0.304	88.865
A_{51}	10.829	0.286	88.885
A_{52}	10.827	0.269	88.904
A_{53}	10.825	0.254	88.921
A_{54}	10.823	0.239	88.938
A_{55}	10.821	0.225	88.954
A_{56}	10.819	0.212	88.969
A_{57}	10.811	0.167	89.022
A_{58}	10.809	0.157	89.034
A_{59}	10.752	0.02	89.227
A_{60}	10.751	0.019	89.23
A_{61}	10.75	0.018	89.232
A_{62}	10.748	0.017	89.235

Table 9 (Continued) Mixture composition in the condensing multiple contact process at 2000 psi

Mixture	mol% of each pseudo-component		
	Pseudo-component1	**Pseudo-component2**	**Pseudo-component3**
A_{63}	10.747	0.016	89.237
A_{64}	10.746	0.015	89.239
A_{65}	10.744	0.014	89.241
A_{66}	10.743	0.013	89.244
A_{67}	10.742	0.013	89.246
A_{68}	10.741	0.012	89.248
A_{69}	10.739	0.011	89.249
A_{70}	10.738	0.011	89.251
A_{71}	10.737	0.01	89.253
A_{72}	10.736	0.009	89.255
A_{73}	10.734	0.009	89.257
A_{74}	10.733	0.008	89.258
A_{75}	10.732	0.008	89.26
A_{76}	10.731	0.008	89.262
A_{77}	10.729	0.007	89.263
A_{78}	10.728	0.007	89.265
A_{79}	10.727	0.006	89.267
A_{80}	10.726	0.006	89.268
A_{81}	10.725	0.006	89.27
A_{82}	10.724	0.005	89.271
A_{83}	10.723	0.005	89.272
A_{84}	10.721	0.005	89.274
A_{85}	10.72	0.004	89.275
A_{86}	10.719	0.004	89.277
A_{87}	10.718	0.004	89.278
A_{88}	10.717	0.004	89.279
A_{89}	10.716	0.004	89.28
A_{90}	10.715	0.003	89.282
A_{91}	10.714	0.003	89.283
A_{92}	10.713	0.003	89.284
A_{93}	10.712	0.003	89.285

Table 9 (Continued) Mixture composition in the condensing multiple contact process at 2000 psi

Mixture	mol% of each pseudo-component		
	Pseudo-component1	**Pseudo-component2**	**Pseudo-component3**
A_{94}	10.711	0.003	89.287
A_{95}	10.71	0.002	89.288
A_{96}	10.709	0.002	89.289
A_{97}	10.708	0.002	89.29
A_{98}	10.707	0.002	89.291
A_{99}	10.706	0.002	89.292
A_{100}	10.705	0.002	89.293
A_{101}	10.704	0.002	89.295
A_{102}	10.703	0.002	89.296
A_{103}	10.702	0.002	89.297
A_{104}	10.701	0.001	89.298
A_{105}	10.7	0.001	89.299
A_{106}	10.699	0.001	89.3
A_{107}	10.698	0.001	89.301
A_{108}	10.697	0.001	89.302
A_{109}	10.696	0.001	89.303
A_{110}	10.695	0.001	89.304
A_{111}	10.694	0.001	89.305
A_{112}	10.693	0.001	89.306
A_{113}	10.692	0.001	89.307
A_{114}	10.692	0.001	89.308
A_{115}	10.691	0.001	89.309
A_{116}	10.69	0.001	89.309

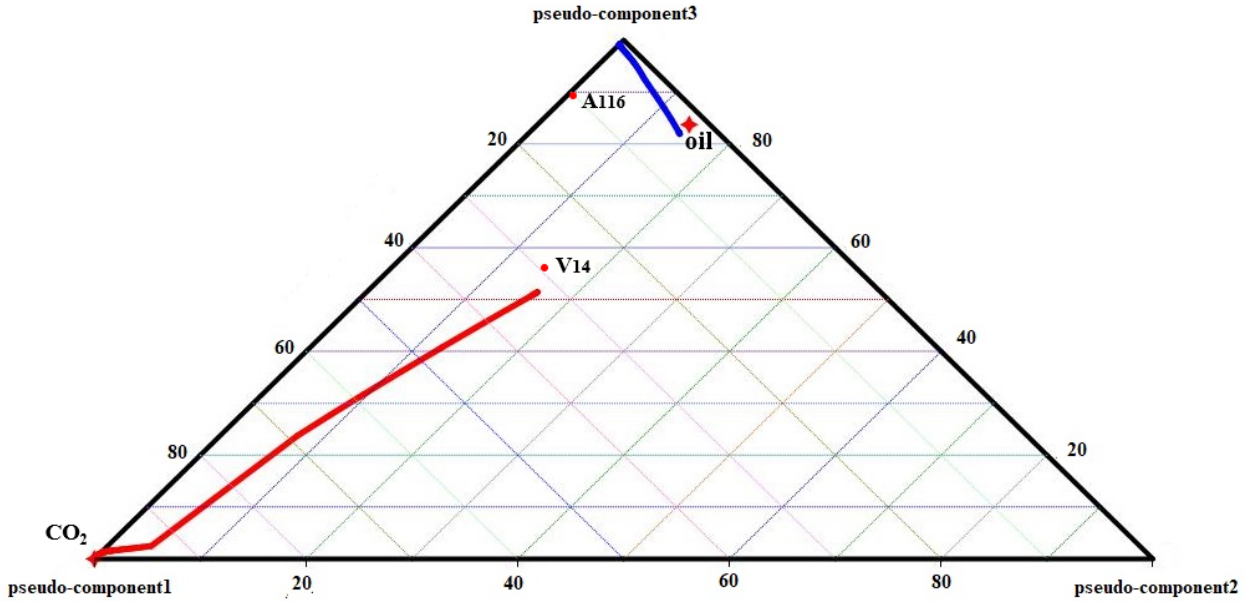

Figure 56 Ternary diagram at 2000 psi generated by CMG WinProp

Tables 10 and 11 conclude the CO_2 and Bakken crude oil mixture through both vaporizing and condensing multiple contact process at 2900 psi. The vaporizing process is terminated after point V_{14} since the mixture composition keeps the same after that point. Figure 57 shows the V_{14} is in the two-phase region, and the miscibility cannot be achieved. For the condensing process, the process is simulated until there is no intercept between the line connecting CO_2 and A_{13} and the two-phase region, which indicates multiple contact miscibility is achieved by condensing process. In addition, Figures 55 to 5 demonstrates the two-phase region shrinks with pressure.

Table 10 Mixture composition in the vaporizing multiple contact process at 2900 psi

Mixture	mol% of each pseudo-component		
	Pseudo-component1	Pseudo-component2	Pseudo-component3
V_1	30.007	15.683	54.31
V_2	29.883	15.712	54.405
V_3	29.772	15.739	54.489
V_4	29.671	15.763	54.565
V_5	29.581	15.786	54.633
V_6	29.5	15.806	54.694
V_7	29.427	15.825	54.749
V_8	29.361	15.842	54.797
V_9	29.302	15.857	54.841
V_{10}	29.248	15.872	54.88
V_{11}	29.2	15.885	54.915
V_{12}	29.157	15.896	54.946
V_{13}	29.118	15.907	54.974
V_{14}	29.084	15.917	54.999

Table 11 Mixture composition in the condensing multiple contact process at 2900 psi

Mixture	mol% of each pseudo-component		
	Pseudo-component1	Pseudo-component2	Pseudo-component3
A_1	13.247	12.626	74.127
A_2	12.785	10.884	76.331
A_3	12.45	9.393	78.157
A_4	12.19	8.114	79.696
A_5	11.978	7.018	81.004
A_6	11.801	6.077	82.121
A_7	11.652	5.27	83.078
A_8	11.524	4.578	83.899
A_9	11.413	3.985	84.602
A_{10}	11.318	3.478	85.204
A_{11}	11.236	3.045	85.719
A_{12}	11.165	2.678	86.157
A_{13}	11.104	2.367	86.529

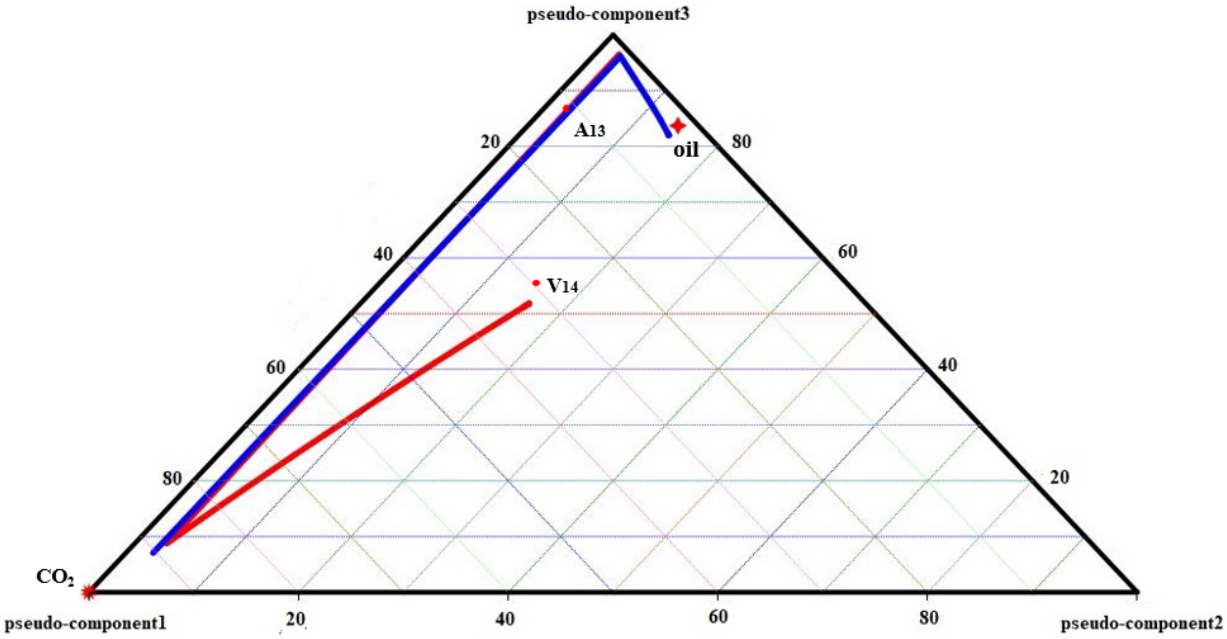

Figure 57 Ternary diagram at 2900 psi generated by CMG WinProp

A more accurate multi-contact MMP result of this CO_2 and Bakken crude oil system at 80 and 120 °C is determined by using different pressure steps (1, 10, 50, and 100 psi) in this cell-to-cell method. Results using different pressure steps are listed in Tables 12 and 13.

Table 12 Multiple contact MMP at 80 °C using different pressure steps (cell to cell)

Pressure Step (psi)	**Multi-contact MMP (psi)**
1	2002
10	2005
50	2012
100	2025

Table 13 Multiple contact MMP at 120 °C using different pressure steps (cell to cell)

Pressure Step (psi)	Multi-contact MMP (psi)
1	2803
10	2805
50	2815
100	2825

It shows that the multi-contact MMP increases with pressure step, and the average MMP determined by cell to cell simulation of this CO_2 and Bakken oil system is 2011 psi at 80 °C and 2812 psi at 120 °C. In addition, multi-contact MMP of the same system at 80 and 120 °C is also determined by multiple mixing cell method with different starting pressure. Results using different starting pressures are listed in Tables 14 and 15. It shows the average MMP is 1757 psi at 80 °C and 2786 psi at 120 °C.

Table 14 Multiple contact MMP at 80 °C using different starting pressures

Starting Pressure (psi)	Multi-contact MMP (psi)
500	1735
700	1890
1000	1646

Table 15 Multiple contact MMP at 80 °C using different starting pressures

Starting Pressure (psi)	Multi-contact MMP (psi)
2300	2564
2400	3032
2500	2764

In conclusion, the multi-contact MMP determined by CMG WinProp is 1884 psi at 80 °C and 2799 psi at 120 °C. Compared with the pressure that leads to a zero IFT, which is 1897 psi at 80 °C and 2732 psi at 120 °C, the error percentage is 0.7% and 2.4%. It implies that the multi-contact MMP is corresponding to MP_{IFT} determined in the previous section.

CHAPTER 6 CONCLUSIONS AND RECOMMENDATIONS

6.1 Conclusions

In this study, experiments are performed to visualize different phase behaviors of the CO_2 and Bakken crude oil system at several temperatures. In every phase behavior experiment, properties such as CO_2 solubility, extraction pressure, and oil swelling factor at different pressures are calculated. In the simulation study, different oil components are lumped into 7 pseudo-components, and properties for each oil pseudo-component are modified to match the oil swelling factor calculated by CMG WinProp flash calculation to the oil swelling factor that is determined in the experimental section. Then, an accurate EOS model is obtained after the matching step. Cell-to-cell simulations are performed by CMG WinProp for multi-contact MMP determination. The MMP determined in the CMG WinProp simulation is then compared and analyzed with pressures ($MP_{swelling}$ and MP_{IFT}) obtained in the experiment section. In this Chapter, major findings are listed as follows:

1. In the phase behavior experiment, CO_2 solubility in the Bakken crude oil is found to increase with the equilibrium pressure at the same temperature. Moreover, it is observed that the CO_2 solubility in the oil phase decreases with temperature at the same equilibrium pressure. In addition, the maximum CO_2 solubility decreases from 0.82 to 0.47 in the temperature ranging from 27 to 120 °C.
2. The onset pressure of the light oil component extraction is defined as the oil extraction pressure. The extraction pressure is determined to be 823, 801, and 499 psi at 27, 80, and 120 °C in the phase behavior experiment, which indicates the oil component extraction in

this CO_2 and Bakken crude happens earlier in higher temperature. In conclusion, the extraction capability of CO_2 increases with temperature.

3. Three types of phase behaviors are observed in the phase behavior experiment, which are liquid-vapor (LV), liquid-liquid-vapor (L_1L_2V), and liquid-liquid (L_1L_2) phase behavior. When the system temperature is below the CO_2 critical temperature (31.1 °C), there are three different types of phase behaviors. While there are only two types phase behaviors (LV, L_1L_2) when the temperature exceeds CO_2 critical temperature.
4. When the system temperature is below the CO_2 critical pressure (Experiment #1), the LV phase behavior is observed in this system in a relative low-pressure region (< 813.47 psi). In this LV region, CO_2 dissolution is dominant and the oil swelling factor increases with equilibrium pressure. When the system pressure exceeds the extraction pressure, parts of CO_2 in the upper phase liquidize, and a L_1L_2V phase behavior is observed. In this three-phase region, light oil components start to be extracted by the liquid CO_2 and the oil swelling factor decreases drastically due to the extraction. When the system pressure increases furthermore, all the CO_2 condense into liquid CO_2 leading a L_1L_2 phase behavior.
5. When the system temperature exceeds the CO_2 critical temperature (Experiment #2 and #3), the oil swelling factor increases with the equilibrium pressure before the extraction pressure. In this swelling factor increasing region, there is a LV phase behavior existing for this system. When the system pressure increases furthermore, the oil swelling factor decreases with equilibrium pressure due to the light oil component extraction until it reaches a plateau. CO_2 in super-critical state has properties of both liquid CO_2 and gaseous CO_2. When the system pressure increases furthermore, it is observed that super-critical CO2 is liquid-like and the swelling factor starts decreasing above 1897 and 2782 psi in

Experiment #2 and #3. The oil swelling factor decreases with equilibrium pressure in this L_1L_2 region until the swelling factor is reduced to zero.

6. In Experiment #1, the phase behavior changes from LV to L_1L_2V at 813 psi, at which the oil swelling factor starts to decrease. In Experiments #2 and #3, super-critical CO_2 firstly becomes liquid-like at 1897 psi and 2782 psi, at which the oil swelling factor restarts to decrease. In this thesis, it is found that the appearance of liquid CO_2 phase will enhance the oil component extraction process.
7. The miscibility pressure defined by the oil swelling factor ($MP_{swelling}$) is determined to be 3795 and 4627 psi at 80 and 120 °C, respectively. The extrapolated miscibility pressure increases with the system pressure.
8. CMG WinProp calculation shows the interfacial tension decreases with the equilibrium pressure. Pressures that results in a zero interfacial tension (MP_{IFT}) are 1897 and 2732 psi at 80 and 120 °C, respectively. The miscibility pressure also increases with the system pressure. Compared with the experimental result, the interface between different phases can still be observed even if the system pressure is above the $MP_{IFT.}$
9. Two miscible pressures are defined along the swelling factor curve. ($MP_{sewelling}$ and MP_{IFT}). Cell-to-cell simulation performed by CMG WinProp implies that the multiple contact MMP is corresponding to MP_{IFT}, at which the super-critical CO_2 starts to be liquid-like.

6.2 Recommendations

1. In the phase behavior experiment, it is found that the oil component extraction pressure decreases with system temperature. However, the oil/gas composition ratio in Experiment #4 is different from the ration in Experiments #1 and #2. Further investigation on the effect of gas/oil composition on the extraction pressure in recommended.
2. In the phase behavior experiment, there are three key pressures: extraction pressure, pressure that leads to a zero interfacial tension, and the pressure leads to a zero-swelling factor. In the oil and gas industry, the primary parameter is the oil recovery factor. In consequence, either experimental or simulation study is needed to investigate the significance of these three pressures in oil production.
3. Cell-to-cell simulation results show that the multi-contact MMP corresponds to the pressure that results in a zero interfacial tension, at which the super-critical CO_2 firstly appears to be liquid-like. In this thesis, a hypothesis is concluded based on the comparison from both results from experiments and simulations. It is found that for a super-critical CO_2 and oil system, the multi-contact MMP is the pressure at which the a L_1L_2 is firstly observed. However, this hypothesis needs more results from future works for validation.

REFERENCE

Adekunle, O. O., and Hoffman, B. T., 2014. Minimum Miscibility Pressure Studies in the Bakken. Paper SPE 169077. Presented at SPE Improved Oil Recovery Symposium, Tulsa, Oklahoma, April 12-16.

Adel, I. A., Tovar, F. D., and Schechter, D. S., 2016. Fast-Slim Tube: A Reliable and Rapid Technique for the Laboratory Determination of MMP in CO_2 - Light Crude Oil Systems. Paper SPE 179673, presented at SPE Improved Oil Recovery Conference, Tulsa, Oklahoma, April 11-13.

Ahmadi, K., Johns, R. T., 2011. Multiple-Mixing-Cell Method for MMP Calculations. *Society of Petroleum Engineers Journal*, *16*(4), 733-742.

Al-Meshari, A.A., 2005. New Strategic Method to Tune Equation-of-State to Match Experimental Data for Compositional Simulation. Ph.D. Dissertation, Texas A&M University, Texas.

Alston, R. B., Kokolis, G. P., and James, C. F., 1985. CO_2 Minimum Miscibility Pressure: A Correlation for Impure CO2 Streams and Live Oil Systems. *Society of Petroleum Engineers Journal*, *25*(2), 268-274.

Ayirala, S. C., and Rao, D. N., 2006. Comparative Evaluation of a New MMP Determination Technique. Paper SPE 99606. Presented at SPE/DOE Symposium on Improved Oil Recovery, Tulsa, Okalahoma, April 22-26.

Ayirala, S. C., and Rao, D. N., 2011. Comparative Evaluation of a New Gas/Oil Miscibility-Determination Technique. *Journal of Canadian Petroleum Technology*, *50*(9/10), 71-81.

Bui, L. H., 2010. Near-Miscible CO2 Application to Improve Oil Recovery. Mater Thesis, the Univerity of Kansas, Kansas.

Carlson, C. G., and Anderson, S. B., 1965. Sedimentary and Tectonic History of North Dakota Part of Willston Basin. *The American Association of Petroleum Geologist Bulletin*, *49*(11), 1833-1846.

Chaback, J. J. (1989). Discussion of Vapour-Density Measurement for Estimating Minimum Miscibility Pressures. *SPE Reservoir Evaluation & Engineering*, *3*(25), 253-254.

Computer Modeling Group Ltd. 2017.*WINPROP Phase Property Program*; Computer Modelling Group Ltd.: Calgary, Alberta, Canada.

Cronquist, C., 1978. Carbon Dioxide Dynamic Displacement with Light Reservoir Oils. Paper Presented at U. S. DOE Symposium. Tulsa, Oklahoma, August 28-30.

Dow, W. G. 1972. Application of Oil-Correlation and Source-Rock Data to Exploration in Williston Basin. *The American Association of Petroleum Geologist Bulletins*, *58*(7), 1253-1262.

Du, F., 2016. An Experimental Study Of Carbon Dioxide Dissolution Into A Light Crude Oil. Master Thesis, University of Regina.

Du, F., Nojabaei, B., 2019. A Review of Gas Injection in Shale Reservoirs:Enhanced Oil/Gas Recovery Approaches and Greenhouse Gas Control. *Energies, 12*(12), 2355.

Elsharkawy, A. M., Poettmann, F. H., and Christiansen, R. L., 1992. Measuring Minimum Miscibility Pressure: Slim-Tube or Rising-Bubble Method?. Paper SPE 24114. Presented at SPE/DOE Enhanced Oil Recovery Symposium, Tulsa, Oklahoma, April 22-24.

Flock, D. L., and Nouar, A., 1984. Parametric Analysis On The Determination Of The Minimum Miscibility Pressure In Slim Tube Displacements. *Journal of Canadian Petroleum Technology*, 23(5).

Green, D.W. and Willhite, G.P., 1998. *Enhanced Oil Recovery*. Richardson, TX: Henry L. Doherty Memorial Fund of AIME, Society of Petroleum Engineers.

Hawthorne, S., Sorensen, J., Miller, D. J., Gorecki, C., Harju, J., and Pospisil, G. 2019. Laboratory Studies of Rich Gas Interactions with Bakken Crude Oil to Support Enhanced Oil Recovery. Paper SPE 961. Presented at SPE/AAPG/SEG Unconventional Resources Technology Conference, Denver, Colorado, July 22-24.

Heck, T. J., LeFever, R. D., Fischer, D. W., and LeFever, J., 2007. Overview of the Petroleum Geology of the North Dakota Williston Basin. North Dakota Geological Survey Report.

Hoffman, B. T. 2012. Comparison of Various Gases for Enhanced Recovery from Shale Oil Reservoirs. Paper SPE 154329. Presented at SPE Improved Oil Recovery Symposium. Tulsa, Oklahoma, April 14-18.

Holm, L. W., and Josendal, V. A., 1974. Mechanisms of Oil Displacement by Carbon Dioxide. *Journal of petroleum Technology*, 1427-1438.

Holm, L. W., and Josendal, V. A., 1982. Effect of Oil Composition on Miscible-Type Displacement by Carbon Dioxide. *Society of Petroleum Engineers Journal*, 87-98.

Huang, E. S., and Tracht, J. H. 1974. The Displacement of Residual Oil by Carbon Dioxide. SPE Paper presented at SPE Improved Oil Recovery Symposium. Tulas, Oklahoma, April 22-24.

Jin, H., and Sonnenberg, S. A. 2013. Characterization for Source Rock Potential of the Bakken Shales in the Williston Basin, North Dakota and Montana. Paper SPE 1581243. Presented at SPE/AAPG/SEG Unconventional Resources Technology Conference, Denver, Colorado, August 12-14.

Jin, H., Sonnenberg, S. A., and Sarg, J. F., 2015. Source Rock Potential and Sequence Stratigraphy of Bakken Shales in the Williston Basin. Paper SPE 2169797. Presented at Unconventional Resources Technology Conference. San Antonio, Texas, July 20-22.

Kesler, M. G., and Lee, B. I., 1976. Improve Prediction of Enthalpy of Fractions. *Hydrocarbon Processing, 55*, 153-158.

Khabibullin, R., Emadi, A., Grin, Z. A., Oskui, R., and Hakan, A., 2017. Investigation of CO_2 Application for Enhanced Oil Recovery in a North African Field - A New Approach to EOS Development. Paper Presented at 19th European Symposium on Improved Oil Recovery, Stavanger, Norway, April 24-27.

Klins, M. A., 1984. *Carbon Dioxide Flooding : Basic Mechanisms and Project Design.* International Human Resources Development Coropration.

Lansangan, R. M., Jangkamolkulchai, A., and Luks, K. D., 1987. Binary Vapour–Liquid Equilibria Behavior in the Vicinity of Liquid-lquid-vapor Loci. *Fluid Phase Equilibra*, *38*, 49-66

Lee, B. I., and Kesler, M. G., 1975. A Generalized Thermodynamic Correlation Based on Three-parameter Corresponding States. *AIChE Journal.*

LeFever, J. A., LeFever, R. D., and Nordeng, S. H., 2011. Revised Nomenclature for the Bakken Formation (Mississippian-Devonian), North Dakota, 11-26.

Li, H., and Yang, D., 2010. Modified α Function for the Peng−Robinson Equation of State To Improve the Vapor Pressure Prediction of Non-hydrocarbon and Hydrocarbon Compounds. *Energy & Fuels*, *25*(1), 215-223.

Meissner, F. F., 1984. Petroleum Geology of the Bakken Formation Williston Basin, North Dakota and Montana. *Petroleum Geochemistry and Basin Evaluation*, 159-179.

Metcalfe, R. S., Fussel, D. D., and Shelton, J. L., 1972. A Multicell Equilibrium Separation Model for the Study of Multiple Contact Miscibility in Rich-Gas Drives. *Society of Petroleum Engineers Journal, 13*(3), 147-155.

Oellrich, L., Ploecker, U., Prausnitz, J. M., and Knapp, H. 1981. Equation-of-state methods for computing phase equilibria and enthalpies. *International Journal of Chemical Enigneering, 21*.

Pedersen, K. S., and Chrisrensen, P. L., 2007. *Phase Behavior of Petroleum Reservoir Fluid.* CRC Press. LLC.

Pitman, J. K., Price, l. C., and LeFever, J. A., 2001. Diagenesis and Fracture Development in the Bakken Formation, Williston Basin: Implications for Reservoir Quality in the Middle Member. *U.S. Geological Survey Professional Paper*.

Poellitzer, S., Florian, T., and Clemens, T., 2009. Revitalising a Medium Viscous Oil Field by Polymer Injection, Pirawarth Field, Austria. Presented at EUROPEC/EAGE Conference and Exhibition. Amsterdam, The Netherlands, June 8-11.

Price, L. C., and Lefever, J. A., 1992. Does Bakken Horizontal Drilling Imply a Huge Oil-Resource Base in Fractured Shales?. *Geological Studies Relevant to Horizontal Drilling: Examples from Western North America*, 199-214.

Reid, R. C., Prausnitz, J. M., and Sherwood, T. K., 1997. *The Properties of Gases and Liquids.*

Schmoker, J. W., and Hester, T. C., 1983. Organic Carbon in Bakken Formation, United States Portion of Williston Basin. *The American Association of Petroleum Geologist Bulletin*, *67*(12), 2165-2174.

Song, C., and Yang, D., 2013. Performance Evaluation of CO2 Huff-n-Puff Processes in Tight Oil Formations. Paper SPE 177212, Presnted at *SPE Unconventional Resources Conference Canada.* Calgary, Alberta, November 507.

Sonnenberg, S. A., and Pramudito, A., 2009. Petroleum Geology of the Giant Elm Coulee Field, Williston Basin. *The American Association of Petroleum Geologist Bulletin, 93*(9), 1127-1153.

Soreide, T., 1989. *Improved Phase Behavior Predictions of Petroleum Reservoir Fluids from a Cubic Equation of State.*

Tsau, J.-S., Bui, L. H., and Willhite, G. P., 2010. Swelling/Extraction Test of a Small Sample Size for Phase Behavior Study. Paper SPE 129728. Presented at SPE Improved Oil Recovery Symposium. Tulsa, Oklahoma, April 24-28.

U.S. Energy Information Adminstration, 2020. Drilling Productivity Report for Key Tight Oil and Shale Gas Regions.

Wang, G., 1986. A Study of Crude Oil Composition during CO2 Extraction Process. Paper SPE 15085. Presented at *SPE California Regional Meeting.* Oakland, CA, April 2-4.

Wang, L., and Yu, W., 2019. Mechanistic simulation study of gas Puff and Huff process for Bakken tightoil fractured reservoir. *Fuel, 239*(1), 1179-1193.

Webster, R. L., 1984. Petroleum Source Rocks and Stratigraphy of Bakken Formation in North Dakota. Hydrocarbon sources of the greater Rocky Mountain region.

Welker, J. R., 1963. Physical Properties of Carbonated Oils. *Journal of Petroleum Technology, 15*(8), 873-876.

Xu, J., and Sonnenberg, S. 2016. Brittleness and Rock Strength of the Bakken Formation, Williston Basin, North Dakota. Paper SPE 2460490. Presented at *SPE/AAPG/SEG Unconventional Resources Technology Conference.* San Antinio, Texas, August 1-3.

Yang, C., and Gu, Y., 2005. New Experimental Method for Measuring Gas Diffusivity in Heavy Oil by the Dynamic Pendant Drop Volume Analysis (DPDVA). *Industrial & Engineering Chemistry Research.*, *44*(12), 4474-4483.

Yin, M., (2015). CO2 Miscible Flooding Application and Screening Criteria.Master Thesis, Missouri University of Science and Technology.

Yu, W., Lashgari, H. R., Wu, K., and Sepehrnoori, K., 2015. CO_2 Injection for Enhanced Oil Recovery in Bakken Tight Oil Reservoirs. *Fuel, 159*(1), 354-363.

Zhang, K., 2016. Experimenal and Numerical Investigation of Oil Recovery From Bakken by Miscible CO2 Injection. Paper SPE 184486. Presented at SPE Annual Technical Conference and Exhibition, Dubai, UAE, September 26-28.

Zhang, K., 2016. Experimenal and Numerical Investigation of Oil Recovery From Bakken by Miscible CO2 Injection.Mater Thesis. Stanford University.

Zhang, K., and Gu, Y., 2016. Two new quantitative technical criteria for determining the minimum miscibility pressures (MMPs) from the vanishing interfacial tension (VIT) technique. *Fuel*, *184*(15), 136-144.